University of California
Los Angeles

Mechanical Control of Enzymes Using DNA Molecular Springs

A dissertation submitted in partial satisfaction
of the requirements for the degree
Doctor of Philosophy in Physics

by

Chiao-Yu Tseng

2013

Abstract of the Dissertation

Mechanical Control of Enzymes Using DNA Molecular Springs

by

Chiao-Yu Tseng

Doctor of Philosophy in Physics

University of California, Los Angeles, 2013

Professor Giovanni Zocchi, Chair

Proteins are compact but flexible molecules; their functions are dependent upon a delicate balance between structural stability and flexibility. Enzymes couple chemical reactions with mechanical motions. More specifically, substrate binding in enzymes drives conformational motion which is an integral part of the catalytic cycle. Understanding the mechanics of the large molecular deformations is the topic of this thesis. Our approach is to use a DNA molecular spring to mechanically stretch an enzyme and measure its enzymatic response. A large part of our work was done on Guanylate Kinase (GK), which showed a decrease in enzymatic activity in response to the mechanical perturbation provided by the DNA spring. A DNA spring is a general tool which can be used to control the activity of an enzyme, and more generally, to explore the mechanical properties of a protein. In addition, the enzyme-DNA chimeras may be developed into interesting biosensors. These are the subjects upon which we will elaborate in this dissertation.

First, we use the DNA spring to exert stresses at three different specific locations on GK, and for each case, determine the changes in substrate binding affinities and catalytic rate. We find that the enzyme's kinetic parameters can be affected separately, depending on where the mechanical stress is applied. For one configuration the applied stress mainly affects the catalytic rate k_{cat}, for another

it mainly affects the binding affinity of the substrate GMP. The anisotropic response of GK shows that the mechanical stress does not only bias the population of the folded and unfolded states of the enzyme. Instead, it is a way to access many intermediate states in the equilibrium situation. This result also leads us to start thinking about continuum mechanics models for our chimera system, which motivates our later work.

Next, we apply the DNA molecular spring to an enzyme from an entirely different class: Renilla Luciferase (RLuc). The successful mechanical control on RLuc shows that the DNA spring is indeed a general tool to manipulate enzymatic activities. We also show proof of concept of the RLuc-DNA chimera as a molecular probe, where the presence of a DNA target sequence can be detected by the decrease in luminescence intensity of RLuc in a one-step solution assay. This probe is also capable of detecting a single-base-pair mismatch on the DNA spring without melting curve analysis. The defect in the DNA spring, caused by the DNA mismatch, results in decreased stress applied by the spring, which leads to a discernible change in enzymatic activity. Inherent in the RLuc-DNA chimera is a reporter system capable of detecting a small change in the stress applied to the enzyme.

In a chimera, the protein and the DNA are mechanically coupled, where the DNA is bent and the protein is mechanically deformed. The DNA is a nonlinear molecule which softens beyond the elastic regime. Using this knowledge, we are able to capture some feature of the mechanics of the protein. Measurements of the response of RLuc for different states of stress suggest that the protein also undergoes a softening transition beyond a few Å deformation. In addition, we find that the sensitivity of the chimera to small changes in the stiffness of the DNA spring, which we observed in both the GK and RLuc chimeras, arises from the mechanical nonlinearities of both the DNA spring and the protein.

The dissertation of Chiao-Yu Tseng is approved.

Anastassia Alexandrova

Dolores Bozovic

Mayank R. Mehta

Giovanni Zocchi, Committee Chair

University of California, Los Angeles

2013

To my dearest family...

Table of Contents

List of Figures

List of Tables

Acknowledgments

This dissertation would not have been possible without the support of many people through my past six years in UCLA. Foremost, my heartfelt gratitude goes to my graduate advisor, Prof. Giovanni Zocchi. He always showed a readiness to discuss my research, share new ideas and give me his support. Whenever I got lost in technical details, he would guide me back to the big picture. From him I learned the most important qualities of a scientist: curiosity, passion and persistence.

I would also like to thank my colleagues, Dr. Andrew Wang, Dr. Yong Wang, Dr. Hao Qu, Amila Ariyaratne, Collin Joseph, Zara Alavi and Daniel Sanchez, for being my faithful companions and partners in the lab. Like other graduate students, most of my time was spent working hard in the basement with machines. However, because of them, life in the lab was more than just work. Not only did we share our experiences in the lab, spending countless hours talking about our research, but we also shared stories (and cookies) from our countries. I treasure the days being with them.

There were many professors who helped me with my lectures and research. They were Dolores Bozovic, Robijn Bruinsma, Alex Levine, Eric D'Hoker, Mayank Mehta and Anastassia Alexandrova. They not only shared their knowledge, but also their ways of thinking. I am honored to have had the opportunities to learn from them.

I would also like to mention the UCLA staff, which was always friendly and patient. I would like to thank Jenny Lee, Cecile Chang, Carol Finn, Elaine Dolals for helping me with academic affairs; Sherin Samaan, Joey De Los Reyes, Ernesto Najar for handling research orders; Craig Reaves for maintaining the building and our lab.

Most importantly, my deepest gratitude is given to my family: my father Ching-Hai Tseng, my mother Hsiu-Wei Wu, my sisters Chiao-Ying and Wan-Yu.

They are the constants of my universe, always by my side and bringing me peace. Their endless love and support accompanied me throughout this endeavor. I am so fortunate to have them in my life and hope to make them proud.

Finally, I would like to thank my friends who never hesitated to show their concern and lend a hand. Doing research is a long and lonely road, but my friends, these twinkling little stars, always light up my way.

Vita

2004	B.S., Physics, National Tsing Hua University, Hsinchu, Taiwan.
2006	M.S., Physics, National Tsing Hua University, Hsinchu, Taiwan.
2008-2013	Teaching Fellow, Department of Physics and Astronomy, University of California, Los Angeles.
2008	Graduate Summer Research Fellowship, Department of Physics and Astronomy, University of California, Los Angeles.
2009-2012	Research Assistant (summer), Department of Physics and Astronomy, University of California, Los Angeles.
2010	M.S., Physics, University of California, Los Angeles.

Publications

Chiao-Yu Tseng and Giovanni Zocchi, Equilibrium softening transition of an enzyme, submitted (2013).

Chiao-Yu Tseng and Giovanni Zocchi, Mechanical control of Renilla Luciferase, *J. Am. Chem. Soc.*, **135**(32), 11879 (2013).

Hao Qu, Yong Wang, **Chiao-Yu Tseng** and Giovanni Zocchi, Critical torque for kink formation in double stranded DNA, *Phys. Rev. X*, **1**, 021008 (2011).

Hao Qu, **Chiao-Yu Tseng**, Yong Wang , Alex J. Levine and Giovanni Zocchi, The elastic energy of sharply bent nicked DNA, *Europhys. Lett.*, **90**, 18003 (2010)

Chiao-Yu Tseng , Andrew Wang and Giovanni Zocchi, Mechanochemistry of the Enzyme Guanylate Kinase, *Europhys. Lett.*, **91**, 18005 (2010)

Chiao-Yu Tseng , Andrew Wang, Giovanni Zocchi, Biljana Rolih and Alex J. Levine, Mechanochemistry of the Enzyme Guanylate Kinase, *Phys. Rev. E*, **80**, 061912 (2009)

CHAPTER 1

Introduction

1.1 Protein Function and Flexibility

Proteins are compact but mechanically soft molecules. While they are covalently-linked polymers, their structures are maintained by rather small forces, such as electrostatic interaction (salt bridge), hydrogen bonding, entropic and *Van der Waals* forces. The continuous breaking and reforming of non-covalent interactions enables the flexibility of proteins, which is essential for protein function. The internal motions of proteins range from thermal fluctuation of atoms and side chains ($<$Å) to large scale conformational changes ($\sim$nm), including open-close hinge motions during enzymatic cycles, and folding and unfolding of proteins. Large-scale conformational changes are dependent upon a delicate balance between structural stability and flexibility. The dynamic properties of proteins are critical to their mechanisms and rate of reactions. For example, the strain and conformational change induced by the binding of an effector in an allosteric enzyme will result in an apparent change in its enzymatic activity.

Proteins can change conformations in different environmental conditions, such as different pH values or salt concentrations. They also often perform conformational changes during biological processes, such as binding events, gene regulation and catalytic cycles, where the interactions between proteins and ligands are highly specific and tightly regulated. Studying these conformational changes may provide information about proteins' mechanical properties (e.g. "How do

proteins deform under stress? What is the force (or energy) needed?"). It may also improve the understanding of the involvement of conformation changes when proteins perform their tasks (e.g. "What roles do conformational motions play in enzymatic cycles?"). Various theoretical and experiment methods have been developed in the past few decades to investigate this issue and we will address a few in the following sections. At the end of this chapter, we introduce our approach: using a DNA molecular spring to probe a protein by mechanically altering the protein's conformation. It is also a method to modulate the activity of an enzyme via perturbing the enzyme's catalytic cycle.

1.2 Theoretical Models and Experimental Techniques

1.2.1 Theoretical Models

Three most popular models in describing the mechanisms of protein-ligand interactions are the key-and-lock, the induced fit and the conformational selection models.

According to Fischer's key-and-lock model proposed in 1894, the active site of an enzyme has a unique geometric shape that only the correct substrate can fit in and initiate the reaction (Fig. 1.1). This model is helpful in understanding why some enzymes only bind to a specific substrate but not a very similar compound which is almost identical in structure. Though the key-and-lock model can explain the specificity of enzymes, it fails to explain the change in enzymatic activity in the presence of allosteric modulators.

In 1958, Koshland proposed a modification to the lock and key model, known as the induced fit theory [1, 2]. It suggests that the precise orientation of catalytic groups is required for enzyme action and only the binding of the correct substrate will bring the catalytic group into proper alignment with the substrate (Fig. 1.1). In other words, a substrate does not only bind to the active site, it also induces the

conformational modification of the enzyme until it is suitable to perform the catalytic function. The induced fit theory is the favored theory in the past fifty years and is supported by abundant experimental evidence. By comparing the x-ray crystal structure of enzymes bound with and without its substrate, the induced-fit effect can be determined. The conformational motion involved in the substrate binding includes small adjustments in orientation of the binding residues and the catalytic residues, and large scale open-close motions of the entire protein [3]. Induce fit conformational changes can be large. For instance, enzyme Guanylate Kinase has a clamp-like shape; upon binding of its substrate GMP, the two lobes are brought together toward a "closed" state, leading to a conformational change of $\sim$1 nm [4].

In comparison to the induced fit theory, the conformational selection model postulates that among the conformations of a dynamically fluctuating protein, the ligand selects and binds to the most favored conformation, shifting the conformation ensemble toward a stabilized state (Fig. 1.1). The concept of selective binding to a single conformation was first suggested by Straub in 1964. It evolves to a generalized concept of "conformational selection and population shift" [5, 6], which challenges the assumption of a conformational difference between the free and ligand-bound states implicated in the induced fit model. In the conformational selection model, the binding interaction merely leads to the population shift of conformational substates instead of inducing a conformational change. This redistribution of substates was difficult to be depicted based on the crystal structures of free and ligand-bound states observed by X-ray. Nowadays, the development in many experimental techniques, such as NMR, enables to the capture of conformational diversity of proteins in solution.

Besides theoretical models, experimental techniques provide another way to investigate protein properties and their interactions with other molecules. We address here some of the widely employed methods.

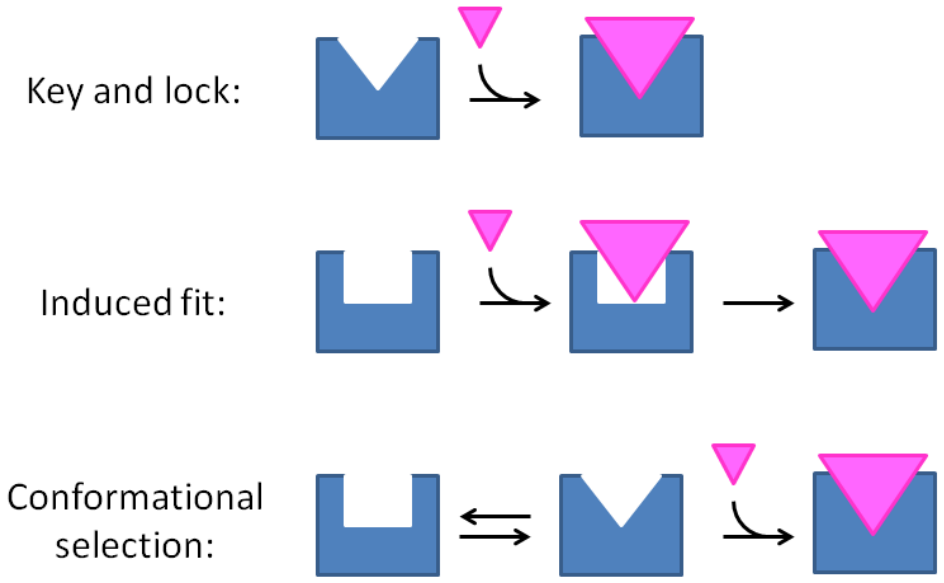

Figure 1.1: Schematic diagrams illustrating the protein motion upon the ligand binding for the key-and-lock, induced-fit and conformational selection models. In the key-and-lock model, a ligand has to be in a specific geometric shape to fit in the protein. In the induced fit model, only the binding of the correct substrate will bring the catalytic group into proper alignment with the substrate to initiate the reaction. On the other hand, the conformational selection model suggests that all the conformation pre-existing and the binding interaction merely leads to the population shift of conformational substates instead of inducing a conformational change.

1.2.2 Experimental Techniques

In this section, we briefly introduce some methods which are relevant to investigating the conformations and mechanical properties of proteins.

X-ray crystallography has been widely used to determine the atomic and molecular structures of biological molecules, including vitamins, drugs, protein and nu-

cleic acids such as DNA and RNA. The first determined crystal structure of protein is myoglobin by Max Perutz and John Kendrew, who won the Chemistry Nobel Prize in 1962. Since then, this technique has been used to elucidate abundant different types of biological molecules. The understanding of structures is usually the first step to investigate molecular properties, dynamics or interactions with other molecules, such as the flexibility of proteins and the ligand binding events. It also has fundamental importance in developing both theories and experimental methods. For example, the induced-fit effect can be determined by comparing the free and ligand bound structures of a protein; the attachment sites of a protein in an AFM pulling experiment are usually chosen based on the information provided from the crystal structure.

The greatest advantage of x-ray crystallography is its outstanding resolution, which is few Å. In addition, it is fairly robust, and the associated experimental and computational methods are now well developed [7]. The disadvantages include that the samples need to be crystalline, which usually takes a lot of effort to find the right conditions, and the crystallized structures may not be the actual structures under biophysical conditions.

Neutron scattering and x-ray scattering have different mechanisms in probing samples. X-rays interact primarily with electron clouds surrounding each atom and thus the diffracted intensity increases with larger atomic number (Z). On the contrary, neutrons interact directly with nucleus of atoms and have a short scattering length ($\sim$fm), which means that neutrons will pass most of atoms without interaction. Therefore, neutrons penetrate deeply into samples and do not damage them. Since H atoms reflect the motion of side chains and backbone where they are bound, incoherent neutron-scattering experiments can provide information on protein dynamics [8]. The mean-square displacement (MSD, denoted as $< x^2 >$) of protein atoms, derived from incoherent elastic scattering intensities, is employed to calculate the environmental force constant of the protein by using

$< k >= k_B/(d < x^2 > /dT$ (equipartition assumption)[9].

An important advantage of neutron-scattering technique in study biological samples is that the samples need not to be crystalline. Thermal fluctuations can be measured in many types of sample, such as powder, solutions and membranes.

The most common single-molecule force spectroscopy techniques are atomic force microscopy (AFM), optical tweezers and magnetic tweezers. The basic scheme of these techniques is to attach one end of the molecule under study to a surface and the free end to a probe: an AFM tip, an optically trapped bead or a magnetic bead. By controlling the tip or the bead, a regulated force can be applied on the molecule to stretch it. These methods are popularly used on force-extension measurements, studying the nonlinear elastic behavior of a protein, the unfolding of protein domains and so on. One advantage of single-molecule force spectroscopy techniques are their wide ranges on manipulation in length and force. For example, AFM can provide force between 10^{-14} - 10^{-8} N and measure the displacement between 10^{-10} - 10^{-4} meter [10]. However, because of being able to study only one or a few molecules at a time, these methods are low throughput and not suitable to measure enzymatic activities.

1.3 Basic Idea of a DNA Molecular Spring

We use an approach which is fundamentally different from the methods mentioned above: using DNA molecular springs to probe and control proteins through altering the conformations mechanically. They are ensemble, mechanical experiments. Since the coupling of mechanical motion with a chemical reaction is one remarkable feature of enzymes, altering the catalysis of enzymes via a mechanical perturbation is conceptually a general method applicable to all (or at least many) enzymes. Besides modulation of enzymatic activity, a DNA molecular spring may be used to elucidate the molecular processes involving the cooperation of mechan-

ical properties and functions of biomolecules.

The molecular spring is composed of 40-60 bp double stranded (ds) DNA (15-20 nm long) with two ends covalently attached to the desired sites on a protein surface. Since the DNA spring is much longer than a typical protein (∼5 nm), in this protein-DNA complex (protein-DNA chimera), the DNA spring has to be bent and thus exerts a mechanical stress on the protein, having a configuration analogous to a bent bow (bent DNA) and a stressed string (protein) (Fig. 1.2). Using a DNA molecular spring has several advantages. First, unlike single-molecular techniques, it is an ensemble measurement at thermal equilibrium, where the enzyme's activity can be measured by using standard assays. In addition, though it is at thermal equilibrium, the protein under study is forced, which is different from neutron scattering experiments. Since the measurements are performed in the working conditions for enzymes, the results can reflect more realistic responses of enzymes under stress. Secondly, DNA is a unique material for our purpose, in which the stiffness can be modulated by the hybridization states and the synthesis can be obtained easily. In addition, its behavior and properties have been studied extensively as well. Third, since protein-nucleic acid conjugates are common in biological systems, the artificial protein-DNA chimeras may have the potential to be designed as smart drugs or sensitive sensors, which can be employed in the cells.

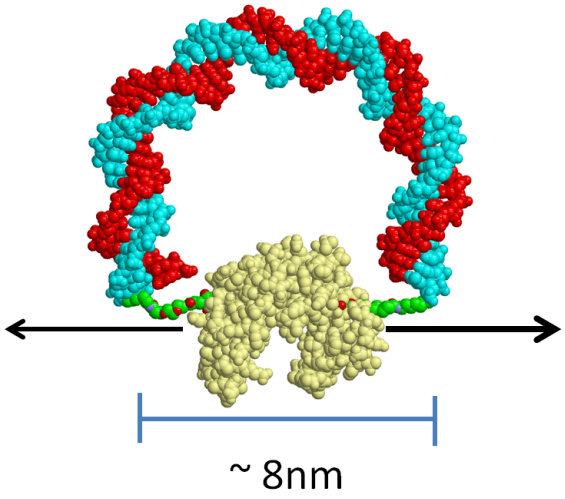

Figure 1.2: Illustration of the protein-DNA chimera. The protein in the figure is Guanylate Kinase, whose crystal structure is from PDB 1ZNX; DNA is from the nucleosome structure 1KX5. The protein, DNA, and cross-linkers are drawn approximately to scale. In this configuration, the DNA has to be bent and thus exerts a stress on the protein in the direction of arrows, perturbing its conformational motion and presumably enzymatic activity.

DNA is a material widely used in constructing artificial biomolecules because of its elastic properties and because it consists of chemical codes (nucleotide sequences). DNA in single-stranded (ss) form is very flexible, with a persistence length of ∼1 nm or 3 bp [11, 12] while it rigidifies drastically when hybridized with the complementary DNA (cDNA), having a persistence length of ∼50 nm or 150 bp [13]. On the other hand, the base pairing rules of DNA, in which only the complementary base pairs (i.e. A and T, G and C) bind together to form double helix structures, enables rational designs of base sequences for specific purposes, such as having a certain structure or melting temperature. These two properties enable DNA to serve as a controllable molecular spring, where the stress provided can be modulated by its structure or length.

We use the worm-like-chain (WLC) model [11] to estimate the elastic energy in the protein-DNA chimera, where the ds DNA is regarded as a thin rod in the linear elasticity regime and its elastic energy is

$$E_{WLC} = \int_0^{2L} \frac{1}{2} \frac{B}{R^2(s)} \, ds \tag{1.1}$$

where $B = 200$ pN $\times$ nm^2 is the bending modulus, $2L$ the contour length of the ds DNA, R the radius of curvature and s the arc length along the rod. A 60 bp ds DNA bent into a half circle has the elastic energy $\sim$10 k_BT. Injecting a 10 k_BT energy into a $\sim$100 amino-acids protein is sufficient to deform it [14].

This DNA molecular method was first developed in our laboratory in 2005. Since then, this method has been applied to Maltose binding protein [15] and Guanylate Kinase [16] to control their molecular processes mechanically. To date, most of the work has been done on Guanylate Kinase (GK) [16, 17, 18, 19, 20, 21]. Guanylate kinase is an enzyme well-known for its induced open-close motion upon binding of the substrate GMP. The DNA spring is coupled to GK in a way that the applied force is against the enzyme's conformation motion upon substrate binding, which is expected to affect the enzymatic activity. We demonstrated that the activity of GK can be affected in a continuously controlled manner [17]. On the path of exploring the molecular processes using this technique, we develop a better understanding about the protein-DNA molecule, which also leads to more interesting issues. In this dissertation, we will be dedicated to solving the following questions:

- How is the elastic energy partitioned in the protein-DNA molecule; which one is the softer part? (Chapter 3)
- Can the kinetic parameters of the enzyme be altered separately by an applied stress? In other words, does the enzyme show anisotropic response to different mechanical stresses? (Chapter 3)

- The DNA molecular spring is conceptually a general method to modulate enzymatic activities. Can we experimentally validate this point of view by applying the DNA spring to a different class of enzymes? (Chapter 4)

- In a chimera, the protein and the DNA are mechanically coupled, where the DNA is bent and the protein is mechanically deformed. Now we understand the bending behavior of the DNA spring. What can we learn about the mechanics of the protein? (Chapter 5)

CHAPTER 2

Synthesis of Protein-DNA Chimera

By using a DNA molecular spring we are able to modulate and probe an enzyme. To precisely apply a mechanical perturbation upon a protein by using a DNA spring, we first construct the protein-DNA chimera, where the DNA is attached to specific sites on the protein surface.

In this chapter, we first introduce the basic concept of protein-DNA chimeras. Then, the synthesis of chimeras is described in detail and the step-by-step protocols are provided.

2.1 Overview of Protein-DNA Chimeras

2.1.1 Protein Functions and Conformational Motion

The protein structures derived from X-ray crystallography or NMR seem rigid and static; in reality, proteins are flexible and dynamic molecules. They are covalently-linked polymers but their structures are maintained by rather small forces, which can be broken by the energy available at the biological temperatures. The continuous breaking and reforming of non-covalent interactions enables the flexibility of proteins, which is essential for protein function. The thermodynamic stability (difference in free energy between folded and unfolded states, under folding conditions) of a ∼100-amino-acid protein is only ∼10 - 20 k_BT [14], which is less than the energy of one covalent bond.

The coupling of mechanics and chemistry is one remarkable feature of en-

zymes, which is highly specific and regulated. Enzymes bind to their substrates, restructure, perform the reactions, release the products and return to their initial conformations. Not only are the conformational changes necessary for chemical reactions, but the chemical energy obtained from a reaction can be converted to direct mechanical motion. For instance, a motor protein is powered by the hydrolysis of ATP and converts this chemical energy to mechanical work. Allostery and induced fit mechanisms are more general examples of conformational changes (static or dynamic [22]) regulating chemical reactions and molecular recognition events.

Exploring this coupling may help us to understand the mechanical properties of enzymes. On the other hand, we may be able to modulate an enzyme's activity by altering its mechanical motion during catalysis. Our strategy is to use a DNA molecular spring to exert a controlled mechanical stress upon a protein and measure its response. Also, it is conceptually a general method of control: what engineers call a "platform".

2.1.2 DNA as a Molecular Spring

DNA is a material widely used in constructing artificial biomolecules because of its elastic properties and because it consists of chemical codes (nucleotide sequences). DNA in single stranded form (ss form) is very flexible, with a persistence length of $\sim$1 nm or 3 bp while it rigidifies drastically when hybridized with the complementary DNA, having a persistence length of $\sim$50 nm or 150 bp [13]. Since DNA is composed of only four types of nucleotides and each nucleotide can bond only with its complementary base, a DNA strand can be designed for specific purpose, such as having a certain structure or melting temperature, by designing its sequence.

Before using DNA as a molecular spring, we want to know first how much force or energy it can provide. To estimate such an energy, we take the continuum linear elastic model (worm-like-chain (WLC) model), where the ds DNA is

regarded as a thin rod in the linear elasticity regime and its elastic energy is

$$E_{WLC} = \int_0^{2L} \frac{1}{2} \frac{B}{R^2(s)}\, ds \tag{2.1}$$

where $B = 200$ pN $\times$ nm^2 is the bending modulus, $2L$ the contour length of the ds DNA, R the radius of curvature and s the arc length along the rod. A 60 bp ds DNA bent into a half circle has the elastic energy $\sim$10 k_BT. Injecting a $\sim$10 k_BT energy into a $\sim$100 amino-acids protein is typically sufficient to deform it [14].

2.1.3 Protein-DNA Chimeras

The principal concept of protein-DNA conjugations is that a DNA is employed as a controllable spring to alter the conformational state of the protein and presumably its enzymatic activity as well. The Ghadiri group built an allosteric control mechanism using a DNA spring to control the binding of an inhibitor to an enzymes active site [23]. Our approach is to construct a protein-DNA chimera, where the DNA spring acts as a mechanical stressor on the protein.

The first protein-DNA chimera was constructed like this: one 60 bp ss DNA attached to the specific sites on the protein surface by two ends (a doughnut chimera) [16, 19]. When hybridizing with the complementary DNA, the DNA spring became semi-rigid and thus stressed the enzyme. Though in this configuration the enzymatic activity could be reduced by a great amount, there was a problem in the chimera construction. Besides the correct products, the "tadpole" chimeras (only one end of the DNA attached to the protein) were also constructed. They were difficult to be removed and did not contribute to the reduction in enzymatic activity. The yield of the correct chimera was always low and the real effect by the mechanical stress was embedded in the background generated by the tadpole chimeras.

To solve this problem, we modified the first scheme and developed the second one. First, we construct the two-armed chimera, in which two ss 30 bp DNA

are attached on specific sites on the protein surface via crosslinkers, respectively (Fig. 2.1). Hybridization to the complementary DNA produces a ds DNA spring with a nick in the middle of the spring, noted as "ds (chimera) with nick". Then, we ligate the two-armed chimera, resulting in one continuous DNA strand attached on the protein surface by two ends (ss chimera or ligated chimera). Hybridization to the complementary DNA produces an intact ds DNA spring (ds without nick).

The mechanical stresses in these four configurations of chimeras described above are (Fig. 2.2):

- Two-armed chimera: no mechanical stress (there ay be a non-mechanical effect)
- ss chimera: no mechanical stress (there ay be a non-mechanical effect)
- ds (chimera) with nick: small stress
- ds (chimera) without nick: large stress

For some mutants, the chimera shows an inhibition of enzymatic activity because of a non-mechanical effect. This effect can be removed by hybridizing the complementary DNA, which is opposite to the effect by mechanical stresses. The non-mechanical effect is due to the interference between the DNA and the protein and we will discuss it in Sec. 3.4.3. Quantitative discussions on the energy partitioning in the chimera and the dynamics of these two coupled molecules will be presented in Chapter 5.

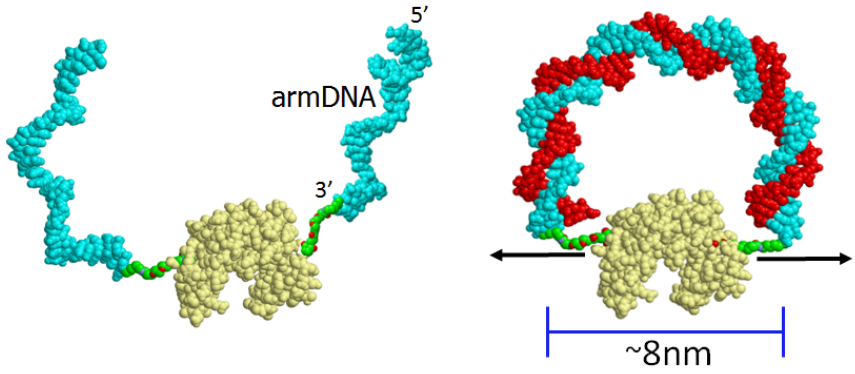

Figure 2.1: Cartoon of the protein-DNA chimera. The protein in the figure, Guanylate Kinase, is from the crystal structure of PDB 1ZNX; DNA is from the nucleosome structure 1KX5. The protein, DNA, and cross-linkers are drawn approximately to scale. Two-armed chimera is first synthesized. When introducing the complementary DNA, the ds DNA becomes semi-rigid and thus exerts a stress on the protein in the direction of the arrows, altering its activity.

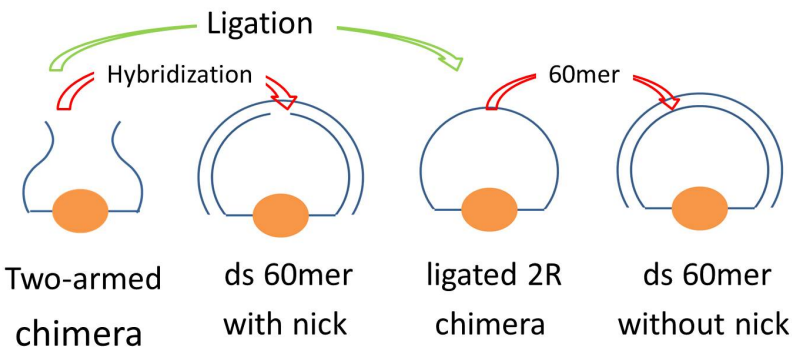

Figure 2.2: Sketch of the different forms of the RLuc chimera used in this study. The molecule is synthesized as a two-armed chimera (2R chimera), with two separate ss 30mer DNA strands coupled to the cross-linkers at the 5' and 3' end, respectively. Ligation of this construct results in the "ligated chimera", sporting one continuous ss 60mer DNA strand attached by the ends to the cross-linkers. Hybridization of the ligated chimera to the complementary 60mer results in an enzyme under stress. Hybridization of the 2R chimera to the complementary 60mer results in an enzyme under a smaller stress because of the nick in the DNA spring.

2.2 Synthesis of Protein-DNA Chimera

2.2.1 Schematics of Chimera Synthesis

Fig. 2.3 is the flow chart of the protein-DNA chimera synthesis (Chapter 2) and measurements to determine enzymatic parameters (Chapter 3). Here is a brief introduction; the step-by-step synthesis protocols are in the following sections.

We first mix the DNA arms with crosslinkers (Cx), followed by High Performance Liquid Chromatography (HPLC) to remove the extra crosslinkers. The DNA-Cx molecule is then attached to the protein, purified with HPLC to obtain the one-armed chimera (1R chimera). Then, the second arm is mixed with the 1R chimera to form the final product: a two-armed chimera, which is purified with Ni-NTA chromatography and identified via SDS gel electrophoresis based on the molecular weight.

2.2.2 Site-directed Mutagenesis

In vitro site-directed mutagenesis is a popularly-employed technique to modify target gene sequences and thus introduce site-specific mutations of the amino acid residues in the proteins of interest [24]. We adopt the commercial QickChange site-directed mutagenesis kit (Stratagene) to produce the mutants needed for Protein-DNA chimera synthesis. Here we address briefly the mechanism of site-directed mutagenesis and the strategies to improve the mutation efficiency.

First, a mutagenic oligonucleotide primer, which is partially complementary to the template DNA plasmid and contains the desired mutations, is designed to serve as the starting point for the DNA replication. The mutations can be adding or deleting a short piece of DNA and changing one or several bases. A primer is usually 20-60 bp with a melting temperature higher than 62 °C. Secondary structures should be avoided while designing long primers. The DNA plasmid is

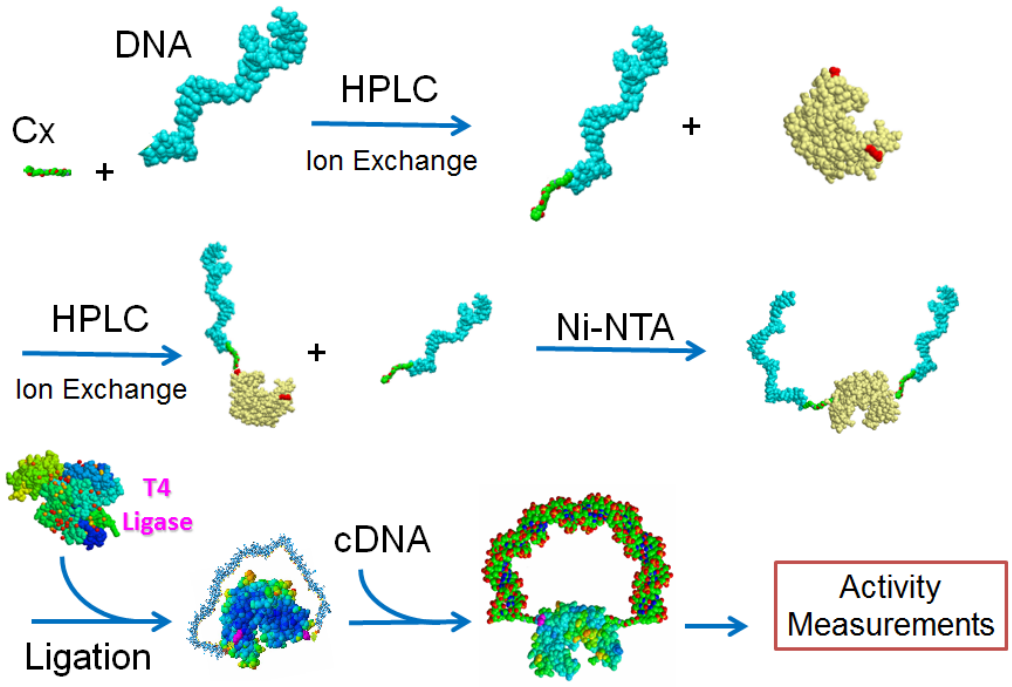

Figure 2.3: Schematics of chimera synthesis. The DNA arms are first linked to crosslinkers and two DNA-Cx conjugations are subsequently coupled to the protein. HPLC is employed to separate the target sample from other by-products. The synthesized two-armed chimera is treated with ligase to generate ligated chimera (ss chimera).

amplified using polymerase chain reaction (PCR) which includes three processes: denaturation (at 95 °C), annealing(at 55 °C) and elongation (at 62 °C). The temperature for elongation should be optimized depending on the length of the primer while the time needed depends on the length of the plasmid (usually the replication rate is $\sim$ 2 kbp/min). During PCR, the mutations are incorporated into the amplicons and the new DNA copies will contain these changes (Fig. 2.4). The total number of cycles is usually 30 - 50.

Because the parental templates produced from *E. Coli* are methylated and will be digested by restriction enzyme *Dpn*1, the sample is treated with *Dpn*1 after the cycles complete to remove the unmutated DNA. The final product is then transformed into *E. Coli* and is amplified, purified and sequenced.

Here, we provide a sample protocol of primer sequences and cycling parameters for site-directed mutagenesis. We used this protocol to obtain the mutant of RLuc, consisting the RLuc-DNA chimera employed in Chapter 4.

- Sample Protocol

Using QuikChang^R Multi Site-Directed Mutagenesis Kit (Stratagene)

Primer Sequences:

(1)G161: GATGAATGGCCTGATATTGAA**TGT**GATATTGCGTTGATCAAATC

(2)T184: GAGAATAACTTCTTCGTGGAA**TGC**ATGTTGCCATCAAAAATCATG

(3)S188: CTTCGTGGAAACCATGTTGCCAT**GT**AAAATCATGAGAAAGTTAGAAC

(*The bold letters are the mutated sites.*)

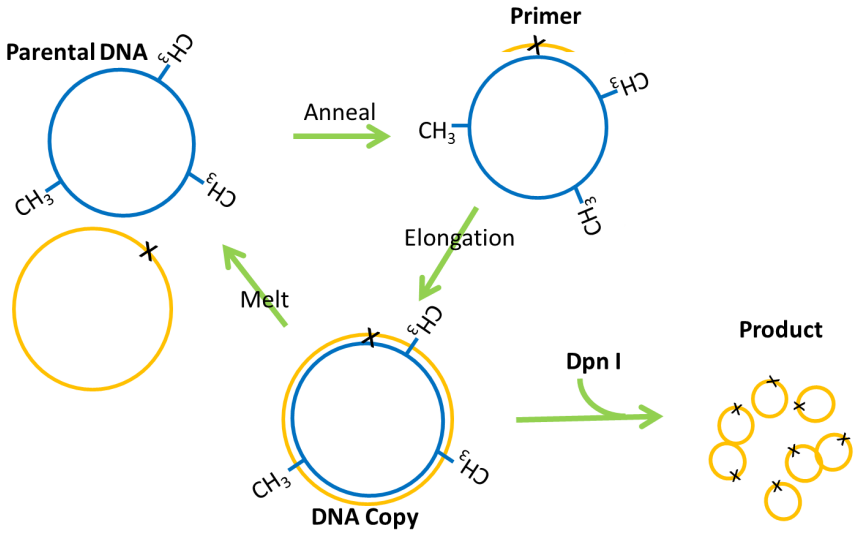

Figure 2.4: Thermal cycling for site-directed mutagenesis. The template plasmid isolated from *E. Coli* is methylated (-CH_3). After each thermal cycle, one copy of mutation-carrying ss DNA is produced from each parental plasmid. After 30-40 cycles, the amount of mutated plasmid is much more than that of original template. The sample is subsequently treated with *Dpn*1 to eliminate the parental templates and thus yields pure mutated plasmids.

Reaction Mixture (25 μL)	
DNA template	RLuc Wild Type in pET28a
10X QickChange Buffer	2.5 μL
d.d.H_2O	11 μL
QickSolution	0.75 μL
ds DNA Template	0.85 μL
Primer (5 μM)	3.5 μL(1) + 2.2 μL(2) + 2.2 μL(3)
dNTP	1 μL
QickEnzyme	1 μL

Thermal Cycling Parameters			
Seqment	Cycle	Temperature	Time
1	1 X	95 °C	1 min
2	32 X	95 °C	1 min
		55 °C	1 min 10 sec
		63 °C	15 min
		4 °C	∞

- The sample is then treated with Dpn1 for one hour at 37 °C to digest the unmutagenized parental strands.
- The Dpn1-treated DNA is transformed into gold competent cells and the minipreperation procedure (Zymo) is followed to isolate the plasmid DNA.
- The plasmid is sent to UCLA GenoSeq Core for sequencing to determine the efficiency of mutagenesis.

Result: RLuH4: Cysteine at 24, 73, 124, 161, 188

Cys161 and Cys 188 are the attachment points for the DNA arms.

2.2.3 Protein Expression

Once the mutated plasmid is prepared, we can use it to express the Cys-mutated protein. The vector containing the protein gene of interest is transformed into *E. Coli*. The successfully-transformed cell colony is incubated from small scale to large scale and then the cell culture is induced with 1 mM IPTG. After growing for 3-6 more hours, the cell is collected and stored at -80 °C for later protein purification.

We express two different enzymes, Gaunylate Kinase and Renilla luciferase, which have different expression protocols. For example, we use bacteria Rosetta(DE3) for guanylate kinase and BL21(DE3)pLysS for Renilla luciferase. Also, they are incubated in different temperatures (37 °C for GK and 30 °C for RLuc). A detailed protocol for each of them is provided below.

Protocol: Guanylate Kinase expression

Our TBGK plasmid is cloned in vector pET17b which is resistant to antibiotic Ampicillin while yGK gene is cloned in vector pET28a, resistant to Kanamycin. The competent cell Rosetta is Chloramphenicol-resistant.

- Day 1: Transformation of *E. Coli*

    1. Remove the competent cells from the freezer and thaw on ice.
    2. Gently mix the cells and dispense 35 μL aliquots into pre-chilled 1.5 ml microfuge tubes and store them at -80 °C. Do not vortex the cells.
    3. Take one tube of Rosetta cells from the freezer and gently thaw on ice for 10 min.
    4. Pipette 2.5 μL of the 200X diluted plasmid (from mutagenesis) into the cells and gently mix by tapping or swirling the tube. Do not pipette

or vortex the cells.

5. Incubate the tube on ice for 30 min.
6. In the meantime, take LB agar plates from 4 °C fridge, add correct antibiotics to the plates and preheat them at 37 °C.
7. Heat-shock the cells for exactly 30 seconds in a 42 °C water bath.
8. Ice the tube for 2 min immediately after heat-shock.
9. Add 250 μL of pre-warmed (37 °C) S.O.C to the tube.
10. Place the tube in an incubator shaker at 37 °C and 250 rpm for 1 hour.
11. Prepare a sterile area and spread 5, 10, 20 μL of the cells from the transformation tube onto the agar plates.
12. Invert the plates and incubate them at 37 °C for 16-20 hours.
13. Store the microtube at 4 °C in case of transformation failure.

- Day 2: Small scale fermentation

1. Prepare a sterile area and three autoclaved tubes. Remove the plates from 37 °C incubator.
2. Add 5 ml LB broth and 5 μL of corresponding antibiotics to each tube.
3. Select a well-isolated colony from the plate with a 1000 μL pipette tip and pipette it gently into the LB broth.
4. Incubate the caped test tubes at 37 °C for 4 - 6 hours.
5. In the meantime, prepare and autoclave one 250 ml LB in 1L flask (for today) and four 1L LB broth in 2L flasks (for Day 3).
6. Wait until the LB is cool, then add 250 μL (1 to 1000 diluted) corresponding antibiotics to the 1L flask.
7. After 4-6 hours, select one test tube which shows normal cell growth and pour it into the 1L flask.

8. Incubate the cells at 37 °C with 250 rpm shaking for 16-20 hours.

- Day 3: Large scale fermentation

1. Prepare a sterile area and place all flasks around the flame.
2. Dilute the overnight cell culture to 10% and measure the O.D. at 600 nm absorbance.
3. Add 1 ml of corresponding antibiotics to 2L flasks.
4. Add the overnight cell culture to the 2L flasks until the final O.D is 0.1.
5. Incubate the culture at 37 °C in the incubator shaker with the rate of 250 rpm.
6. After about 90 min, when the O.D. reaches 0.6 - 0.8, induce expression with 1 mM IPTG.
7. Incubate the culture for 4-6 more hours. Spin down the cells, discard the supernatant and store the cells at -80 °C.

Protocol: Renilla Luciferase expression

Our RLuc plasmid is cloned in vector pET28a, which is resistant to Kanamycin. The competent cell BL21(DE3)pLysS is Chloramphenicol-resistant.

- Day 1: Transformation of *E. Coli*

  1. Remove the competent cells from the freezer and thaw on ice.
  2. Gently mix the cells and dispense 40 μL aliquots into pre-chilled 1.5 ml microfuge tubes and store them at -80 °C. Do not vortex the cells.
  3. Take one tube of BL21(DE3)pLysS cells from freezer, add 2 μL of β-ME and gently thaw on ice for 10 min. Swirl it gently every two minutes.
  4. Pipette 2.5 μL of the 200X diluted plasmid (from mutagenesis) into the cells and gently mix by tapping or swirling the tube. Do not pipette or vortex the cells.
  5. Incubate the tube on ice for 30 min.
  6. In the meantime, take LB agar plates from 4 °C fridge, add correct antibiotics onto the plates and preheat them at 37 °C.
  7. Heat-shock the cells for exactly 40 seconds in a 42 °C water bath.
  8. Ice the tube for 2 min immediately after heat-shock.
  9. Add 500 μL of pre-warmed (37 °C) S.O.C to the tube.
  10. Place the tube in an incubator shaker at 37 °C and 250 rpm for 1.5 hour.
  11. Prepare a sterile area and spread 50, 100, 300 μL of the cells from the transformation tube onto the agar plates.
  12. Invert the plates and incubate them at 37 °C for 16-20 hours.
  13. Store the microtube at 4 °C in case of transformation failure.

- Day 2: Small scale fermentation

    1. Prepare a sterile area and three autoclaved tubes. Remove the plates from 37 °C incubator.
    2. Add 5 ml LB broth and 5 μL of corresponding antibiotics to each tube.
    3. Select a well-isolated colony from the plate with a 1000 μL pipette tip and pipette it gently into the LB broth.
    4. Incubate the caped test tubes at 37 °C for 4 - 6 hours.
    5. In the meantime, prepare and autoclave one 250 ml LB in 1L flask (for today) and two 1L LB broth in 2L flasks (for Day 3).
    6. Wait until the LB is cool, then add 250 μL (1 to 1000 diluted) corresponding antibiotics to the 1L flask.
    7. After 4-6 hours, select one test tube which shows normal cell growth and pour it into the 1L flask.
    8. Incubate the cells at 30 °C with 250 rpm shaking for 16-20 hours.

- Day 3: Large scale fermentation

    1. Prepare a sterile area and place all flasks around the flame.
    2. Dilute the overnight cell culture to 10% and measure the O.D. at 600 nm absorbance.
    3. Add 1 ml of corresponding antibiotics to 2L flasks.
    4. Add the overnight cell culture to the 2L flasks until the final O.D is 0.2.
    5. Incubate the culture at 30 °C in the incubator shaker with the rate of 250 rpm.
    6. After about 2 hours, when the O.D. reaches 0.6, induce expression with 1 mM IPTG.

7. Incubate the culture for 3 more hours. Spin down the cells, discard the supernatant and store the cells at -80 °C.

2.2.4 Ni-NTA Purification

Nickel-nitrilotriacetic acid (Ni-NTA) metal-affinity chromatography (Qiagen) is used to purify the expressed protein carrying a His-tag from *E. coli* cells. NTA occupies four of the six binding ligand of the nickel ion, leaving two sites free to interact with the 6xHis tag (Fig. 2.5). The six-histidines chain in the his-tag ensures the binding with metal ion while the irrelevant proteins from bacterial cell lysate bind rather weakly with Ni-NTA resin and thus can be washed away even though they are abundant. Imidazole can bind to Ni-NTA and compete with the his-tagged protein. When present in high concentration (> 300 mM), the imidazole molecules occupy most of the binding sites and the his-tagged protein is eluted in the Elution buffer. However, low concentration of imidazole (< 20mM) in the lysis or wash buffers can reduce the nonspecific binding of contaminating proteins. The buffer compositions should be adjusted for different proteins. Here is a sample protocol we used to purify Mycobacterium Tuberculosis Guanylate Kinase (TBGK). However, the modifications needed for Renilla Luciferase are specified as well.

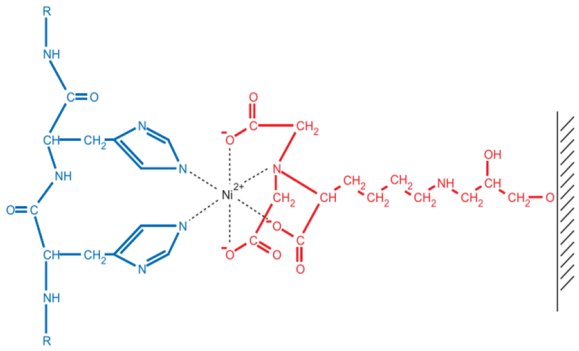

Figure 2.5: This figure is adapted from 6xHis-tagged protein purification handbook(Qiagen). Interaction between neighboring residues in the 6xHis tag and Ni-NTA matrix. Ni-NTA is colored red while the 6xHis-tag of the target protein is colored blue.

Protocol: Protein Purification using Ni-NTA chromatograph

- Preparation of cell lysate using French Press

  1. Remove the expression cells from -20 °C and thaw the cells on ice until them melt.
  2. Prepare Lysis buffer: lysozyme 10 mg, protease inhibitor cocktail (PIC) one tablet (Roche), 7 μL β-ME in 50 mM Phosphate, 100 mM NaCl buffer at pH 8.
  3. Add the Lysis buffer into cells. Swirl gently to resuspend the cells.
  4. Use a French Press to mechanically rupture the cells (consult the standard protocol for operation)

- Preparation of cell lysate using Freeze-Thaw strategy

  Note. This is an alternative method to prepare cell lysate when a French Press is not available. It has been used for obtaining GK and RLuc. It is convenient; however, it does not work for all kinds of protein.

1. Follow the previous steps 1-3.
2. Aliquot the mixture into small volumes (<15 ml).
3. Freeze the aliquots in the -80 °C freezer. Usually 10 min will be sufficient. (Or freeze them quickly on dry ice for three minutes)
4. Thaw the frozen aliquots in warm water to speed up melting.
5. Repeat steps 3-4 at least five times.

- Purification using Ni-NTA

1. Pour the lyate into spin columns with proper balancing.
2. Spin down at 15,000 rpm for 30 min and collect the supernatant.
3. In the meantime, set up a gravity column and add 2 ml of Ni-NTA resin. Discard the storage buffer and wash the resin with 20 ml Native Wash Buffer (20mM Sodium Phosphate,10 mM NaCl and 20 mM Imidazole buffer at pH 8.0)
4. Pour the supernatant into the resin column and then into a collecting tube several times until most of the Ni-NTA beads are washed into the tube.
5. Leave the supernatant at 4 °C for 1 hour.
6. Pour the supernatant back into the gravity column and collect the Flow Through (FT).
7. Wash the beads with 30 ml of Native Wash Buffer and 30 ml of Hi-salt Wash Buffer (20mM Sodium Phosphate,100 mM NaCl and 20 mM Imidazole buffer at pH 8.0).
8. Wash the beads with Imidazole Wash Buffer (IWB; 20mM Sodium Phosphate,10 mM NaCl and 50 mM Imidazole buffer at pH 8.0). A different volume of IWB is used depending on the affinity of his-tagged

protein to the Ni-beads. For GK, we use at least 5 ml of IWB. On the other hand, for RLuc, the beads are washed with 3 ml IWB and every milliliter of IWB is collected separately. The imidazole washed collection from RLuc contains much fewer impurities and can be directly used for chimera synthesis after we check its purity via gel electrophoresis.

9. Elute channel protein 7 times with 1 ml of Elution Buffer (20mM Sodium Phosphate,10 mM NaCl and 350 mM Imidazole buffer at pH 8.0). For RLuc, 3 times of 1 ml Elution Buffer is used to elute the proteins. Phosphate buffer at pH 7 is added to the elution until the final concentration of protein is less than 25 μM to prevent self-association of RLuc (see Sec. 4.1.2).
10. Store the purified protein at 4 °C.
11. Aliquot 20 μL of FT, 20 μL of NW, 10 μL of IW and 5 μL of Elution for SDS-PAGE gel electrophoresis to assess purification performance.

2.2.5 Bio-conjugation Procedures

The DNA arms are conjugated to the protein via SM(PEG)$_n$ (Pierce), which is a hetrobifunctional crosslinker with N-hydroxysuccinimide (NHS) ester and maleimide groups, allowing covalent conjugation of amino- and sulfhydryl-containing molecules (Fig. 2.6).

Polyethylene glycol (PEG) is the spacer in the crosslinker which improves the solubility and flexibility of the linker. Throughout the thesis, we use SM(PEG)$_2$, whose length is 17.6 Å unless specified otherwise. The distance between the two conjugated molecules, in this case the DNA arm and the protein, can be controlled by using crosslinkers with different numbers of PEG spacers. Both reactive groups are sensitive to the pH values of the reaction buffers, whereas the optimized pH for NHS ester is 7-9 and that for maleimide is 6.5-7.5.

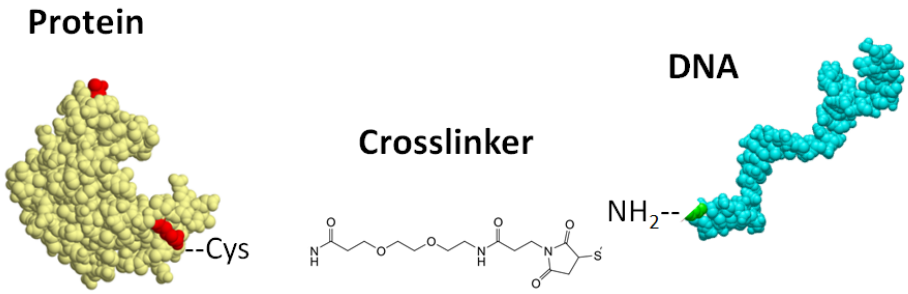

Figure 2.6: Protein-DNA conjugation through the crosslinker NHS-PEO_2-Maleimide. The amino-modified DNA arm is coupled with the crosslinker (Cx) through the NHS group. The intermediate DNA-Cx molecules are then linked to the Cysteine-mutated protein via the Maleimide group to form the protein-DNA chimera. The protein, crosslinker and DNA are not to scale.

Before the first use, $SM(PEG)_n$ is dissolved in Dimethyl sulfoxide (DMSO), divided into small aliquots and then stored at -20 °C. Minimization of exposure to moisture is required since NHS-ester group is susceptible to hydrolysis. Because the the NHS-ester group is more fragile than the maleimide group and can become inactive easily. Cross-linking of the amine-containing molecule to the crosslinker is always the first step in the conjugation processes. For two-armed (2R) protein-DNA chimera construction, end-linked amino-modified DNA arms are first incubated with crosslinkers and then passed through ion exchange column to remove extra crosslinkers. The DNA-crosslinker molecules are ready for the subsequent conjugation of DNA and protein (see Sec. 2.2.6)

2.2.6 High Performance Liquid Chromatography (HPLC)

We introduce two cysteines on the protein surface, allowing later two-armed chimera construction. However, the cysteines may form disulfide bonds between

proteins and cause aggregation as well, prohibiting the conjugation of DNA arm and the protein. To improve the conjugation efficiency, GK is incubated with 5 mM TCEP to reduce the possible disulfide bond and purified by size-exclusion column to remove TCEP before adding the DNA arm.

We measure the concentration of the freshly purified protein and mix it with the DNA-crosslinker as soon as possible. The major products in this step, besides our target one-armed chimera, are unattached protein and DNA, and two-armed (2R) chimera. For TBGK, the ratio of protein to DNA in the mixture is usually between 1.5 : 1 and 2 : 1. A higher ratio will improve the efficiency of making the target 1R chimera; however, there will be a significant amount of unattached protein as well, which is a waste. On the other hand, if the ratio is lower than 1 : 1, more two-armed 2R chimera rather than 1R chimera is produced. One-armed chimera synthesis is the most critical and delicate step, as well as the problematic step in 2R chimera construction usually. The optimal ratio of protein to DNA varies with different proteins, even with different mutants. Sometimes not only the ratio, but the concentration is important. For example, the ratio of protein to DNA during Renilla Luciferase (RLuc) DNA chimera synthesis is 9 : 1, which will be discussed in detail in Sec. 4.2.4. A sample HPLC profile of 1R purification is also shown in that section. The products collected in different fractions will need to be identified through SDS-PAGE electrophoresis to correctly collect 1R chimera [19]. The collected one-armed chimera is subsequently added with as much as e2eB arm, at least in the 1R to DNA ratio of 1 : 2. The mixture is incubated overnight at 4 °C, followed by a buffer exchange step to reduce the concentration of EDTA, facilitating the later Ni-NTA purification. The purification protocol is the same as the one in protein Ni-NTA purification except without the Imidazole wash step. The yield of two-armed chimera is then determined with SDS gel electrophoresis.

2.2.7 Ligation of Two-armed Chimera

As we will see both in GK-DNA chimera (Chapter 3) and RLuc-DNA (Chapter 4), the nick in the middle of the DNA spring (two arms hybridized with the complementary DNA) limits the mechanical stress applied on the enzyme, leading to merely a small or no effect on the enzymatic activity. The mechanisms of this feature will be discussed in detail in Chapter 5. In order to study the functional response of an enzyme to a mechanical stress, we need a stiffer spring which can be obtained by repairing the nick using DNA ligases.

We employ T4 ligase (New England Biolabs) to link the two DNA arms, facilitated by the phosphate modification of one of the arms. First, a short piece of DNA (12-18 bp), which is partially complementary to the DNA arms, is used as a splint to hold the two arms. The reaction mixture is then incubated under the conditions suggested by the manufacturer (sample protocols will be provided later). The ligation products include unligated 2R chimera, successfully ligated chimera (ss chimera), 1R chimera (by-product from the chimera synthesis) and other polymers, which will be purified through Ni-NTA chromatography to remove ligases. Because the ligated chimera is circular, we expect it has a smaller mobility under denaturing conditions than that of 2R chimera, enabling us to separate them and determine the yield using SDS gel electrophoresis. The yield is typically 0.4-0.75.

Here, we provide a sample protocol for GK-DNA chimera, which is adopted from [25]. We modify the protocol for RLuc-DNA chimera due to its low concentration ($\sim$200 nM) which will be provided in Sec. 4.2.5.

- **Ligation protocol of GK two-armed chimera** 2 μM of two-armed chimera and 2 μM of 18mer are incubated overnight with 4 unit μL^{-1} of ligase and 0.4 mg/ml BSA in the reaction buffer provided by the manufacturer at room temperature.

2.3 Measurements of Enzymatic Activity

The reaction rate is measured with the GK-NADH activity assay first used by Agarwal *et. al* [26], where the GK reaction is coupled to two other downstream reactions:

$$\begin{cases} ATP + GMP \overset{\text{GK}}{\rightleftharpoons} ADP + GDP \\ ADP(GDP) + PEP \overset{\text{GK}}{\rightleftharpoons} ATP(GTP) + \text{pyruvate} \\ 2 \text{ pyruvate} + 2 \text{ NADH} \overset{\text{LDH}}{\rightleftharpoons} 2 \text{ lactate} + 2 \text{ NAD}^+ \end{cases} \tag{2.2}$$

where PK is the pyruvate kinase catalyzing phosphoryl transfer from phosphoenolpyruvate (PEP)to ADP or GDP and producing pyruvate; LDH is the lactate dehydrogenase catalyzing the interconversion of pyruvate and lactate with concomitant interconversion of NADH and NAD^+. The consumption of ATP and GMP is therefore monitored by the decrease of NADH, whose concentration is derived from the fluorescence at 465 nm with calibrated standards (excitation at 365 nm) [19].

For each measurement the reaction mixture consisted of 100 mM Tris HCl, 100 mM KCl, 10 mM $MgCl_2$, 150 μM NADH, 0.5 mg/ml BSA, 100 mM PEP, 10 units/ml pyruvate kinase, and 13.2 units/ml lactate dehydrogenase. A final concentration of 50 nM GK chimera was added to the aforementioned mixture except GMP (or ATP). Each sample contains 45 μL of mixture and the reaction was initiated with 5 μL GMP (or ATP).

CHAPTER 3

Probing Mechano-chemistry of Guanylate Kinase

Using DNA molecular springs to mechanically perturb enzymes and then measure their enzymatic responses may be the most direct way to investigate mechano-chemical coupling in enzymes.

In the previous work we observed that the enzyme stressed by the DNA spring showed a decrease in enzymatic activity. However, the enzyme could not be "turned off" completely. In Chapter 1 we estimated that the elastic energy provided by the DNA spring was $\sim$10 k_BT and injecting a 10 k_BT energy into a $\sim$100 amino-acids protein is sufficient to deform it. This brings out the question of why the elastic energy provided by the DNA spring is large while the effect on the enzymatic activity is comparably small? In other words, how is the elastic energy partitioned in the chimera?

In the beginning of the chapter, we compare the elastic energies in two different protein-DNA chimeras, leading to the conclusion that the DNA spring is the softer part. Then, we use the DNA spring to exert stresses at three different specific locations on the enzyme Guanylate Kinase, and for each case determine the changes in substrate binding affinities and catalytic rate. We discover that the enzyme kinetics parameters can be affected separately, depending on where the mechanical stress is applied. For one chimera the applied stress mainly affects the catalytic rate k_{cat}, for another it mainly affects the binding affinity of the substrate GMP. The anisotropic response of GK shows that the mechanical stress

does not only bias the population of the folded and unfolded states of the enzyme. Instead, it is a way to access many intermediate states in the equilibrium situation. This result also leads us to start thinking about continuum mechanics models to describe our chimera system, which motivates our work in Chapter 5.

At the end, we provide a new configuration of the protein-DNA chimera, where multiple DNA arms are attached to one protein and multiple DNA springs can form when introducing the complementary DNA. Though this multi-spring structure fails to apply a sufficiently large stress on the enzyme to turn off the enzyme completely, it may be used to design a self-assembly macrostructure.

3.1 Introduction

3.1.1 Mechanical Chemical Coupling in Enzymes

The coupling of mechanical motion with a chemical reaction is one remarkable feature of enzymes. For example, motor proteins transduce a chemical reaction into directed motion. Allostery and induced fit mechanisms are more general examples of conformational changes (static or dynamic [22]) regulating chemical reactions and molecular recognition events. Beyond the structural characterization of mechano-chemical coupling, a thermodynamic description is lacking, in terms of the forces required to affect the chemical reaction catalyzed by the enzyme. The most direct method to experimentally explore mechano-chemical coupling is to affect the conformational change of an enzyme mechanically and measure its enzymatic response. To follow this concept, we use a DNA "molecular spring" [16, 23, 27] to apply such a mechanical stress at specific locations on the surface of an enzyme and measure the effect on the catalysis. A DNA spring is in principle a general tool to alter enzymatic activities and to probe protein properties. However, to date most of our work has been done on the enzyme Guanylate Kinase (GK), which is also the sample protein explored in this chapter.

3.1.2 Conformation-Catalysis Relation in Guanylate Kinase

Guanylate Kinase catalyzes phosphoryl transfer from ATP to GMP and releases ADP and GDP as products. The conformational transition from the "open" to the "closed" state characteristic of NMP kinases is driven by substrate binding [4] and is a well-known example of induced fit though it is not an allosteric enzyme. It consists of three domains, which are LID, CORE and GMP binding domain. (Fig. 3.1) The CORE domain carries the P-loop, which is an essential motif associated with the phosphate transfer between substrate ATP and GMP. In most of the studies in this chapter, we use the GK from *Mycobacterium tuberculosis* (TBGK). We also use yeast GK to construct a multi-armed chimera, which is discussed in Sec. 3.5.

3.1.3 Three Stress Application Schemes

We mutated the two internal Cysteins (at positions 40 and 193) of the wild type to Ser in order to be certain of the specificity of the DNA spring attachment points and we expressed three different mutants of this molecule, each with a pair of Cys substitutions (which are thus the only Cys in the molecule). In the following, we refer to these three molecules as the 75/171, 40/171, and 40/130 mutants, respectively, where the numbers indicate the residues which were substituted to Cys. The locations of these residues are indicated in Fig. 3.2. We synthesized the corresponding 3 protein-DNA chimeras, and for each one we determined, in the presence and absence of mechanical stress (i.e. with the DNA spring hybridized or not hybridized), the binding affinities for the two substrates (GMP and ATP) and the catalytic rate.

For GK, the kinetic parameters are the binding affinities for ATP ($1/K_A$) and GMP ($1/K_G$) and the catalytic rate k_{cat}. The three pairs of points where we apply the mechanical stress (Fig. 3.2(b)) were chosen by the following qualitative

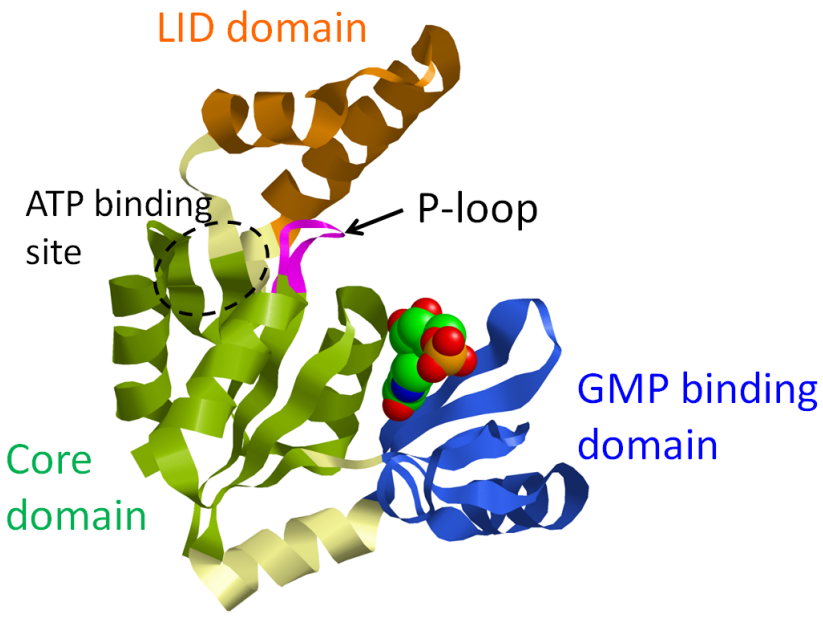

Figure 3.1: Crystal structure of Guanylate Kinase from Mycobacterium tuberculosis (PDB structures 1ZNX, bound with GMP). The CORE domain is colored green while the LID and GMP binding domain are colored orange and blue, respectively. GMP is shown in space-filling spheres. P-loop is in pink, which is an essential motif associated with the phosphate transfer between substrate ATP and GMP. Large conformational change occurs upon binding the substrate GMP.

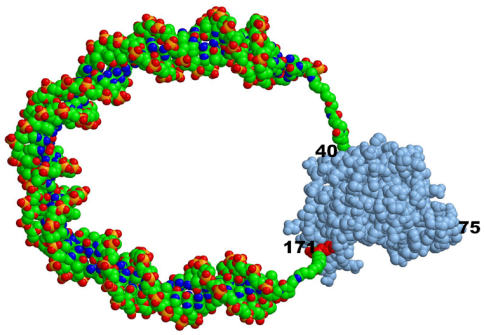

(a)

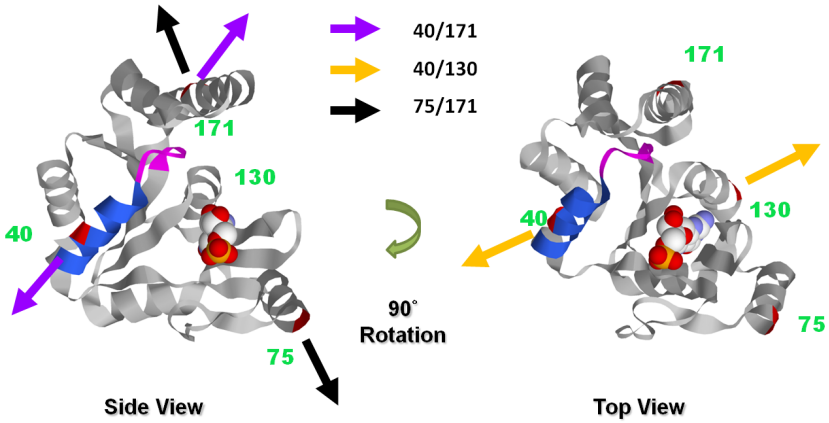

(b)

Figure 3.2: (a) Cartoon of a protein-DNA chimera with the DNA spring attached at the sites 40/171. The protein (Guanylate Kinase) is from the PDB structure 1ZNX, the DNA is from the nucleosome structure 1KX5. Protein and DNA (60 bp) are drawn approximately to scale. The distance between residues 40 and 171 is $\sim$ 2.7 nm.

(b) The GK structure (1ZNX) with bound GMP (shown in the spacefill representation); the four separately modified sites (residues 40, 75, 130 and 171) are colored red, the p-loop is shown in pink, and the α-helix connecting the p-loop is blue.

considerations. For the 75/171 mutant, the applied stress works against the open to close conformational change of the two lobes of the molecule. Since this conformational change is driven by substrate binding, we reasoned by Le Chatelier's principle that the mechanical stress would lower the binding affinity of one or both substrates. For the 40/171 mutant, the mechanical stress pulls on an α-helix which, at the other end, connects to the p-loop, a conserved motif essential for catalysis in this class of kinases. We reasoned that if the helix moves as a whole as a result of pulling along its axis, we would affect the p-loop and thus the catalytic rate k_{cat}. Alternatively, the stress might specifically affect the ATP binding site and thus K_A. In the 40/130 mutant we pull on the same spot of the same helix (i.e. at position 40), but in a different direction (sideways with respect to the axis of the helix).

3.2 Enzymatic Inhibition by Mechanical Perturbation

We measure the enzymatic inhibition for 40/171 and 75/171 chimera hybridized with varying length of complementary DNA l (Fig. 3.3). When the contour length of the ds DNA spring is smaller than the distance of the protein plus two crosslinkers (in this case, l <30 bp), there should be no or very little mechanical stress from the molecular spring. When l becomes longer, the ds part has to be bent eventually and thus exert an increasing force on the enzyme, expected to induce bigger changes in enzyme catalysis.

In the case with a nicked DNA spring, the results of 40/171 and 75/171 are very different. For 40/171 chimera, the evolution of the enzymatic activity for increasing hybridization length l is rather flat, indicating that the stress is not sufficient to significantly perturb the enzyme. On the other hand, an activation is observed on 75/171 chimera. This activation effect is dependent on the attachment sites and the DNA sequences as reported in [19]. It may be associated with the

interference between the arm DNA (in ss form) and the enzyme, which vanishes when the DNA is removed from the enzyme surface upon hybridization. After repairing the nick in the DNA by ligation (see Sec. 2.2.7), both 40/171 and 75/171 exhibit a considerable repression on the enzymatic activity.

From the measurements we conclude:

1. With a nick in the middle of the spring, there exists no or an undetectable effect on the enzymatic reaction due to the mechanical perturbation.

2. When repairing the nick, the enzymatic inhibition is drastic in both 40/171 and 75/171.

These bring up our questions of interest:

1. Why is there such a big difference when repairing the nick of the DNA spring given that we know that repairing the nick does not stiffen the DNA very much? (Discussed in Chapter 5)

2. Does the mechanical stress on 40/171 and 751/171 affect the enzymes in the same way? How do the kinetic parameters, such as substrate binding and reaction rate, change? (Discussed in Sec. 3.4)

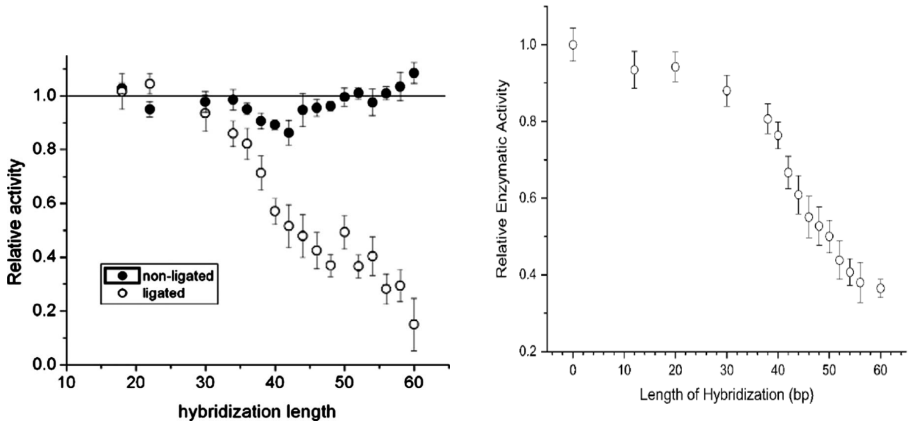

(a) (b)

Figure 3.3: Relative activity vs hybridization length (in bp). (a) For 40/171 chimera, before ligation (filled circles) and after ligation (open circles). The ligated curves are corrected for the yield of ligated chimeras measured from a gel. (b) For 75/171 chimera. The configuration of this chimera used here is one 60 bp ss DNA attached to the specific sites on the protein surface by two ends (a doughnut chimera) (see Sec. 2.1.3). This figure is adapted from [17].

3.3 Elastic Energy Partitioning in GK-DNA Chimeras

3.3.1 Elastic Energy Driven Polymerization

Upon hybridization with complementary DNA, the DNA spring rigidifies and has to bend for having the same end to end distance (EED) as the protein, introducing elastic energy in the system. However, monomer (one chimera coupled with one cDNA) is not the only possible configuration. To release the elastic energy, dimer and other polymers will form as well since in these molecules the ds DNAs are straight and relaxed. (See Fig. 3.4) On the other hand, forming polymers entails entropic cost and is less favored when the entropic cost is higher than the elastic energy reduced. These two factors compete with each other until equilibrium is reached. Considering the equilibrium between monomers and dimers, the essential components of the chemical potentials are, respectively:

$$\begin{cases} \mu_M = F_{el} + k_B T \ln(X_M) \\ \\ \mu_D = k_B T \ln(X_D) \end{cases} \tag{3.1}$$

where F_{el} is the elastic energy of monomer, $k_B T \ln X$ is the chemical potential of a dilute solution associated with chimera concentrations: X_M the molar fraction of monomer and X_D the molar fraction of dimer. Two monomers make one dimer, thus the equilibrium condition is:

$$2\mu_M - \mu_D = 0 \tag{3.2}$$

So from Eq. 3.1 and Eq. 3.2 we obtain:

$$2F_{el} = k_B T \ln\left(\frac{X_D}{{X_M}^2}\right) \tag{3.3}$$

Experimentally, the monomers and dimers are separated using electrophoresis technique and then X_M and X_D are determined based on the intensities of the corresponding band.

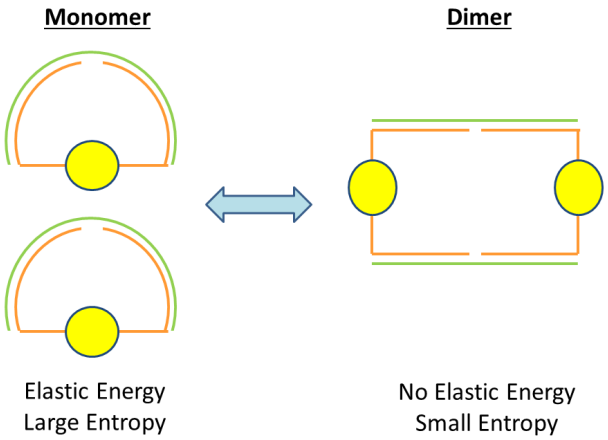

Figure 3.4: Schematic of polymerization process. Forming dimers will release the elastic energy in the monomers, however, it will reduce the entropy as well. The equilibrium population of monomer and dimer is a balance between these two factors.

3.3.2 A Simplistic Elastic Model of GK-DNA Chimera

The elastic energy measured using Eq. 3.3 is contributed from both the protein and the DNA. Either of them is not a simple molecule and the coupling of both makes it difficult to understand how the enzyme responds to the energy residing in it. Our first step is to ask the question: how is the elastic energy partitioned between the protein and the DNA? This is equivalent to asking whether the DNA or the protein is stiffer. To see this, consider two springs with spring constants K_1, K_2 and relaxed end-to-end distances (EEDs), X_1, X_2 (Fig. 3.5). If the springs are now constrained to have the same EED, the systems elastic energy is

$$E = E_1 + E_2 = \frac{1}{2}(X_1 + X_2)^2 \frac{K_1 K_2}{K_1 + K_2}$$

and the ratio of the energies in the individual springs is $E_1/E_2 = K_2/K_1$, which means that more energy resides in the softer spring.

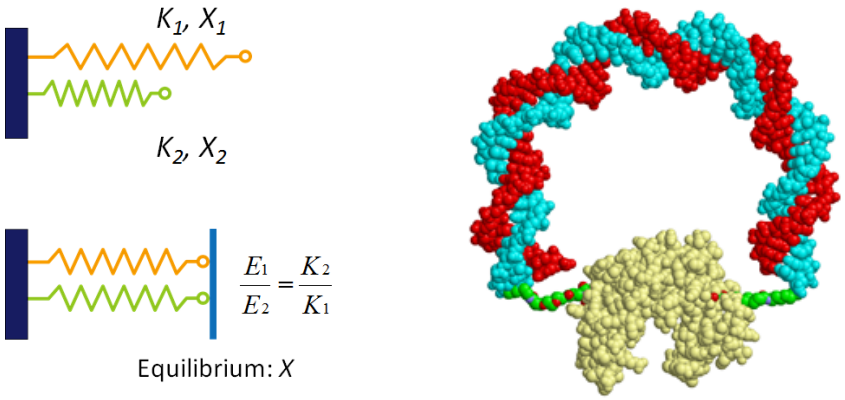

(a) (b)

Figure 3.5: Two coupled springs. (a) Two coupled springs in parallel with spring constants K_1, K_2 and relaxed end-to-end distances (EEDs), X_1, X_2. When they are constrained to have the same EED X, the energies in the individual springs is inversely proportional to the spring constant. (b) Two coupled nonlinear springs consisting of a bent DNA and a stretched protein. In analogy to (a), more elastic energy resides in the softer spring.

3.3.3 Results

To find out whether the DNA or the protein is stiffer, we examine F_{el} for two different chimeras, where the DNA springs are attached on residues 40 and 171, 75 and 171, respectively. The distance between residue 40 and 171 is $\sim$ 2.7 nm while that between 75 and 171 is $\sim$ 3.8 nm. In addition, in 75/171 the applied force works against the open to close state upon the GMP binding while in 40171 the applied force is expected to alter the p-loop (see Sec. 3.1.3). Therefore, in these two cases, the proteins are in principle different springs while the DNA springs are identical. This indicates that if the F_{el} of the two chimeras are very different, the protein is the softer part, otherwise DNA is softer.

Fig. 3.6 shows a gel picture of the monomer-dimer equilibrium for the two mutants, for l=58 bp, the length of the complementary DNA hybridized to the chimera. The amount of dimers is similar for the two mutants, so the elastic energy is almost the same. Quantitatively, we find

$$\Delta F_{el} = F_{el}(75/171) - F_{el}(40/171) \approx 0.4 \pm 0.2 k_B T$$

and $F_{el} \approx 9.2 \pm 0.2 k_B T$ [18].

These values are averaged over several experiments and hybridization lengths l, for $42 < l < 60$ (the elastic energy vs is flat in this region); the quoted errors are the corresponding standard deviation.

From this result we infer that the DNA is the softer part and most of the elastic energy resides in it.

To make progress, we need a better understanding of at least one of the spring. Qu el al. studied in detail the bending behavior of a short piece of DNA and determined an analytic expression for the bending energy of the DNA [28, 29, 30]. This new understanding allows us to study the energy partition between the DNA and protein and to investigate the dynamics of these molecules more (see Chapter 5).

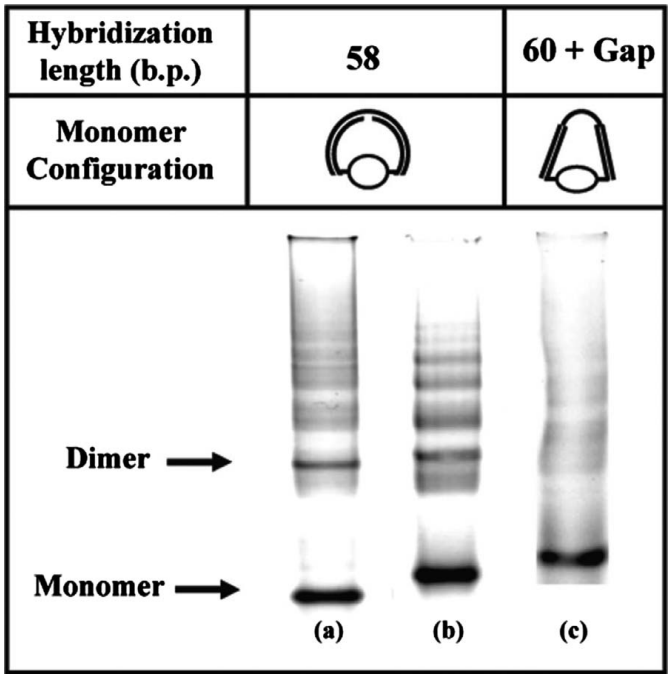

Figure 3.6: Gel electrophoresis of a sample of hybridized chimeras, showing monomer and dimer bands, as indicated. For lane (a), the measured concentrations were 0.13 μM and 0.030 μM for monomers and dimers, respectively. Lane (a) is the 75/171 chimera, lane (b) is the 40/171 chimera, both constructed with the same 60mer DNA and hybridized to the 58mer complementary. Lane (c) is a control: the same chimera of lane (b) is hybridized with a 68mer such that the 8 bases in the middle are unpaired. This relaxes the elastic energy and correspondingly dimers and higher-order polymers disappear.

3.4 Anisotropic Responses of GK to Mechanical Stresses

Now we know that DNA is the softer part in the chimera and the elastic energy in the molecule is $\sim 9\ k_BT$. In addition, the enzymatic activity decreases with increasing mechanical stress (see Sec. 3.3).

Next question, how does the enzyme respond to stresses in different directions? Can the kinetic parameters be affected separately? To explore the enzymatic response of the enzyme under stress in different directions, we attach the same DNA molecular spring in turns to three different locations (40/171, 75/171, 40/130) on the surface of the enzyme of Fig. 3.2(b), and the effect of the mechanical stress on substrate binding and catalytic rate is measured.

3.4.1 Michaelis-Menten Mechanism and Analysis

In order to understand how the kinetics of GK is affected by different mechanical perturbation, we perform GMP and ATP titration experiments, where the Michaelis-Menten constants K_G, K_A for the two substrates GMP and ATP, and the catalytic rate k_{cat} are measured. Each titration curve is obtained for the two cases: in the presence and absence of mechanical stress, for the same chimera sample. The measurements in the absence of stress are obtained from the ss protein-DNA chimera, the measurements under stress from the chimera hybridized with the complementary 60mer.

The three parameters K_G, K_A, k_{cat} are measured within the Michaelis-Menten (MM) description, where the rate of producing ADP (and GDP) is given by:

$$\frac{d}{dt}[ADP] = \frac{[E]k_{cat}}{\left(1+\frac{K_A}{[A]}\right)\left(1+\frac{K_G}{[G]}\right)} \tag{3.4}$$

where [E] is the total enzyme concentration, [G] and [A] are the equilibrium concentrations of GMP and ATP. At short times, [ADP](t) $\propto$ t and the slope S of this relation is the RHS of Eq. 3.4 with the initial values of the substrates' concentra-

Table 3.1: The kinetic parameters K_A, K_G, k_{cat} measured for the three different GK chimeras in the presence (hybridized without nick) and absence (unhybridized or hybridized with nick) of mechanical stress. The uncertainty reflects the standard deviation over 4-6 measurements.

Mutant	**040171(M1)**			**040130(M2)**			**075171(M3)**		
	K_A	K_G	k_{cat}	K_A	K_G	k_{cat}	K_A	K_G	k_{cat}
unhybridized	1400 ±149	243 ±37	9.6 ±0.6	739 ±50	221 ±33	9.3 ±0.5			
hybridized with nick							2304 ±365	137 ±9	10.9 ±1.6
hybridized without nick	1301 ±108	186 ±33	6.4 ±0.3	620 ±57	173 ±16	8.8 ±0.5	2072 ±270	195 ±10	9.2 ±0.8

tions, $[G]_0$ and $[A]_0$. The speed S of the reaction is measured with the GK-NADH activity assay (see Methods). Thus to extract K_A, K_G and k_{cat}, we use the form:

$$S = P_1/(1 + P_2/X) \tag{3.5}$$

to fit the titration curves, where P_1 stands for $k_{cat}[E]/(K_G/[G]_0 + 1)$ (or $k_{cat}[E]/(K_A/[A]_0 + 1)$), P_2 for K_A (or K_G), X for $[A]_0$ (or $[G]_0$), in ATP and GMP titrations, respectively. For example fitting the plot of S vs $[G]_0$ to the form (3.5) one extracts K_G and [E] k_{cat} ; knowing [E] we also obtain k_{cat}. Some titration curves are displayed in Fig. 3.7. The results of these measurements are summarized in Table. 3.1, where the parameters listed are directly from the titration measurements, without taking into account the yields of the correct chimeras.

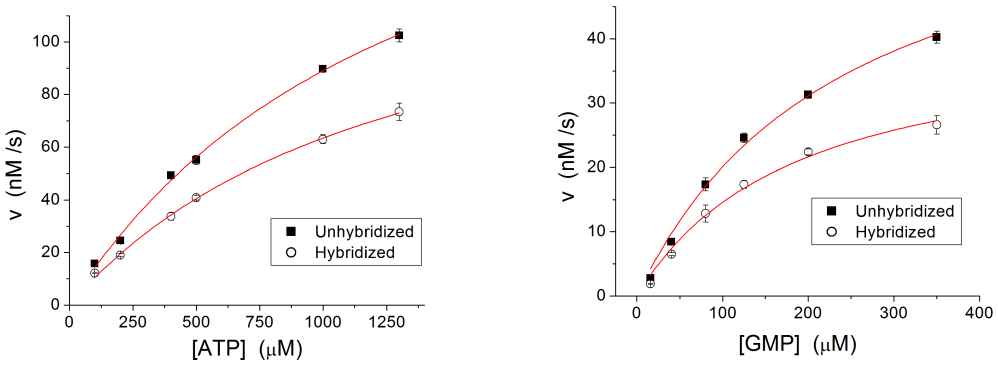

(a)

(b)

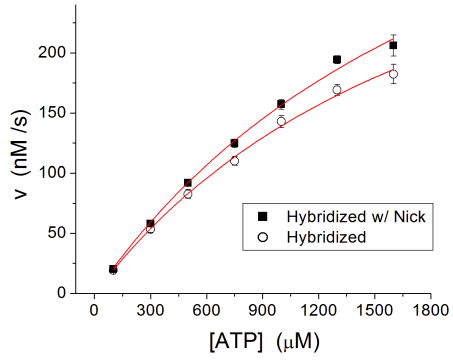

(c)

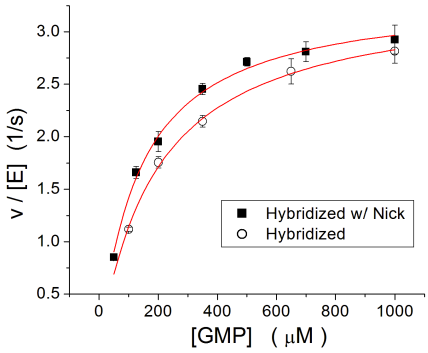

(d)

Figure 3.7: ATP and GMP titration curves (reaction rate vs. initial substrate concentration) for the 40/171 chimera, unhybridized (solid squares) and hybridized to the complementary 60mer (open circles). The curves are fits to the experimental data points using Eq. 3.5. Every data point is the average of 4-6 measurements and the error bar is the standard deviation.

(a) GMP titration experiments. Enzyme concentration 21 nM, ATP concentration 0.5 mM. (b) ATP titration experiments. Enzyme concentration 25 nM, GMP concentration 2 mM.

3.4.2 Experimental Results

For the 40/171 mutant we find that the mechanical stress has the effect of decreasing the catalytic rate k_{cat}, while there is little or no effect on K_G and K_A (Table. 3.1). Here we are comparing the chimera hybridized to the complementary 60mer with the unhybridized (ss) chimera (we do not detect "non-mechanical" effects for this chimera, see Fig. 3.10). The result is consistent with the qualitative hypothesis of the beginning, that pulling on the α-helix connected to the p-loop would affect the catalytic rate. Contrary to the next case below, here the application of the mechanical stress is not designed to take advantage of a structurally recognized "hinge". Under stress, the catalytic rate is decreased by a factor ~ 0.67; factoring in the yield $p \approx 0.51$ for this sample, we obtain $k_{cat}^{ds}/k_{cat}^{ss} \approx 0.36$ (Fig. 3.8).

For the 75/171 mutant we find a similarly specific response to the mechanical stress, which now has the effect of decreasing the binding affinity for GMP (increasing the MM constant K_G), while it has little or no effect on K_A and k_{cat}. Here we are comparing the chimera hybridized to the complementary 60mer with the chimera hybridized to two separate complementary 30mers, i.e. the latter configuration has a nick in the middle of the molecular spring, which reduces the mechanical stress to the extent that there is no effect on the protein [20, 19]. We use this reference configuration in order to subtract the "non-mechanical" effects, as explained above. The apparent binding affinity for GMP is reduced by a factor ~ 0.7, and factoring in the yield $p \approx 0.42$ for this sample (see gel of Fig. 3.9), we find $K_G^{ss}/K_G^{ds} \approx 0.4$ (Fig. 3.8). This result is consistent with our previous measurements reported in [17]; we performed these measurements again because this is a slightly different molecule compared to the one in [17], lacking the two internal Cys.

Finally, for the 40/130 mutant the mechanical perturbation has essentially no effect on any of the three parameters. Here again we compare hybridized and

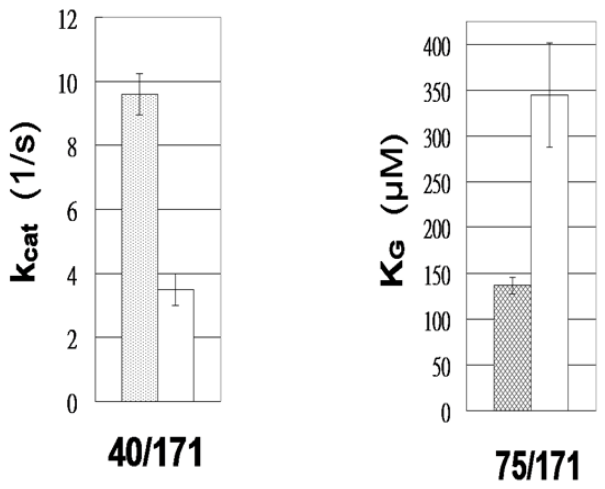

(a)

Figure 3.8: Main effects on the kinetic parameters by the mechanical stress in different directions, factoring the yield. (a) For 040/171, the catalytic rate k_{cat} decreases ($k_{cat}^{ds}/k_{cat}^{ss} \approx 0.36$) while there is little or no effect on K_A and K_G. (b) For 75/171, the apparent binding affinity for GMP is reduced ($K_G^{ss}/K_G^{ds} \approx 0.4$) while it has little or no effect on K_A and k_{cat}. For 40/130, the three parameters are essentially unaffected.

unhybridized chimera; although some "non-mechanical" effects are present in this case (see Fig. 3.10), the end result is that changes in the parameters in this case, if present, are within experimental error.

3.4.3 Corrections from Yield and Non-specific Effect

For the final quantitative analysis, there are two correction factors to be considered. One is the yield of correctly constructed chimeras. This we measure by gel electrophoresis, where the different species are distinguished by their different electrophoresis mobilities. The final yields in our samples are of order $\sim 50\%$.

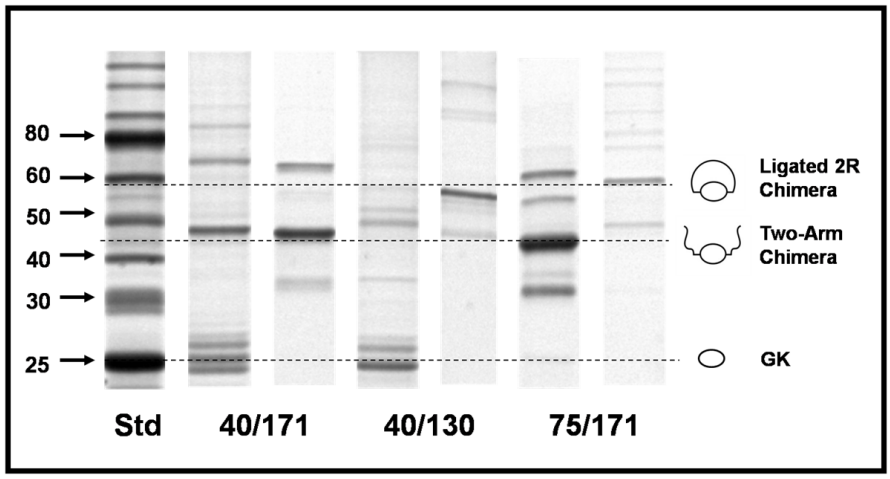

Figure 3.9: Gel Electrophoresis of different mutants (*) and their unligated(**) or ligated(***) chimeras.The cartoon above each lane illustrates schematically the different construction. The different lanes are: (a) Protein molecular weight standard (25-80 kDa, as indicated). (b) 40/171 mutant of GK (the band at 45 kDa corresponds to disulfide bond induced protein dimers) (c) 40/171 two-armed chimera (d) 40/130 mutant of GK (e) 40/130 ligated two-armed chimera (f) 75/171 two-armed chimera (g) 75/171 ligated two-armed chimera Yields of correct constructions (ligated two-armed chimeras) are determined from these gels.

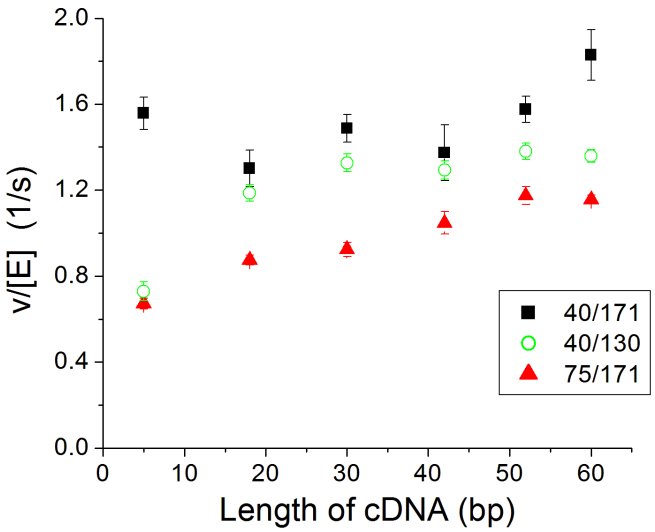

Figure 3.10: Reaction rates of the two-armed chimera (normalized by the chimera concentration) vs. length of cDNA for the 40/171 (filled squares), 40/130 (open circles), and 75/171 (filled triangles) chimeras. Initial substrates concentrations were $[\mathrm{GMP}]_0 = 200\ \mu\mathrm{M}$ and $[\mathrm{ATP}]_0 = 500\ \mu\mathrm{M}$.

The other concerns certain "non-mechanical" effects of the DNA spring on the enzyme, which are present for some chimeras. The mere presence of the DNA, in the absence of mechanical stress, generally does not perturb the enzyme kinetics significantly, and moreover, when such "non-mechanical" effects are present they can be distinguished from the effects of stress. This we established through control experiments where the chimera DNA is removed using DNase [16], or a second DNA strand is brought in but in a stress-free configuration (see [19] and Fig. 3.10). In some cases, the DNA spring in the ss form can partially inhibit the enzyme, possibly by partially occluding the active site. The inhibition is lifted by partial hybridization of the DNA; in this state, mechanical effects are not present because the stress is too small, so in this case this is the reference state to which we compare the stressed (fully hybridized) molecule. We have documented this correction extensively in previous work [19].

In Fig. 3.10 we show the results from control experiments designed to evaluate the "non-mechanical" effects of the DNA on the enzyme.In these experiments, the non-ligated chimera is hybridized with complementary DNA of varying length, such that in all cases there is a nick or ss gap in the molecular spring; in this configuration there is no stress. For the 40/171 chimera, the curve is essentially flat. For the 75/171 chimera the activity increases gradually with the length of cDNA, therefore in Table. 3.1 we use the hybridized nicked chimera as the reference state. For the 40/130 chimera there is a jump in activity after hybridization, independent of the cDNA length. Ideally we should compare to a partially hybridized reference state in this case, but we do not have those measurements. However, from the ATP titration curves, which are identical for this mutant in the hybridized and unhybridized state, we know there is no effect on K_A and k_{cat}. Considering the activation effect seen in Fig. 3.10 and the measurements of Table. 3.1 for this chimera we conclude that if there is a small effect of the mechanical stress on K_G, it is within experimental error.

3.4.4 Concluding Remarks

To summarize, for the 40/171 chimera we find that only k_{cat} is affected (decreased) as a result of the mechanical stress; for the 75/171 chimera only K_G is affected (increased, corresponding to a lower binding affinity for GMP); for the 40/130 chimera there is no effect on k_{cat} and K_A, and either no effect or only a small effect on K_G.

With respect to the wild type GK, the mutagenesis involved in preparing the different chimeras does alter the kinetic parameters, but not drastically. Removing the internal Cysteines results in a lowering of ATP binding affinity of about a factor 3. The differences in parameters between the three double-Cys mutants are smaller and in fact almost within our precision in determining the absolute values of the parameters. Thus we can say that the above experiments with the DNA spring are performed on molecules which are structurally intact and essentially identical.

Overall, the effect of the mechanical stress as applied here is small: factors of 2 or 3 changes in substrates' binding affinities and catalytic rate. Thus we must be deforming the structure very little. One main finding of this study is that a mechanical stress applied by pulling at two spots on the surface of the enzyme can affect the (static or dynamic) conformation of far away residues in between the pulling spots. This is not a priori obvious, another possible scenario being that the DNA spring pulls out a short piece of the polypeptide chain while the conformation of the rest of the structure remains unchanged.

3.5 Another New Molecule: Multi-armed Chimera

A DNA spring is conceptually a general method to study the dynamics of proteins by providing a nondestructive stress to modulate enzymatic activity. However, we are unable to completely shut down the activity of any of the GK-DNA chimeras

because the DNA spring is too soft compared to the protein. Since one spring is not sufficient to turn off the enzymatic activity completely, multiple springs might provide a satisfactory overall stress to inactivate the enzyme. In other words, a multi-armed chimera, which allows the formation of multi-springs, might be a biomolecule which can be switched "on" or "off" in the presence of the trigger, in this case the complementary DNA. We constructed a multi-armed chimera to test our conjecture, nevertheless, we find that this multi-armed chimera cannot be switched "on" and "off".

Despite the fact that the multi-armed chimera is not the solution to turn off enzymatic activity, it provides an opportunity to construct a Protein-DNA chimera lattice, where a chimera serves as a single tile to construct an organized macrostructure.

3.5.1 Selecting Yeast GK as a Sample Protein

Our method to synthesize Protein-DNA chimeras is to attach the DNA arms on specific Cys-mutated sites on the protein via crosslinkers. However, it is impractical to substitute several amino acid residues on the protein surface to Cysteines not only because it is difficult but also because it may cause serious aggregation due to the formations of disulfide bond between Cysteines. Instead, we used the inverse strategy of synthesis of two-armed chimera, namely, crosslinkers were conjugated to the protein via a primary amine-NHS ester reaction and to the DNA arms via a maleimide (sulfhydryl-targeted) reaction. Due to this requirement, we selected yeast GK as our sample enzyme. Yeast GK has 19 Lysines, which is an amino acid having primary amine, and 15 of them are on the surface, accessible to the crosslinkers for conjugation (Fig. 3.11).

Compared with TBGK, yGK has a larger conformational motion upon binding of GMP. It also has a much higher reaction rate k_2 [31]. Table 3.2 lists a brief comparison between TBGK and yGK.

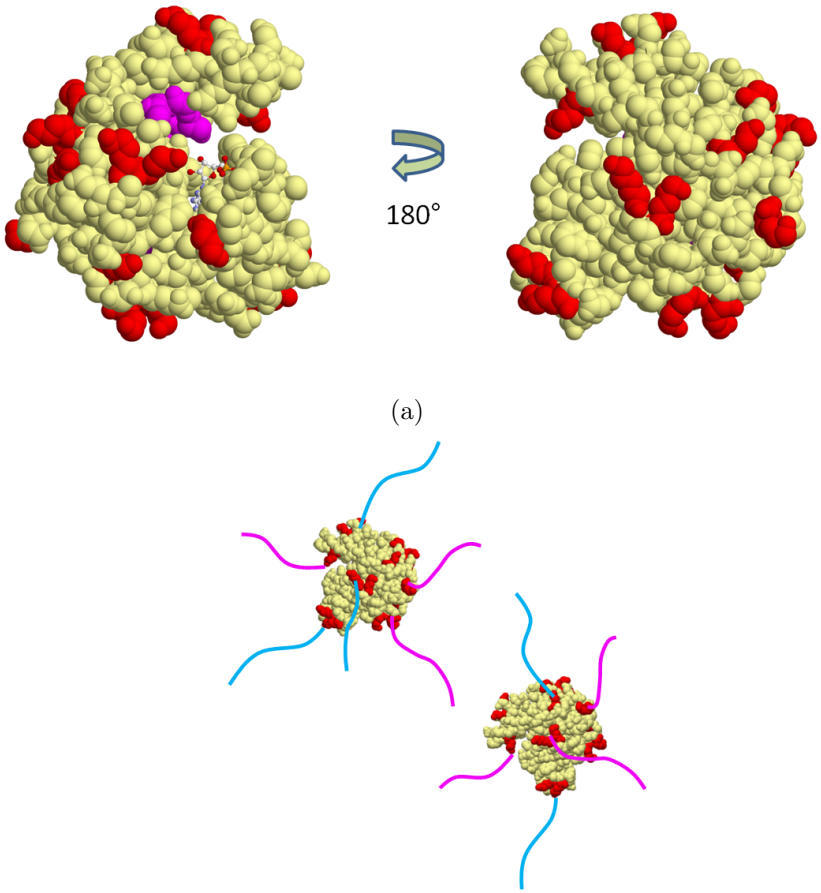

Figure 3.11: (a) Both surfaces of the crystal structure of yeast Guanylate Kinase (yGK) from PDB:1EX7. From one view, the substrate GMP (displayed ball-and–stick) can be visualized. All Lysines on the yGK surface, which are available for later DNA arm conjugations, are colored red. 15 out of 19 Lysines are found on the surface. (b) Cartoon of multi-armed chimeras.

Table 3.2: Kinetic parameters of Guanylate Kinase from *Mycobacterium Tuberculosis* (TBGK) and Yeast (yGK). The parameters are from [30].

	TBGK	**yGK**
Forward reaction (Formation of ADP and GDP)		
$K_{ATP}(\mu M)$	237	204
$K_{GMP}(\mu M)$	80	91
$k_{cat}(s^{-1})$	23	394
Backward reaction (Formation of ATP and GMP)		
$K_{ADP}(\mu M)$	137	17
$K_{GDP}(\mu M)$	98	97
$k_{cat}(s^{-1})$	17	90

3.6 Synthesis of Multi-armed yGK Chimeras

3.6.1 Attachment of Crosslinkers to yGK

To test the efficiency of attaching a crosslinker to yGK, yGK was incubated with the crosslinker for different periods of time and then fresh crosslinkers added every 30 minutes. yGK is incubated with crosslinkers for 30 minutes, 2.5 and 3.5 hours. The yield of crosslinker attachment was checked by gel electrophoresis, showing that 3.5 hours is sufficient for the crosslinkers to saturate the attachment points (Lysines) on the protein. (Fig. 3.12)

3.6.2 Preparation of DNA Arms

The thiol-modified DNA arms purchased from IDT are in the protected form with the disulfide linkage intact to minimize the potentials for oxidation, which results

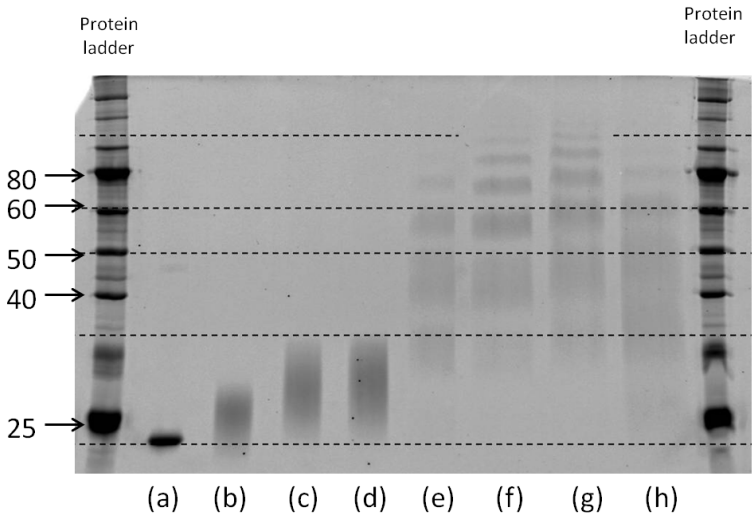

Figure 3.12: Gel electrophoresis of yGK, yGK-Cx and 1R chimeras. The different lanes are: (a) yGK protein, (b)-(d) yGK attached to crosslinkers and (e)-(h) yGK coupled to DNA arm A via crosslinkers. To test the efficiency of attaching the crosslinker to yGK, yGK was incubated with crosslinker for different periods of time and then additional crosslinker was added every 30 minutes. yGK was incubated with crosslinkers for (b) 30 minutes, (c) 2.5 hours and (d) 3.5 hours. Using the yGk samples with crosslinkers, (e)-(h) show the coupling of yGK and DNA arms with different ratio and incubation times. (e) and (f) were sample (b) subsequently mixed with arm A for 4.5 hours in the ratio 1 : 2 and 1 : 4, respectively. (g) and (h) were sample (c) subsequently mixed with arm A in the ratio of 1 : 4 for 100 and 40 minutes, respectively.

in the formation of dimers. Before incubation with the yGK-crosslinker (yGK-Cx), the DNA arms are incubated with 30 mM TCEP for reduction and then purified through HPLC ionic-exchange column to remove the TCEP. Once both arms are prepared, they are added to yGK-Cx as soon as possible with a desired protein-DNA ratio. Old DNA will form disulfide bonded dimers, unable to link to the protein.

3.6.3 Multi-armed Chimera with Two Types of Arms

We mix the same amount of arm thiol-A-25 and arm thiol-B-25 to the protein using different protein to DNA ratios and the mixture is incubated for 3 days to maximize the number of linkage. The final products are identified using gel electrophoresis. Fig. 3.13 is a gel picture of yGK coupled with various numbers of DNA arms, varying from 4 to 12.

3.6.4 Multi-armed Chimera with the Same Type of Arms

We also construct the chimera using the same type of arms. Namely, yGK is coupled with only A arms or only B arms. These chimeras may be a potential material to design a Protein-DNA lattice (see Sec. 3.8.2).

3.6.5 Ligation and Purification of Multi-armed Chimeras

We adopt and modify the Ligation protocol in Sec. 2.2.7 for NR-chimeras. The reaction conditions are: 300 nM of NR-chimera, 1.3 units of T4 ligase, 1 μM of 18mer as a splint, 0.2 mg/ml of BSA in buffer recommended by the manufacturer. The mixture is incubated overnight at 16 °C to ensure a sufficient efficiency.

After one night incubation, the sample is passed through an HPLC ionic-exchange column to collect only chimeras. However, there is neither any method to determine the efficiency of the ligation nor any way to separate the successfully

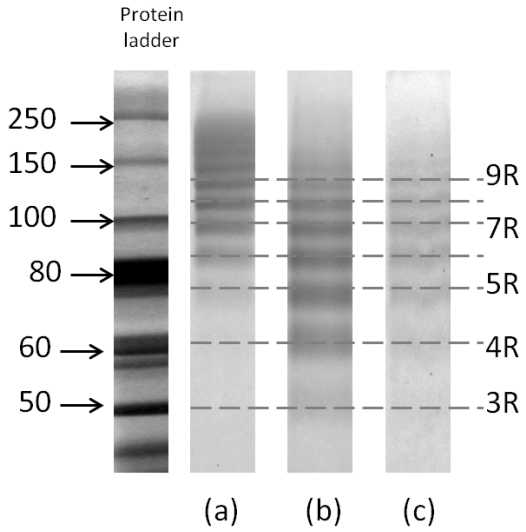

Figure 3.13: Gel electrophoresis of yGK coupled with different numbers of DNA arms. yGK was incubated with DNA arms at different ratios for 3 days at 16 °C and then the products of yGK attached to different numbers of DNA arms were separated and identified using gel electrophoresis. The lanes show: (a) the result of yGK incubation with A-thiol-25 and B-thiol-25 DNA arms in the ratio of 1 : 8 : 8; (b) and (c) are yGK incubation with A-thiol-25 and B-thiol-25, respectively, in the ratio of 1 : 8.

ligated chimeras. In addition, chimeras having a different number of DNA arms cannot be separated. Fig. 3.14 shows an HPLC profile, where chimeras with more DNA arms tend to be eluted later though there is no clear cut method for separation. However, this process is not optimized and there may be a better method to obtain a purer collection of chimera with a certain number of arms.

3.6.6 A Sample Protocol

Below is the example protocol, which has not been optimized.

1. Add 5 mM TCEP to Yeast GK ($\sim$ 100 μM) and incubate for 40 min. The mixture is subsequently purified through an HPLC size-exclusion column. The eluted yGK is in sodium phosphate buffer at pH 7.25.

2. Add crosslinkers to yGK ($\sim$ 10 μM) in a ratio of 1:200. Every 30 min, the same amount of fresh crosslinkers are added to the mixture to ensure the maximum efficiency in linkage. The total incubation time is 3 hours.

3. The mixture is then passed through another HPLC size-exclusion column to remove extra crosslinkers. The products are yGK conjugated with different numbers of crosslinkers, noted as yGK-Cx. (Fig. 3.12)

4. Arm DNA is reduced by TCEP for 30 min in the condition : 5 μM DNA and 30mM TCEP in sodium phosphate buffer at pH 7.

5. Arm DNAs are added to the purified yGK-Cx as soon as both arms are ready. Then the mixture is incubated for 3 days at 4 °C. The final products are purified through an HPLC ionic-exchange column and determined via SDS gel electrophoresis. The ratio of DNA to protein affects the number of DNA arms on the final products. Fig. 3.13 is a gel picture, displaying the products corresponding to different DNA to protein ratios.

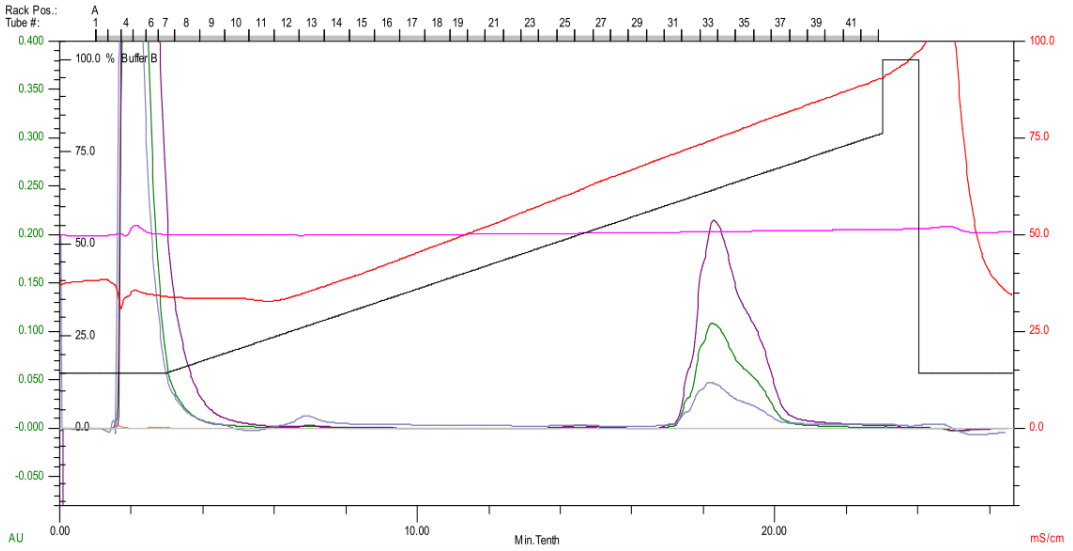

Figure 3.14: HPLC ionic column profile for nR-chimera purification after the ligation. The samples from fraction 32 to 36 were collected; the later samples should have larger molecular weight (i.e. more DNA arms) on average. We measured the enzymatic inhibition of the samples from different collections with different hybridization states (i.e. with or without nick); the results are listed in Table 3.3. The left Y-axis is the absorption at 280 nm (green) and 260 nm (purple) in arbitrary units; the right Y-axis is the salt concentration in mS/cm; and the X-axis is the elution time in minutes.

6. For the ligation of a multi-armed chimera, the reaction conditions are: 300 nM of NR-chimera, 1.3 units of T4 ligase, 1 μM of 18mer as a splint, 0.2 mg/ml of BSA in manufacturer-recommended buffer. The efficiency cannot be determined by gel due to the complexity of all the possible products.

3.7 Results of Controlling Enzymatic Reaction by Multiple Springs

Introducing the cDNA reduces chimera activity, but not significantly. A comparison of activity measurements for different multi-armed chimeras is listed Table. 3.3. Conclusively, these chimeras with more arms display a greater inhibition of enzymatic activity when hybridized with cDNA. However, this effect is only comparable to, rather than much greater than, that of the normal ligated two-armed chimera, indicating that using this multi-armed chimera is not a efficient method to turn off the enzyme.

There might be several possible reasons for this. First, the number of the effective spring is less than expected. Assume that on average there are 10 DNA arms on the protein, including arm A and arm B, the statistical average number of formations of ds spring is ~ 4. Steric effects also need to be considered, where the first ds DNA spring may hinder the formation of the other springs. As a result, the number of effective springs will be less than 4. Moreover, since Lysines (the attachment sites for DNA springs) on yGK surface distribute quite uniformly, the forces applied by DNA springs are rather isotropic. Based on our previous conclusion that the response of enzyme to mechanical stress is anisotropic, most of the springs may not contribute to altering enzymatic reaction. Certain non-mechanical effects were observed on TBGK mutant 75/171, stemming from protein-DNA interaction. Though this was not observed in other mutants, many DNA strands in close proximity to the enzyme may have an impact on its catal-

Table 3.3: Reaction rates (relative unit) of nR-chimeras from different fractions after HPLC ionic column purification. The nR-chimeras were from HPLC fraction 32 to 36 (see Fig. 3.14). The samples came out later should have more DNA arms on average. The samples from different fractions were mixed with 50 bp complementary DNA (50mer) and two 25mer cDNA (Rab), separately. The enzyme with the 50mer spring was under large stress while that with the Rab spring was under no or little stress because the nick in the middle of the spring released most of the tension. The comparison of the 50mer and Rab shows that multiple springs does not induce a significant decrease in enzymatic activity of GK with respect to the two-armed chimera. The concentrations of chimeras used here were undetermined and the efficiency of the ligation was unknown.

Fraction	**32**		**33**		**34**		**35**		**36**	
Hybridization	50mer	Rab	50mer	Rab	50mer	Rab	50mer	Rab	50mer	Rab
ATP@750 μM	1743	2080	2655	3101	1579	1962	503	755	312	469
GMP@ 300 μM	$\pm$33	$\pm$53	$\pm$29	$\pm$66	$\pm$68	$\pm$68	$\pm$54	$\pm$13	$\pm$12	$\pm$13
Ratio (50mer/Rab)	0.84		0.86		0.8		0.67		0.66	
ATP@750 μM	2227	2686	3496	4332	2068	2863	780	1107	402	588
GMP@ 300 μM	$\pm$21	$\pm$39	$\pm$154	$\pm$34	$\pm$44	$\pm$58	$\pm$31	$\pm$42	$\pm$12	$\pm$42
Ratio (50mer/Rab)	0.83		0.81		0.72		0.7		0.68	

ysis, screening the effect by mechanical stress.

Despite the fact that this multi-armed chimera is not the solution to turn off the activity of the enzyme, it provides an opportunity to construct a Protein-DNA chimera lattice, where a chimera serves as a single tile to construct an organized microstructure.

3.8 Building Macrostructure from Nanoscale Materials: DNA Tiles and Multi-armed Chimeras

3.8.1 DNA Origami

Molecular self-assembly is the process where molecules adopt an organized arrangement without guidance or management from external sources. This process is essential in biological systems, associated with lipids to form the membrane and the formation of double helical DNA through hydrogen bonding of the individual strands, for example.

DNA tile based self-assembly is one of the most popular methods in DNA nanotechnology, used to organize a variety of nanoarchitectures with controlled spacing and pattering. [32] A DNA tile consists of multiple connected interwoven strands and can bind to each other by hybridizing their single-stranded ("sticky") ends, enabling the structure to grow [33, 34].

Under slightly satuated conditions, the attachments of a tile to a crystal by two or more ends if favorable, presumably allowing complex assembly with less error, but the attachment of one end is unstable [35, 36]. Controlling the supramolecular DNA assembly is often achieved in nucleation and growth processes. A programmable DNA seed is essential to initiate the growth of a structure and different seeds nucleate different types of crystals [35, 36].

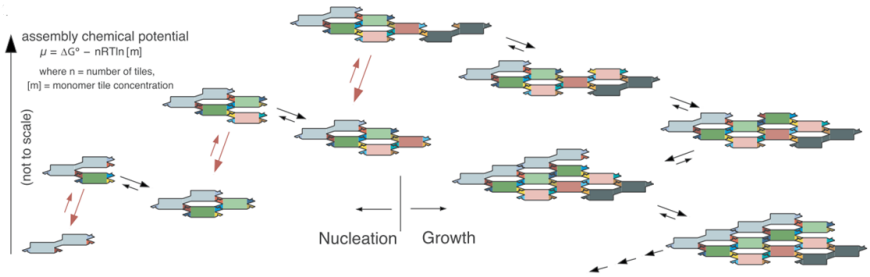

Figure 3.15: This figure is adapted from [34]. Illustration of the self-assembly of DNA tiles into a ribbon structure. Nucleation steps (at left) culminate in the critical nucleus (at top), followed by growth (at right). Arrows depict the reaction rates of transition between two structures, which can be controlled by the design of DNA tiles .

3.8.2 Principle of Design of Macrostructure Using Multi-armed Chimeras

Despite the fact that the multi-armed chimera is not the solution to turn off the activity of enzymes, it provides an opportunity to construct a Protein-DNA chimera lattice, where a chimera serves as a single tile to construct an organized microstructure.

The principles of designing a macrostructure from Protein-DNA molecules are as follows: first, prepare two kinds of multi-armed chimeras having different arms A and B, respectively; an ss DNA complementary to A plus B is used to crosslink chimera A and B (see Fig. 3.16); find the optimal condition of mixing chimera A, chimera B and complementary DNA, allowing the formation of a microscale structure Protein-DNA lattice. A seed for nucleating is essential to this process, where a programmable DNA seed may be considered. The difficulties are how to design suitable DNA arms and find the right conditions which allow forming one (or a few) macrostructure rather than many small structures.

A macroscale structure allows for better and easier manipulation of enzymatic

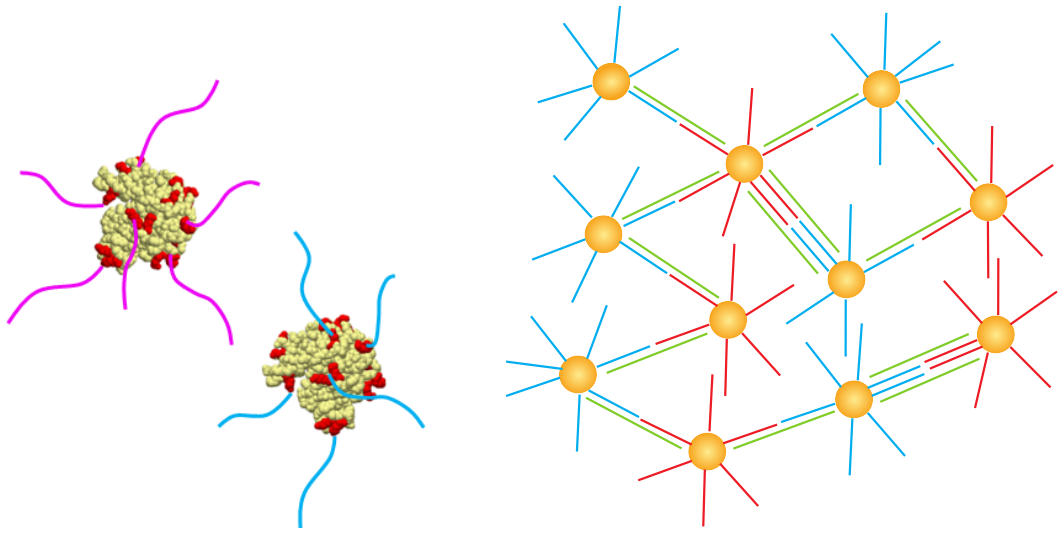

(a) (b)

Figure 3.16: Sketch of Protein-DNA lattice. (a) Two different types of multi-armed chimeras. One chimera has A DNA arms (pink) while the other has B arms (blue). (b) With the complementary DNA of A plus B (green), the two chimeras of different types are linked together. With the proper environment (e.g. the buffer conditions and the ratio of chimeras to cDNA), a "seed" (a conjugation of few chimeras) may grow into a macrostructure (lattice).

reactions. Protein-DNA lattices would also be designed to have various shapes and orientations, leading to anisotropic responses to different kinds of mechanical perturbations. Much more work needs to be done before obtaining a practical Protein-DNA lattice, however, the research associated to this new material will be interesting and it is worthwhile to try .

CHAPTER 4

Mechanical Control of Renilla Luciferase

Using a DNA molecular spring to mechanically perturb an enzyme is conceptually a general method applicable to all (or at least many) enzymes. However, most of our work was performed with the enzyme Guanylate Kinase (GK) (see Chapter 3) though the method was originally demonstrated with the Maltose Binding Protein (MBP) [16]. In this chapter, we demonstrate a new chimera, where the enzyme Renilla luciferase (RLuc) is the sample protein controlled by the DNA molecular spring. Renilla luciferase belongs to an entirely different class of enzymes from Guanylate Kinase and does not perform a conformational transition from the "open" to the "closed" state like GK. Therefore, the successful control of RLuc validates the concept that the DNA molecular spring is indeed a general method with which to modulate enzymatic activities and probe protein properties as well.

We also show proof of concept that the RLuc chimera can be constructed as a sensitive molecular probe, where a specific DNA target sequence can be detected in an easy, one-step and homogeneous assay. This Rluc-DNA probe is able to detect the presence of the target DNA (e.g. the complementary DNA of the arm DNA) with a quantity as low as $\sim$10 fmol, dependent on the luminescence detector being used. It is also capable of detecting a single-base-pair mismatch on the DNA spring without melting curve analysis. The defect in the DNA spring introduced by the DNA mismatch causes a decrease in the stress applied by the spring, leading to a discernible change of enzymatic activity. Inherent in the RLuc-DNA chimera is a reporter system which is capable of converting a small change in the stress

applied to the enzyme into a detectable change in luminescence intensity.

Because of the sensitivity and specificity demonstrated in the RLuc-DNA chimera, the RLuc-DNA chimera has the potential to be developed into a molecular probe, though certainly more work needs to be done to obtain a practical biosensor. At the end of this chapter, we provide some possible steps to improve and further develop this biomolecular sensor.

4.1 Construction of a New Protein-DNA Chimera

4.1.1 Selection of a New Enzyme: Renilla Luciferase

In principle, DNA molecular spring is a general strategy to perturb protein mechanically and study the responses of proteins to moderate mechanical forces (~ 5 pN). However, the previous studies were mostly done on Guanylate Kinase (GK). To validate the view that this method is universal, we are looking for another enzyme which is fundamentally different from GK and will respond to mechanical stress by the DNA spring as well.

We select Renilla Luciferase for an RLuc-DNA chimera construct for several reasons. First, the overall structure of this enzyme (Fig. 4.1) is quite different from the structure of GK (and MBP): there is no "hinge" or hinge motion, and it is not a nucleotide binding protein. In addition, the enzymatic activity of RLuc is measured as luminescence intensity and this measurement is rather easy and sensitive. Inherent in the RLuc-DNA chimera is a reporter system which facilitates the measurements of the mechanical response of the chimera. Besides, when incorporated with other techniques, such as aptamers, the RLuc-DNA chimeras may be developed into practical biosensors for different targets (see Sec. 4.6.5).

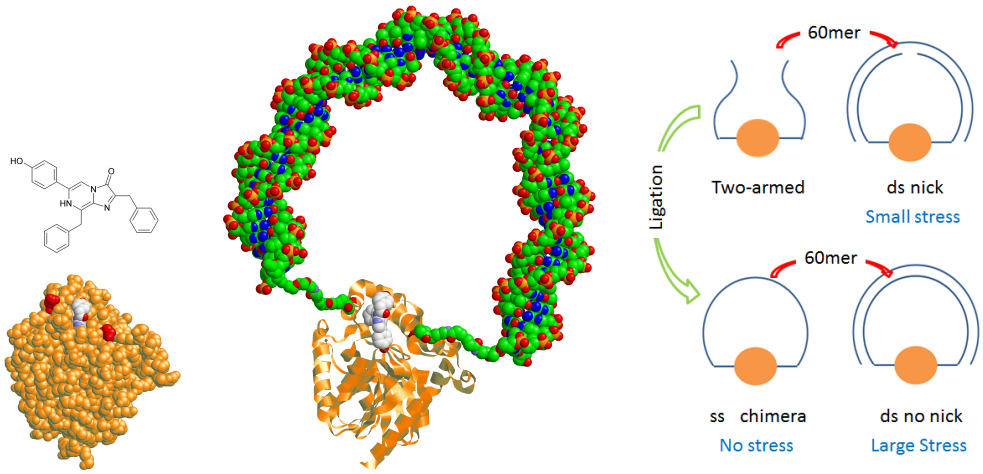

(a) (b) (c)

Figure 4.1: (a) Crystal structure of Renilla luciferase (colored light yellow) with bound substrate (coelenterazine) from Protein Data Bank (PDB) structure 2PSJ. Residues 161 and 188, mutated to cysteins in the experiment, are colored red. The distance between these two residues is $\sim 2\,nm$. (b) Cartoon of the RLuc-DNA chimera with the DNA spring attached to sites 161/188. The RLuc structure is from PDB 2PSJ and DNA is from the nucleosome structure 1KX5. The protein, DNA, and cross-linkers are drawn approximately to scale. (c) Sketch of the different forms of the RLuc chimera used in this study. The molecule is synthesized as a two-armed chimera (2R chimera), with two separate ss 30mer DNA strands coupled to the cross-linkers at the 5' and 3' end, respectively. Ligation of this construct results in the "ligated chimera", sporting one continuous ss 60mer DNA strand attached by the ends to the cross-linkers. Hybridization of the ligated chimera to the complementary 60mer results in an enzyme under stress. Hybridization of the 2R chimera to the complementary 60mer results in an enzyme under a smaller stress because of the nick in the DNA spring.

4.1.2 Overview of Renilla Luciferase

Luciferase from renilla reniformis (RLuc) is a 36 kD enzyme which catalyzes the oxidation of luciferin coelenterazine by molecular oxygen, producing coelenteramide, CO_2 and light (470 nm), with a rather low quantum yield of 5 % [37, 38]. The Michaelis-Menten constant of the coelenterazine-h (a modified substrate we use) is 220 nM. [37] The bioluminescent process actually involves three components: RLuc, green fluorescent protein (RrGFP), and Ca^{2+}-activated luciferin binding protein [39].In the presence of Ca^{2+}, the luciferin binding protein releases luciferin, initiating catalysis by RLuc. The energy generated by this oxidation is transferred to RrGFP and then emitted as a green-wavelength photon. This process can presumably lead to a larger effective quantum yield, and indeed this is utilized in biotechnology. [40, 41]

In structural terms, RLuc consists of two domains, an α/β hydrolase domain and a cap domain; the latter contains a binding pocket for the substrate and is expected to be comparatively flexible [42]. Wild-type RLuc has three cysteins at residues 24, 73 and 124, forming no disulfide bond. At high concentrations (>1 mg/ml), RLuc slowly self-associates; this phenomenon does not involve disulfide bond formation of the internal cysteins [43]. The product of the RLuc catalyzed reaction is a strong competitive inhibitor of the enzyme (Ki $\sim$ 23 nM)[43]. Another feature of RLuc is that the enzyme inactivates after a relatively small number of catalytic cycles. The wild-type enzyme can catalyze about 100 reactions before inactivating [44].

4.2 Synthesis of RLuc-DNA Chimeras

The synthesis of RLuc-DNA two-armed chimera is adapted and optimized from the method described in [19] and explained in detail in Chapter 1. All the modifications specially for RLuc will be addressed clearly in this section.

4.2.1 Selection of Mutation Sites

The Luciferase must probably "breathe" in order for the substrate to get in and out of the binding pocket. One possibility is to perturb this motion via mechanical stress. Unlike Guanylate Kinase (GK), which has a well-known conformational transition from the "open" to the "closed" state, the crystal structures of Renilla luciferase with and without substrate bound (PDB: 2PSJ and 2PSH) are almost identical, so there is no obvious way of pulling Rluc against its reaction motion as was done with GK.

Therefore, the spring attachment points E161/S188 were chosen on the qualitative expectation that the stress applied at these locations would probably deform the substrate binding site and lead to an effect on the activity, which indeed succeeded. We also tested some other attachment pairs, however, we ran into problems with the expression of these mutants or chimera construction. The progresses are listed in Table 4.2.

4.2.2 DNA Arms Preparation

The synthetic DNA oligonucleotides were purchased from Integrated DNA Technology (IDT). The sequences of the two DNA 30mer arms with which the chimera was constructed were:

A: 5'-[AminoC_6]-GAGTGTGGAGCCTAGACCGTGAG-TTGCTGG-3' and

B: 5'-[Phos]-CAGTGGTGCGACCGACGTGGAGCCTC-CCTC-[AmMO]-3'

where [AminoC_6] and [AmMO] are amino terminal modifications at the 5 end and 3 respectively. [Phos] is the phosphate modification, enabling to subsequently link the two DNA arms by ligation. These two DNA arms are the same ones used to construct GK-DNA chimera.

The amino-functionalized DNA strand is attached to the Cys residues through a hetero-bifunctional crosslinker (NHS-PEO2-Maleimide), which reacts with the

amine group on the DNA via the NHS to from an amide bond and the sulfhydryl group of the Cys via the maleimide group to form a stable thioehter bond.
The 60 b.p. DNA complementary to A plus B was:
60mer: 5'- CAGCTGCTTGGATGGTACCGTGGACTCCTGCCAGCAACTC-ACGGTCTAGGCTCCACACTC-3'
and was used to obtain the ds chimera. We also designed two 60 b.p. DNA oligomers having one and three mismatches relative to the chimera DNA; the sequences were:
1MC: 5'-CAGCTGCTTGGATGGTACCGTGGACTCCT**T**CCAGCAACTCA-CGGTCTAGGCTCCACACTC-3'
and 3MC: 5'-CAGCTGCTTGGATGGTACCGTGGACTCC**ATT**CAGCAACT-CACGGTCTAGGCTCCACACTC-3'
The bold letters represent the mismatched nucleotides.

We also constructed a chimera with a shorter DNA spring 40mer, having two DNA 20mer arms, whose sequences were:
A-20: 5'-[AmMC$_6$]GAGTGTGGAGCCTAGACCGT-3'
B-20: 5'-[Phos]CGGTACCATCCAAGCAGCTG[AmMO]-3'
The synthesis of this 40mer spring chimera is similar to that of the 60mer spring chimera, but it results in a higher yield. See Sec. 4.2.4 for more details.
We use both chimeras (60mer and 40mer) to investigate the nonlinear dynamics of molecules in Chapter 5. For this chapter, all the measurements are based on the RLuc-60mer chimera.

4.2.3 Mutagenesis, Protein Expression and Purification

The wild-type gene of Renilla luciferase (RLuc) was obtained from the pRL-null vector (Promega) and subcloned into the pET28a vector (Novagen) with a His-tag at the C-terminal to facilitate the purification after protein expression. To con-

struct the mutant, the wild-type gene was modified by site-directed mutagenesis to substitute two cysteins at residues 161 and 188 for later DNA conjugation. The mutant proteins were expressed in *E. Coli* strain BL21(DE3)pLysS and induced with 1 mM IPTG for 3 hours at 30 °C [44]. The product proteins were purified by Ni-NTA chromatography (Qiagen) through the His-tag. Because this protein tends to self-associate, the concentration of RLuc is kept under 25 μM and we generally avoid vortexing and centrifugation of the samples.

4.2.4 Two-armed Chimera Construction

The protocol for constructing the RLuc chimera is based on that of the GK chimera but is rather different in the one-armed chimera construction and purification. The main reason for this is that RLuc tends to self-associate so we avoid vortexing and centrifugation. RLuc seems to prefer joining with two DNA arms rather than just one even when the protein to DNA ratio is bigger than 1.

Figs. 4.2(a)&(b) show the HPLC profiles of 1R purification with different protein to DNA ratios during incubation. We observed that even though the ratio was 2, the product contains many more 2R chimeras (peak 3) than 1R chimeras (peak 2). (Fig. 4.2(a)) Longer incubation of RLuc with the DNA arm did not improve the yield of 1R chimera. However, when mixing the recollected RLuc with new DNA arm, both 1R and 2R chimera were produced, indicating that the RLuc was still reactive to crosslinkers. Thus, unreactive RLuc was not the cause for the low yield. Though the reason for the preference of RLuc to attach two DNAs is still unclear, we solved this low-yield problem by increasing the protein:DNA ratio to 9 : 1, which provided acceptable yield of the 1R chimera (Fig. 4.2(b)).

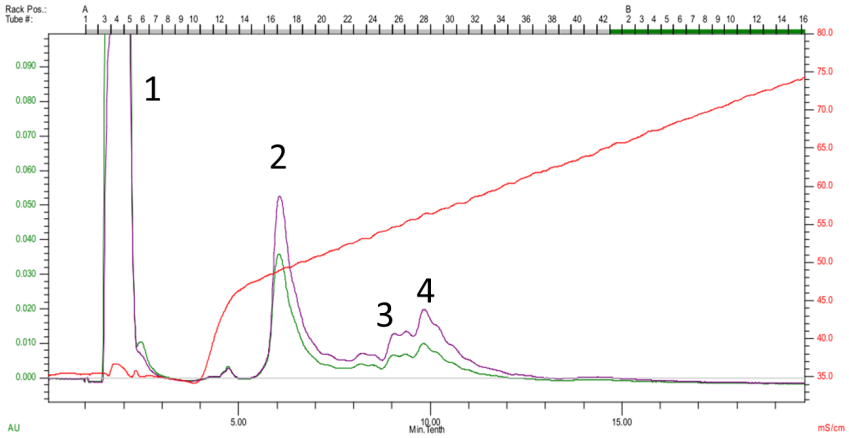

(a)

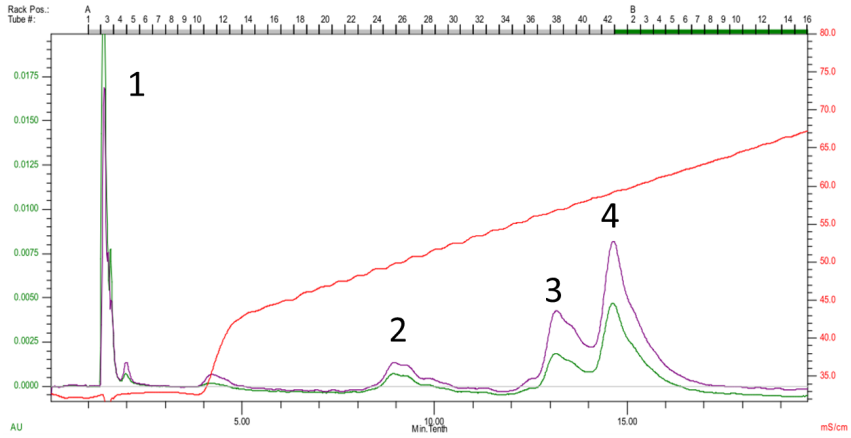

(b)

Figure 4.2: HPLC profiles of a 1R purification through an ion-exchange column for (a) the mixture with protein to 30mer in the ratio of 9 : 1, which is used in our chimera synthesis, and (b) the mixture with protein to 30mer in the ratio of 2 : 1, which has a rather low yield of the 1R chimera. Through 1R purification, by-products, such as the 2R chimera (peak 4), unbound DNA (peak 3) and proteins (peak 1), will be separated from 1R chimeras (peak 2). The left Y-axis is the absorption at 280 nm (green) and 260 nm (purple) in arbitrary units ; the right Y-axis is the salt concentration in mS/cm; and the X-axis is the elution time in minutes.

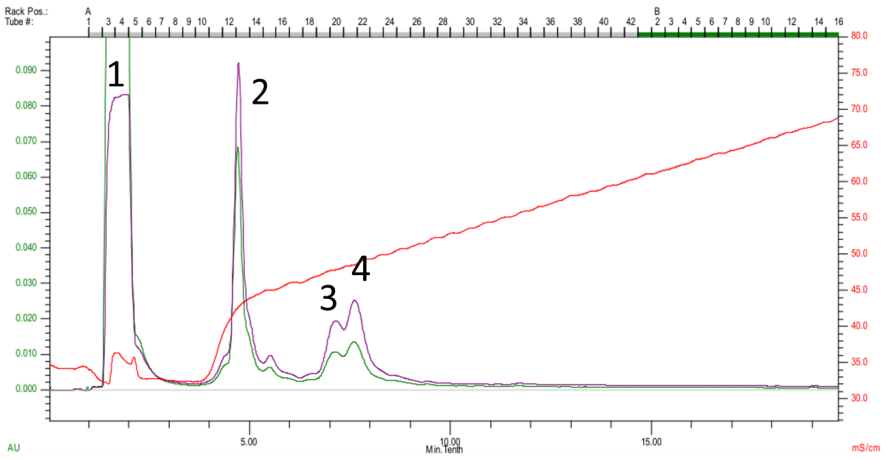

(a)

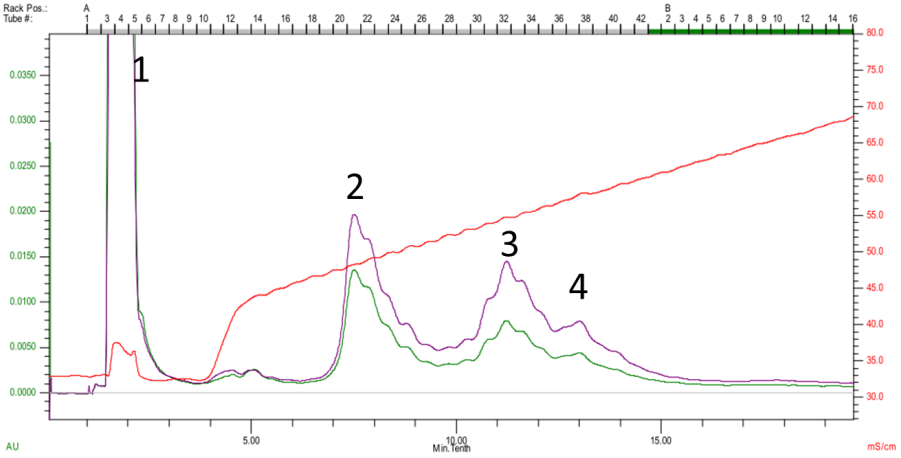

(b)

Figure 4.3: Same HPLC profiles as Fig. 4.2 for 1R purification of (a) protein coupled to one 20mer arm DNA, and (b) protein coupled to one normal 30mer arm but via a longer crosslinker .

The proteins (peak 1), 1R chimeras (peak 2), unbound DNA (peak 3) and 2R chimeras (peak 4) can be readily separated. The left Y-axis is the absorption at 280 nm (green) and 260 nm (purple) in arbitrary units; the right Y-axis is the salt concentration in mS/cm; the X-axis is the elution time in minutes.

We constructed two other chimeras: a chimera with a 40mer DNA spring (RLuc40) and another 60mer chimera but this one with a longer crosslinker (NHS-PEG8-Maleimide, length ∼4 nm). The synthesis protocol of these two chimeras is the same as the one for the ordinary RLuc-60mer chimera (RLuc60). The HPLC profiles of the one-armed purification are shown in Figs. 4.3(a) and (b). We used RLuc40 and RLuc60 to study the nonlinear dynamics of molecules in Chapter 5.

The product from HPLC purification and the final two-armed construction can be determined by gel electrophoresis and identified based on molecular weight (Fig. 4.4).

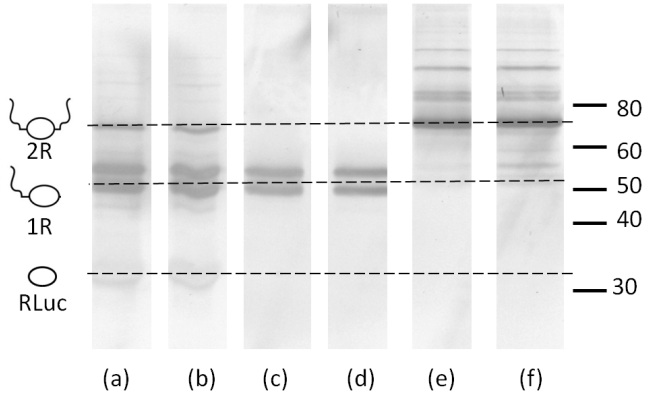

Figure 4.4: Gel electrophoresis of different products during the chimera construction , stained with Sybr Gold. RLuc and A arm were incubated at a ratio of 9 : 1. (a) before HPLC ion-exchange purification, the major product is one-armed chimera. (c) the fractions we selected after HPLC purification to perform subsequent 2nd arm coupling, which contains mostly one-armed chimera. (e) sample (c) mixed with B arm for overnight incubation, showing that the yield of the two-armed chimera is high. We added βME to samples (a), (c) and (e) to check that there is no serious aggregation, represented by (b), (d) and (f), respectively.

4.2.5 Ligation and Purification

We employed T4 DNA ligase (New England Biolab) to link the A and B arms of the chimera. The sample is incubated for two days at 16 °C under the following conditions: 20 nM chimera, 1.25 μM 18mer cDNA, which serves as splint to hold the two free ends of the DNA arms, 0.1mg/ml of BSA (New England Biolab), and 1.2 units/μL of ligase in the recommended reaction buffer (Biolab). After ligation, Ni-NTA purification is performed to remove the DNA splint, ligase, and ATP. Products of the ligation reaction are identified by gel electrophoresis; the yield of the correct construction (ligated chimera) was more than 75 %.

Because we avoid vortexing and centrifugation of RLuc, the RLuc-DNA chimera concentration in the elution buffer was always low ($\sim$ 150 nM) compared to the GK chimera. The yield and concentration of chimeras were determined via SDS gel electrophoresis (see next section).

4.2.6 Determination of Enzyme Concentration

Protein concentration was measured with the Bradford assay (Bio-Rad) or, for small quantities, from the intensity of the bands on SDS-PAGE pictures, where proteins were stained with SYPRO Ruby Protein Gel Stain (Invitrogen). Fig. 4.5 shows the gel picture of different chimeras, where the protein quantities were determined by the intensities of the corresponding lanes.

From the result of the cDNA detection experiment, it turns out that using the titration of cDNA and finding the minimum concentration which saturates the effect of reducing luminescence is a more precise way to determine chimera concentration. (Fig. 4.9(c))

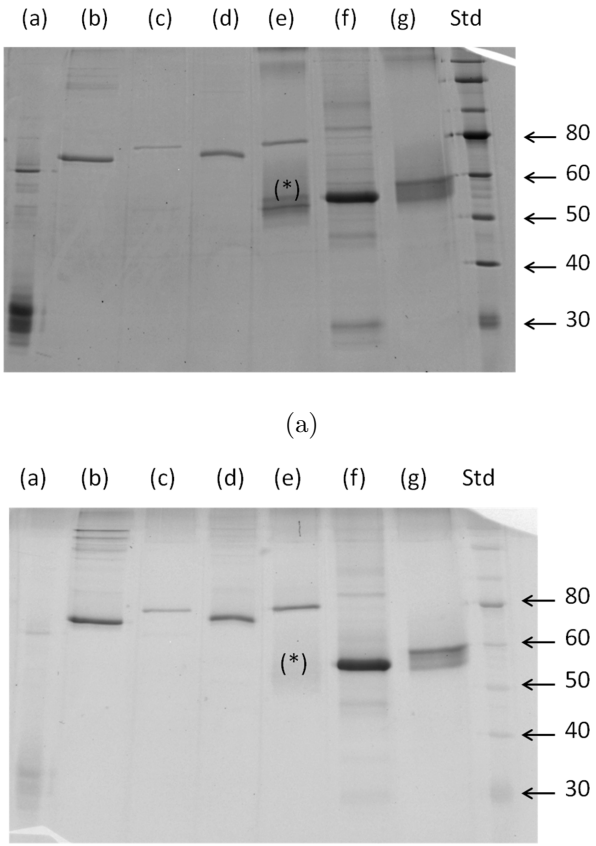

Figure 4.5: Gel electrophoresis of three different RLuc-DNA chimeras with two separate DNA arms or one ligated ss DNA arm. The gels were stained either with (a) Sypro Ruby to visualize proteins or (b) Sybr Gold to visualize DNA. Though Sybr gold is used to stain DNA, a faint band will appear if the quantity of protein is high. The lanes are: (a) RLuc, (b) and (c) are RLuc-60mer chimera with SM(PEG)$_2$ crosslinker, where (b) has two separate 30mer DNA arms and (c) has a ligated 60mer ssDNA. (d) and (e) are RLuc-60mer chimera with a longer crosslinker SM(PEG)$_8$ before and after ligation, respectively. The asterisk denotes T4 ligase, which contained no DNA and disappeared after the Sybr Gold staining. (f) and (g) are RLuc-40mer chimera with SM(PEG)$_2$ crosslinker, where (f) has two separate 20mer arms and (g) represents the sample after ligation, however, it is unclear what the yield of the successfully ligated sample was. The estimate was that more than 50% was ligated ss40mer chimera.

4.2.7 Kinetics of Enzyme Activity

RLuc-DNA chimera was incubated with or without target DNA at room temperature overnight in PBS (pH 7.4) with 0.4 mg/ml BSA. In the mixture, the chimera concentration was between 1 to 6 nM while the target DNA concentration was 60 times the chimera concentration unless otherwise specified. The stock concentration of Coelenterazine-h substrate (Promega) was 50 μM in methanol. Substrate solution was further diluted in PBS (pH 7.4) right before the luminescence measurements. Due to the fast inactivation of RLuc, the microplate was modified to allow the substrate solution to be manually injected to mix with the chimera sample and initiate the luminescence, enabling to monitor the beginning of the reaction with our commercial microplate reader (Synergy HT, BioTech) For each measurement, 160 μM substrate solution was added to 40 μL sample.

4.3 Dynamics of RLuc and Fitting of Luminescence Measurements

4.3.1 Dynamics of RLuc

Mechanical control of Luciferase activity is shown in Fig. 4.6, where we report the time course of luminescence measurements under no stress (blue circles), a small stress (green squares: nicked DNA spring), a larger stress (red triangles: ligated ds DNA spring). The mechanical stress exerted by the DNA spring in the ligated, ds form leads to partial inhibition of the enzyme. Fig. 4.6(c) is a control where the two-armed chimera is hybridized with two separate 30mers (i.e. the DNA spring is disjoint so there is no stress), showing that the mere presence of DNA in close proximity to the enzyme does not affect the activity. Luciferase activity is often quantified by the integrated light intensity emitted over a time period (area under the curves of Fig. 4.6); this measure is reported in Fig. 4.6(d).

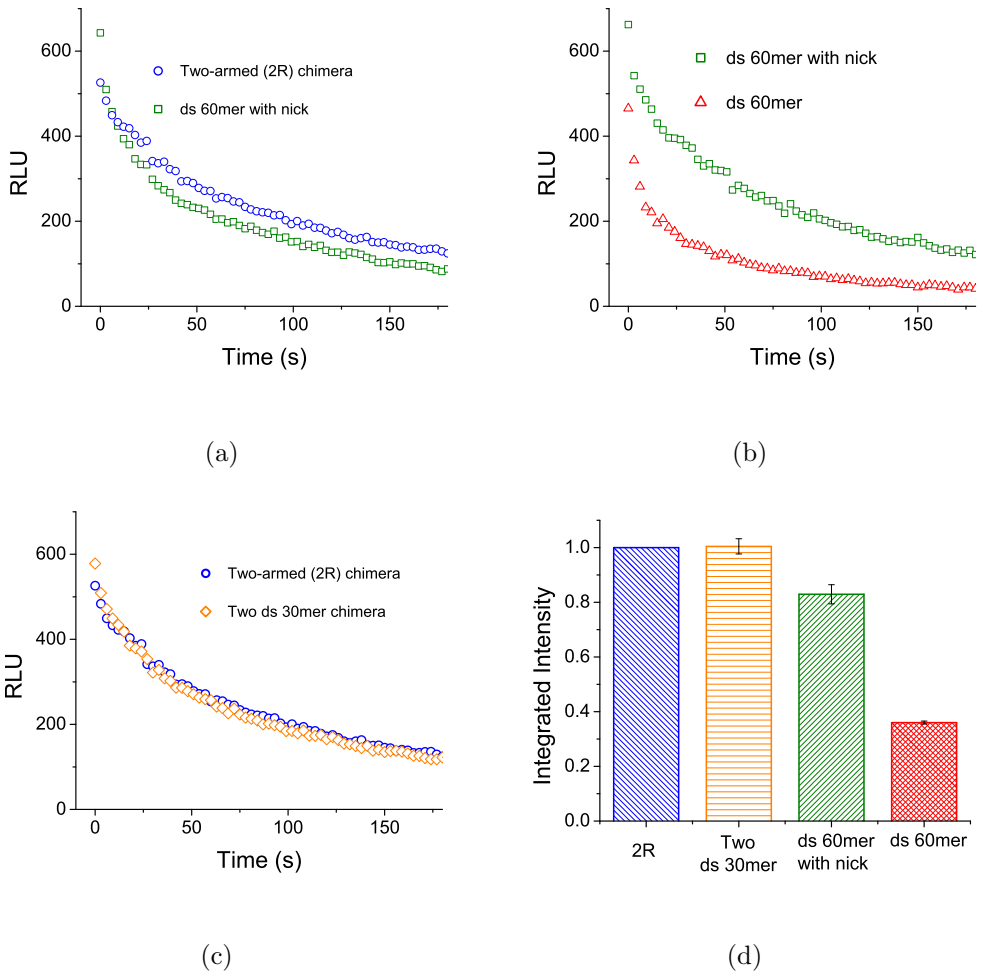

Figure 4.6: The time course of luminescence intensity (arbitrary units) for the RLuc chimera under different states of mechanical stress The conditions are: 2 nM chimera concentration, 1 μM initial substrate concentration. (a) Two-armed chimera (circles) and two-armed chimera hybridized to the complementary 60mer (ds with nick:squares). The DNA spring with the nick has only a small effect on the speed of the enzyme. (b) Ligated chimera hybridized with two complementary 30mers (DNA RA and RB: ds with nick:squares) and ligated two-armed chimera hybridized to the 60mer (ds without nick:triangles). The DNA spring without nick has a larger effect on the speed of the enzyme. (c)Two-armed chimera (circles)and two-armed chimera hybridized with two separate complementary 30mers (DNA RA and RB: two ds 30mer: diamonds). This is a control which shows that merely bringing DNA in close proximity to the enzyme, without stress, has no effect on the enzymatic activity. (d)Integrated luminescence intensity (area under the curves in (a), (b), (c) from $t = 0$ to $t = 120$ seconds) for the two-armed chimera(no stress), the chimera with two separately hybridized arms(control with no stress), the ds chimera with nick (small stress), and the ds chimera without nick (larger stress), normalized by the result of the two-armed chimera. The error bars are generated from three measurements for each construction.

In order to analyze the activity curves in more detail, we need a fit for the time course measurements of Fig. 4.6. These are actually not simple exponential or sum of exponentials curves, and though the effects which produce this peculiar time course are known, we do not find corresponding fits in the literature. The main effects to be considered are product inhibition [43] and a stochastic process whereby the enzyme goes irreversibly into an inactive state after so many turnovers on average [44]. This "bleaching" is presumably related to the low quantum yield Q $\sim$ 5% [37, 38] of the photon emitting reaction. Qualitatively, under conditions where the molar ratio of enzyme to substrate is small, the steep decrease in luminescence at the beginning of the time measurements (Fig. 4.6) is due to the inactivation of the enzyme; gradually, inhibition by the accumulated products slows down the reaction, leading to the long tail in the graphs (Figs. 4.6 and 4.8).

Within a Michaelis-Menten description of the reaction speed:

$$E + S \leftrightarrow ES \begin{cases} \xrightarrow{k_{cat}} EP \leftrightarrow E + P \\ \xrightarrow{k_d} E^*P \quad (dead) \end{cases} \tag{4.1}$$

where E is the enzyme, S the substrate, P the product, k_{cat} the catalytic rate and k_d the inactivation rate of the enzyme, the rate of emitting photons is:

$$\frac{d}{dt}N_\gamma = \frac{[E]k_{cat}VQ}{1 + \frac{K_S}{[S]} + \frac{K_S}{K_P}\frac{[P]}{[S]}} \tag{4.2}$$

where V is the reaction volume, Q the quantum yield, K_S, K_P the Michaelis-Menten constants of substrate and product, [S] and [P] the concentration of substrate and product, respectively, and [E] = [E](t) is the total concentration of active enzymes at time t, governed by the rate equation:

$$\frac{d[E]}{dt} = -[ES]k_d = -\frac{[E]k_d}{1 + \frac{K_S}{[S]} + \frac{K_S}{K_P}\frac{[P]}{[S]}} \tag{4.3}$$

$$\Rightarrow \frac{d[E]}{dt} = -\frac{dN_\gamma}{dt}\frac{1}{VQ}\frac{k_d}{k_{cat}} \tag{4.4}$$

To fit the time course measurements, we integrate the system of equations (4.2-3) (see Sec. 4.3.2), keeping in mind that

$$\frac{d[S]}{dt} = -\frac{1}{VQ}\frac{dN_\gamma}{dt}, \qquad \frac{d}{dt}[P] = -\frac{d}{dt}[S] \tag{4.5}$$

and adjust the parameters to reproduce the experimental curves. In the following, we show the details of the fitting and the results are listed in Table 4.1 and discussed in Sec. 4.3.3.

4.3.2 Fitting of Experimental Data

Luminescence measurements were performed with many different substrate concentrations, from 200 to 1000 nM, but we particularly fitted the data with concentrations of 600, 750 and 1000 nM. Because there are many parameters (see Eqs. 4.2 and 4.3), we employ the following strategy. First, we calculated K_S by using a double reciprocal plot: reciprocal of reaction rate vs. reciprocal of substrate concentration. Since the molar ratio of substrate to enzyme is large (>500), in the beginning of the reaction the substrate concentration can be approximated as a constant and [P]/[S] is approaching zero. Taking the reciprocal of Eq. 4.2 gives

$$\frac{1}{\frac{d}{dt}N_\gamma} = \frac{1}{[E]k_{cat}VQ}(1 + \frac{K_S}{[S]}) \tag{4.6}$$

We therefore plot 1/(Luminescence Signal) vs. $1/[S]_0$ (the initial substrate concentration), fit a straight line, and obtain K_S as the slope over the intercept (Fig. 4.7). We took the first ("zero time") data point of each reaction as the reaction rate for that specific initial substrate concentration, analyzed all the data for different substrate concentrations (Fig. 4.7) and calculated K_S for the ss chimera and the ds chimera (Table 4.1).

Next, we write the measured luminescence intensity I as:

$$I(t) = A\frac{dN_\gamma}{dt} \tag{4.7}$$

where A is an instrument dependent numerical factor (the conversion factor between rate of emitting photons and luminometer reading). From Eq. 4.5:

$$\frac{d}{dt}N_\gamma = VQ\frac{d[S]}{dt} \tag{4.8}$$

$$\Rightarrow I(t) = BV\frac{d[S]}{dt} \qquad where\ B = AQ \tag{4.9}$$

The equations which evolve the quantities [S], [E] and [P] are (see Eqs. 4.2-4.5)

$$\begin{aligned}
\frac{d[S]}{dt} &= -\frac{[E]k_{cat}}{1+\frac{K_S}{[S]}+\frac{K_S}{K_P}\frac{[P]}{[S]}} \\
\frac{d[E]}{dt} &= \frac{k_d}{k_{cat}}\frac{d[S]}{dt} \\
\frac{d[P]}{dt} &= -\frac{d[S]}{dt}
\end{aligned} \tag{4.10}$$

while the intensity at time zero is

$$I(0) = I_0 = B\ \frac{[E]_0 k_{cat} V}{1+\frac{K_S}{[S]_0}} \tag{4.11}$$

We fit the three parameters k_{cat}, k_d and K_P as follows. Starting from the known initial values $[S]_0$, $[E]_0$, $[P]_0 = 0$, and K_S determined above, and choosing values for k_{cat}, k_d andK_P, we evolve Eq. 4.10 in time. B is determined from the luminescence at zero time I_0 using Eq. 4.11. Then the luminescence intensity in the course of time, $I(t)$, is determined from Eq. 4.9. This is compared to the experimental curve and the parameters k_{cat}, k_d and K_P are varied to minimize the square difference (least square fit). The procedure returns values for k_{cat}, k_d, K_P and the parameter B which is proportional to the quantum yield Q (see Eq. 4.9). In this way, we generated the reaction curves numerically and fit the luminescence measurement with substrate concentrations of 600, 750 and 1000 nM by adjusting k_d, k_{cat} and K_P. The best-fit set of values of k_d, k_{cat}, and K_P for each construction is reported in Table 4.1. We also report the value of B, since the ratio of the B values with and without stress is equal to the ratio of the corresponding Q values (the instrumental parameter A being the same for all experiments).

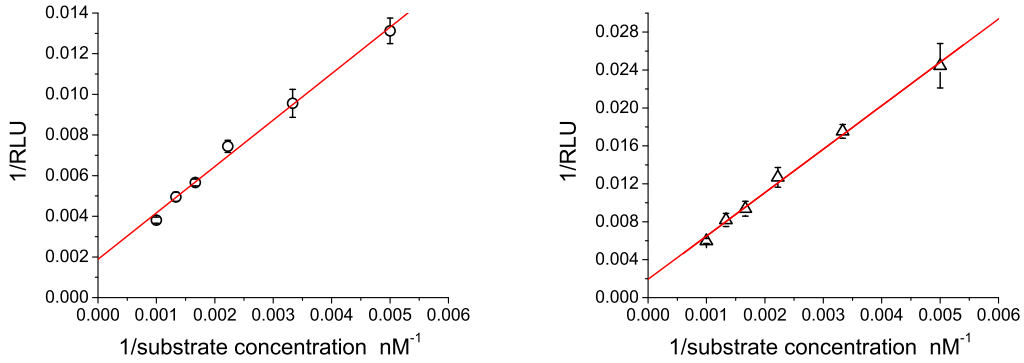

(a) (b)

Figure 4.7: Determination of K_S for ss chimera and ds 60mer using double reciprocal plot:reciprocal of reaction rate vs. reciprocal of substrate concentration. The slope divided by the intercept is K_S.

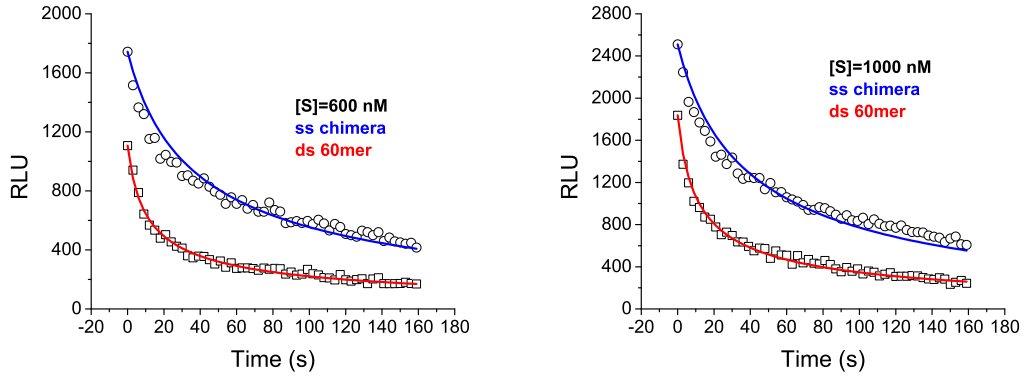

(a) (b)

Figure 4.8: Experimental data (dots) and fits (lines) of the luminescence intensity vs. time. (a) is the time course of luminescence intensity for the unhybridized chimera (no stress; circles) and ds chimera (stressed; squares) with initial substrate concentration of 600 nM while (b) is with initial substrate concentration of 1000 nM. The somewhat complicated fit is explained in Sec. 4.3.2, and the parameters extracted from it are reported in Table 4.1.

4.3.3 Effects of Mechanical Stress

In Eq. 4.4, k_{cat}/k_d represents the average turnover number of an enzyme before inactivation. Under stress, both k_d and k_{cat} increase by ∼30 %, and the parameter B, which is proportional to the quantum yield Q (Eq. 4.9), is reduced by ∼25 % , so that the average turnover number before inactivation is essentially unaffected by the stress, while the quantum yield is lower. Further, K_S is doubled, while K_P is reduced by a factor 4. These parameter changes are reflected in the change of shape of the time course curves (Figs. 4.6, 4.8) under mechanical stress: the increase in the rates k_d and k_{cat} causes the curve to be steeper at short times, while the decrease in K_P (stronger product inhibition) causes it to be flatter at long times. In contrast, if only the quantum yield Q was changing then the curve under stress could be rescaled to look like the stress-free curve (see Eq. 4.2). In summary, the effect of the mechanical stress with the DNA spring in this particular position is complex: in terms of Michaelis-Menten parameters, the rates are sped up, but the quantum yield and the binding affinity for the substrate are reduced, while product inhibition is increased, so that overall luminescence is reduced. Thus the integrated luminescence intensity of the chimera is a detector for the appearance of stress and therefore hybridization of the DNA spring.

Table 4.1: Kinetic parameters obtained from fitting the time course measurements as in Fig. 4.8, for the ss (no stress) and ds (stressed) chimera. Results for 3 different initial substrate concentrations are reported. Since the values of the kinetic parameters are in principle independent of initial substrate concentration, the corresponding variations in the Table are a measure of the uncertainty in the values extracted from the model Eqs. (4.2 - 4.3).
The values of K_S were instead obtained from the graphs of Fig. 4.7.

		ss chimera	ds 60mer chimera
	substrate conc.	$K_S = 1.2 \pm 0.2 \times 10^3$	$K_S = 2.4 \pm 0.5 \times 10^3$
	(nM)	(nM)	(nM)
$\boldsymbol{k_d}$ (1/s)	600	1.8×10^{-2}	2.4×10^{-2}
	750	1.5×10^{-2}	2.5×10^{-2}
	1000	1.6×10^{-2}	2.5×10^{-2}
$\boldsymbol{K_P}$ (nM)	600	17	4.3
	750	20	4.0
	1000	19	5.9
$\boldsymbol{k_{cat}}$ (1/s)	600	1.3	1.8
	750	1.3	1.7
	1000	1.2	1.9
$\boldsymbol{B}$	600	1.6	1.2
	750	1.6	1.3
	1000	1.8	1.3

4.4 Comparison of the GK-DNA Chimera and the RLuc-DNA Chimera

Comparison of the results of GK chimera and RLuc chimera is interesting. GK has a known, large conformational change from the "open" to the "closed" structure upon binding the substrate GMP; therefore it could perhaps be expected that pulling with the DNA spring against this conformational motion would affect substrate binding, which is correct. With the Luciferase there is no such easy prediction, as this enzyme is a regularly shaped globule and substrate binding is not (at least not dramatically) of the induced fit kind. The fact that we are able nonetheless to modulate this enzyme's activity with the DNA spring shows the generality of the principle that mechanically stressing an enzyme will affect activity, whether or not the enzyme has naturally occurring large conformational motion during the catalytic cycle.

Another interesting fact is that in both cases (GK and RLuc), the forces we are able to apply with the DNA spring significantly reduce enzymatic activity but do not shut off the enzyme completely. So at this level the mechanical response of these two very different structures is not entirely different.

Moreover, there is a rather small effect (~ 20 % change or less) with the nicked DNA 60mer spring (in the case of GK, this effect, if present, is below the resolution of the measurements; for RLuc it is visible thanks to the higher resolution of the measurements); however, repairing the nick has a rather dramatic effect on the activity for both enzymes. We believe this behavior is due in essence to a nonlinearity of the mechanics of these systems, an issue which we will discuss in Chapter 5.

In Chapter 2 we showed that GK has an anisotropic response to mechanical stresses. It would be also an interesting topic for RLuc though now we can only construct one RLuc-DNA chimera.

4.5 RLuc-DNA Chimera as a Biomolecular Detector

Here, we demonstrate the RLuc-DNA chimera as a molecular probe for the detection of specific DNA sequences. RLuc and other Luciferases are of course commonly used as bioluminescent reporters in studies of gene expression and regulation. The advantage of using a luciferase reporter gene is that bioluminescence is typically not endogenous to the cell of interest, and that the corresponding assay is sensitive, quantitative and easy. A molecular probe based on Luciferase retains these advantages, and the present construction represents one such probe.

4.5.1 Sensitivity in Detecting the Target DNA

We now demonstrate the use of the Luciferase-DNA chimera as a molecular probe. The target is the 60mer DNA sequence complementary to the chimera DNA; the RLuc-DNA chimera (in ligated, ss form) is the probe. The following is the condition of the measurements. Luminescence measurements were conducted for ligated RLuc-DNA chimera mixed with different concentrations of DNA 60mer, from 500 pM to 1 μM. The estimated chimera concentration was 2 nM (see Determination of concentration section). The luminescence intensities were integrated over two minutes and normalized by the integrated luminescence of the ligated, unhybridized RLuc-DNA chimera sample.

Fig. 4.9(a) shows the time course of luminescence measurements in a 40 μL sample volume containing approximately 2 nM RLuc-DNA chimera probe and varying amounts of the target oligo, reacting with 160 μL substrate solution that the final substrate concentration is 1 μM. As the fraction of chimera hybridized to the target increases, luminescence decreases. The fraction of chimera hybridized is given, in this case, essentially by the stoichiometry, because the dissociation constant of this 60mer duplex is much smaller than 2 nM, the probe concentration in these measurements. This is shown in Fig. 4.9(c), where the luminescence signal

(reported here as the area under the curves of Fig. 4.9(a)) is seen to decrease linearly down to its asymptotic minimum value (see also Fig. 4.9(b)). This minimum value is not zero because the DNA spring is not stiff enough to completely shut down the enzyme [20]. Since the dynamic range of this probe is roughly a factor 2 in light intensity (Fig. 4.9), the detection limit in this particular format, in terms of amounts of target, is given essentially by the smallest amount of RLuc detectable with a signal/background of order 1, with the detector one is using. With our commercial luminometer, this is roughly 10 fmole. Of course, the concentration of the target must also be large enough that hybridization to the probe occurs.

4.5.2 SNP Detection

We also tested the sensitivity of the RLuc-DNA probe in detecting mismatches in the target DNA. To this end, we used two 60 bp target strands carrying one and three (consecutive) mismatches at the center (oligomers 1MC and 3MC, see Sec. 4.2.2). Fig. 4.10 shows that a single mismatch is easily detected by comparing the luminescence level with that of the chimera hybridized to the true complementary. Several mismatches are even more easily detected. It is apparent that this probe has a peculiar sensitivity to localized defects in the DNA spring, which may release the mechanical tension.

Here we show that this RLuc-DNA probe is capable of detecting a single-base mismatch at the center of a 60mer target DNA.

Here is the condition for mismatch detection experiment. RLuc-DNA chimera was incubated alone or with different target DNA, including 60mer, 1MC and 3MC, in PBS (pH=7.4) with 0.4mg/ml BSA. The concentration of chimera and DNA were 2 nM and 5 nM, respectively. The luminescence measurements were conducted as described in the Sec. 4.2.7.

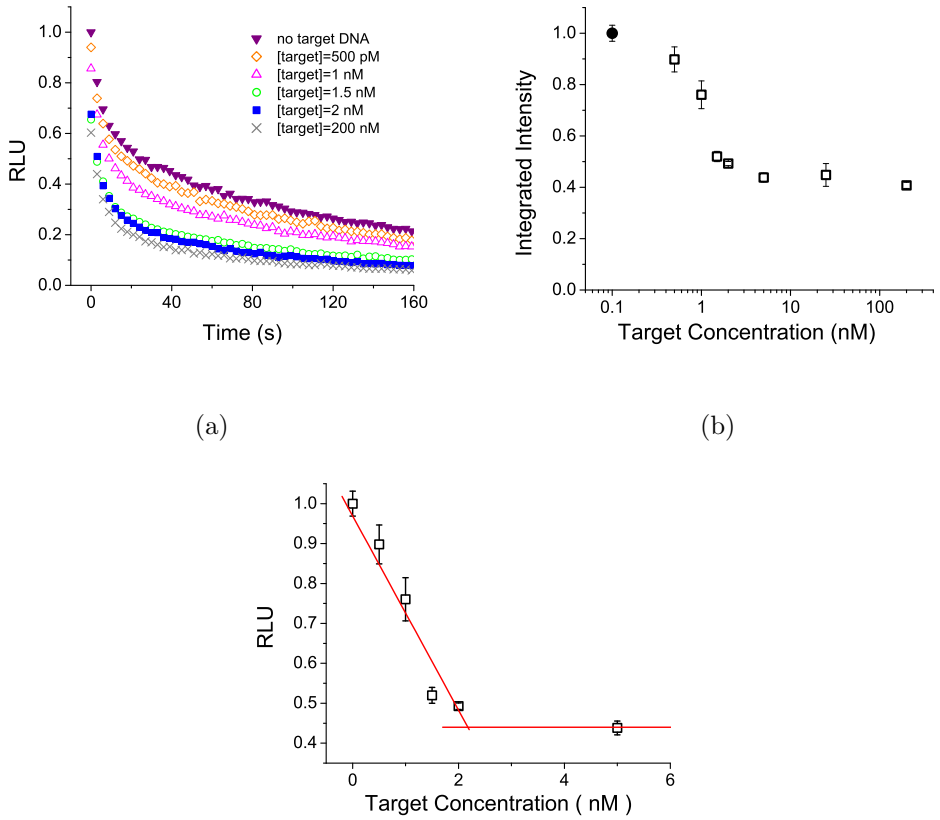

(a) (b)

(c)

Figure 4.9: The RLuc chimera as a molecular probe. The figure shows the results from a titration experiment where different amounts of target DNA (the 60mer complementary to the chimera DNA) are added to samples of the RLuc chimera; different amount of target varying from 0.5 to 200 nM concentration in 40 μL incubation volume were incubated overnight with the chimera at 2 nM concentration. To start the reaction, these samples were mixed with 160 μL substrate solution for a final substrate concentration of 1 μM.
(a) Time courses of the luminescence intensity for the ligated RLuc-DNA chimera mixed with different final concentrations of target 60mer, from 500 pM to 200 nM in the 40 μL incubation volume. (b) The integrated luminescence intensity (area under the curves in (a)) over two minutes for the chimera with different target concentrations, normalized by the intensity without target DNA. The solid circle represents the result without target DNA. (c) The same data as in (b) plotted on a linear concentration scale, showing that the integrated intensity decreases linearly with the concentration of target DNA until it saturates. Thus the fraction of hybridized chimera is stochiometric with the target in this regime of concentrations. The lines are linear fits for the linear decrease and saturated regions. The intersection provides a good estimate of the actual chimera concentration in the experiments.

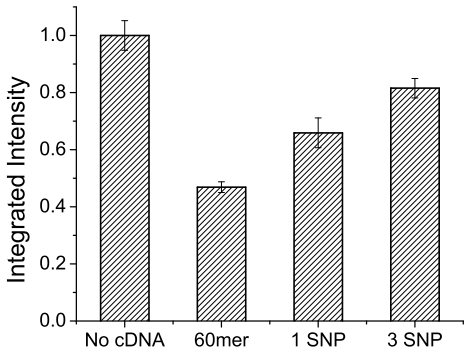

Figure 4.10: SNP detection with the RLuc chimera. We show the integrated luminescence intensity for the ligated chimera mixed with different targets. The results are normalized by the integrated intensity of the chimera alone (no target DNA). 1SNP and 3SNP represent the chimera hybridized with target 1MC and 3MC, having one mismatch and three consecutive mismatches in the center of the DNA spring, respectively. The conditions were: chimera concentration 2 nM and DNA target concentration 5 nM, incubation volume 40 μL. The figure shows that a single mismatch at the center of a 60mer target can be detected with this probe without the need to compare different temperatures.

4.5.3 Other Biomolecular Detectors

It is not our purpose here to present a detailed comparison with other DNA detection assays; we merely mention that other homogeneous assays, such as the molecular beacons [45, 46, 47] and the enzyme-DNA-inhibitor probe of Saghatelian et al [23] are not bio-luminescence based, while other sensitive detection schemes such as cyclic voltammetry [48], scanometric DNA array[49] and Electrochemical DNA sensors [50, 51, 52] are surface bound. As regards SNP detection, for existing assays the hybridized sequence is shorter than 20 bp, while our longer 60 bp construct presumably should translate to the ability of detecting mismatches at very low target concentrations. Ours is also, we believe, the only homogeneous

assay where SNP detection is achieved without some form of melting curve analysis.

4.6 Feasible Improvements: Making a New Detector

We show that the Rluc-DNA chimera can be engineered to be a sensitive detector which is easy to operate *in vitro*. However, the limitations are the turnover number and the fast inactivation of RLuc which may be an obstacle to the applications *in vivo*. Here, we provide some possible methods which may improve things in practice and create a better biomolecular sensor.

4.6.1 Other Mutants of RLuc

We have tested several mutants of RLuc, nevertheless, none of them has been successfully constructed into an RLuc-DNA chimera yet. Table 4.2 lists the mutants we have tried and the progress so far.

On the other hand, besides experimental exploration, it would be useful to have theoretical predictions for "hotspots"[53] on the surface of the enzyme where an applied stress has a large effect, if such spots exist. Different approaches to this question have been proposed, based on phylogenetic analysis [53, 54, 55] and MD simulations [56, 57]; we expect the dialogue between numeric analysis and experiments to intensify as more measurements with the enzyme-DNA chimeras become available.

4.6.2 RLuc8 and Firefly Luciferase

There are several alternative luciferases which might improve the utilizations of luciferase-DNA detectors. Rluc8, a mutant of Renilla luciferase having 8 mu-

Table 4.2: Progress of chimera construction for RLuc mutants. Here we list all the mutants we tested and the progress and the problems of turning them into chimeras. All the cysteine residues in the mutants are listed.

Mutant	**Cysteine**[a]	**Progress / Problems**
RF5	24, 73, 124, 184, 227	We constructed a two-armed chimera, which shows little effect when hybridized with the complementary DNA. However, we have not tried to ligate the 2R chimera and do not know if there will be an effect on the enzyme activity when a larger stress is applied.
RJ4	124, 161, 268	The product of protein expression is of a higher molecular weight ($\sim$ 80 kD), which is suspected to be in a dimer form. However, adding a reducing agent, such as βME and TCEP, does not change the molecular weight, which is checked by SDS gel.
RG1	24, 73, 124, 173, 268	We successfully expressed the protein but have not constructed the chimera yet.
RI3	124, 173, 268	We have not tested this mutant yet.
RK2	124, 184, 268	We have not tested this mutant yet.
RL1	24, 124, 173, 264	We have trouble in protein expression for this mutant.
RM3	73, 124, 161, 268	We successfully expressed the protein but have not constructed the chimera yet.

[a] The Cysteine residues in wild-type RLuc are residue 24, 73, 124. The highlighted residues are the attachment points for the DNA spring.

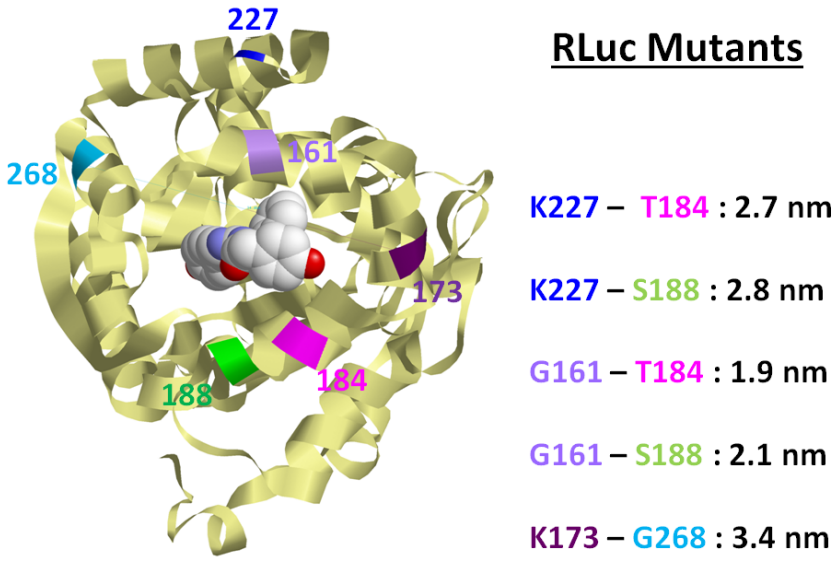

Figure 4.11: Visualization of the residue positions for DNA arm linkage of the different chimeras listed to Table 4.2. The distances between a specific pair of attachment points are listed on the right of the figure. The information about the spatial positions of attachment points on the RLuc surface may be helpful in designing a new chimera.

tated amino acids, may be the best choice since it is 200-fold more resistant to inactivation and exhibits a 4-fold better light output [38, 42]. Beetle luciferases, including firefly luciferases, may also be good options since they are versatile and have a variety of luminescence colors. One mutated site on firefly luciferase can lead to a change in luminescence color from yellow-green to red because of the variation in the hydrophobic microenvironment around the active site [58]. Therefore, a stressed firefly luciferase may display a different emission color instead of a change in intensity, which can be adopted as a subtle detector as well.

4.6.3 Using DNA Binding Enzyme as a Target

RLuc shows a significant drop in luminescence intensity when the nick of the DNA spring is repaired, leading to the idea that the RLuc-DNA chimera may be capable of detecting any binding events that changes the rigidity of the spring. For example, a protein that binds and holds the nick will cause a change in luminescence intensity (Fig. 4.12).

Among DNA-binding proteins, Ligase may be a good option for demonstration purposes. since Ligase has non-specific, i.e. sequence independent, interactions with DNA. Restriction enzymes[59] are other candidates, where the DNA spring needs to be designed such that the sequences around the nick can be recognized by the restriction enzyme. Of course, the most important requirement is that the enzyme binds but does not cleave DNA unless triggered or to the contrary, the enzyme can be inactivated by inhibitors. For instance, BamHI is a good option for the first trial because it can be inhibited by Ca^{2+} [60].

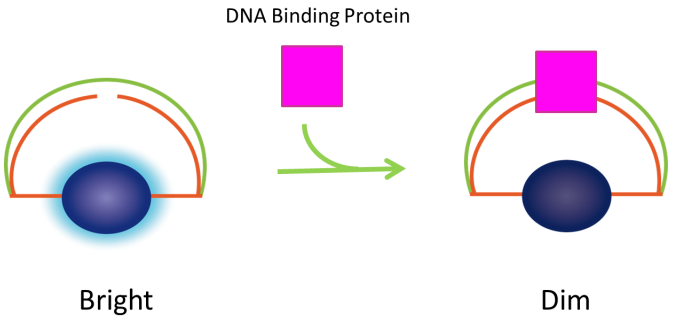

Figure 4.12: Schematic of using a DNA-binding protein to reduce the luminescence intensity of an RLuc-DNA chimera. Binding of a DNA-binding protein to the nick of the DNA spring may rigidify the spring and cause a decrease in luminescence intensity.

4.6.4 Double-spring Chimeras

Double-spring chimeras are RLuc-DNA chimeras having DNA arms with a fork-like structure, where the crosslinker is conjugated to the middle of the DNA arm (Fig. 4.13). In principle, double-spring chimeras should be capable of detecting two different target cDNAs. With a nick at the center of the DNA spring, the activity of the RLuc-DNA chimera decreases slightly (see Sec. 4.3.1), which is a small but detectable signal. We expect that the double-spring chimera has a similar behavior upon hybridization with one cDNA, however, when hybridized to both cDNAs, the activity will decrease even further. The difference between these two cases allows us to design double-spring chimeras as a Boolean logic gate to differentiate NOT, OR and AND operations. For Boolean algebra of two conditions, NOT means none of the conditions is satisfied, while OR means one of the conditions is satisfied and AND means both conditions are satisfied.

Fig. 4.13 shows the concept of using double-spring chimeras as a Boolean logic gate to detect the presence of target cDNAs. In the absence of any target DNA, the double-spring chimera works normally and the luminescence intensity is high;

in the presence of either target DNA, the luminescence intensity decreases while when both target DNAs appear, the luminescence intensity becomes even dimmer . In analog to Boolean algebra, the bright signal means NOT, the intermediate signal means OR and the dimmest signal means AND. With this design, the double-spring chimera may be a potential computing artificial biomaterial since Boolean logic is the basis of computer-based computation. This is not an irrational and crazy idea. Several principles of the design of logic gates in living cells have been proposed recently [61, 62].

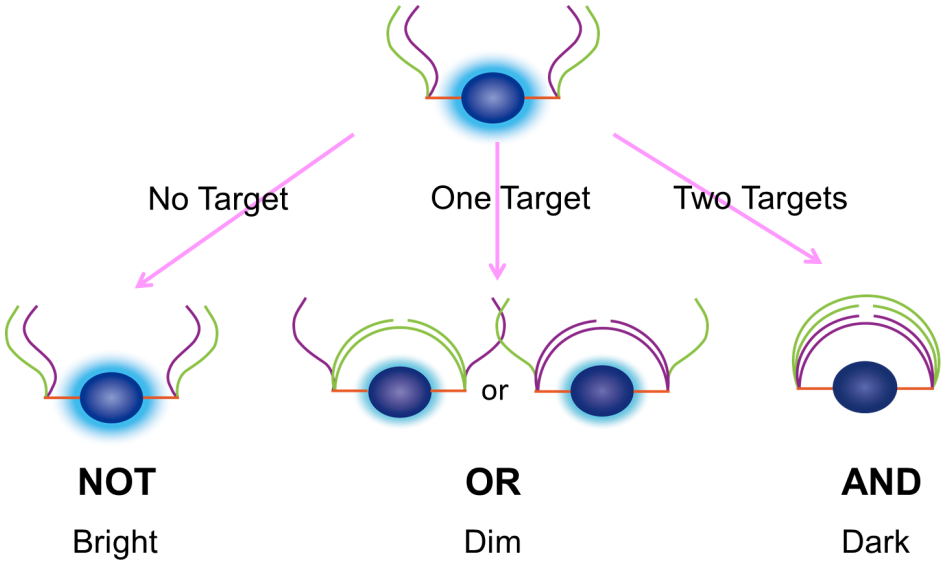

Figure 4.13: The concept behind use of double-spring chimeras as Boolean logic gates. The luminescence intensity (LI) of the chimera will change in response to the presence of the targets, which are the cDNAs of the two pairs of DNA arms (green and purple, respectively). In the absence of any target, the luminescence intensity of the chimera remains intact. With the presence of either of the targets, the LI decreases due to the stress induced by the rigidification of the DNA spring. When both the targets appear, the stress increases even further, leading to an even dimmer luminescence intensity. In this manner, the presence of the target DNA may be detected by the corresponding luminescence intensity of the chimera.

4.6.5 Incorporation of Aptamers into RLuc Chimeras

Future work may address the question of whether the present probe, or derivations thereof, can be useful for *in vivo* detection inside the cell, and whether incorporating aptamers in the DNA spring [63, 64, 65] can lead to a more general design of small molecules detectors.

Aptamers are single-stranded DNA or RNA oligonucleotides that bind to a specific molecule. Currently, more and more people use aptamers as molecular recognition elements instead of antibodies because there are several advantages. First, they are easier and more economical to produce. Second, they are also capable of greater specificity and affinity than antibodies [66]. Moreover, a wide variety of targets have been discovered, including small molecules [67], proteins [68], viruses [69], and whole cells [70]. The combination of the RLuc-DNA probe with aptamers, where the presence of aptamer targets can be detected merely by the change in luminescence of the probe, may lead to versatile applications for sensing and diagnostic purposes, as well as eventually, *in vivo* applications. There are other aptamer-based biosensors, such as Electrochemical DNA sensors [50, 51], however, they are surface-bound and more complicated to prepare and measure.

In order to obtain a probe which can detect a variety of targets in an easy and simple method, there are several technical challenges to be solved to make a practical RLuc-aptamer probe. For example, can binding of the target provide a sufficient change in stiffness of the DNA spring to alter the luminescence of the luciferase? Is there a requirement in aptamer-target structure to create a signal? What would the proper length of the DNA spring be in order to optimize the signal when binding with a target? Delicate designs of the DNA spring and trial and error would be essential and necessary to fulfill this goal.

To test the practicality of RLuc-aptamer probe, one can synthesize RLuc-DNA

chimeras where the ss DNA molecular spring contains an aptamer sequence. For an initial demonstration, one might start with the following three aptamers:

1. Aptamer of cocaine: 5'-GGGAGACAAGGAAAATCCTTCAATGAAGTGGG-TCGACA-3'. This aptamer binds to cocaine with $K_d = 0.4$ μM [71].

2. Aptamer of dopamine: 5'-GTCTCTGTGTGCGCCAGAGAACACTGGGGCA-GATATGGGCCAGCACAGAATGAGGCCC-3'. This aptamer binds to dopamine with $K_d = 0.4$ μM [72].

3. Aptamer of human thrombin: 5'-GGTTGGTGTGGTTGG-3'. This aptamer binds to human thrombin with $K_d = 0.025$-0.2 μM [73, 74].

We think Human Thrombin is the best sample to start with because of several reasons. First, it has a molecular weight of 37 kD, enabling to check the efficiency of aptamer-Thrombin binding by using gel electrophoresis to separate the aptamer-bound and unbound Thrombin. Second, the structure of Human Thrombin-aptamer complex has been solved by X-ray crystallography. The visualization of structure is helpful in designing an aptamer incorporating DNA arm. Third, there are already many aptamer-based assays, such as aptamer microarrays, designed to detect Human Thrombin, providing abundant useful information in designing an aptamer-incorporating DNA spring.

On the other hand, cocaine and dopamine are molecules of interest on biosensor targets because of the health effects of cocaine abuse and the effects of dopamine in brain processes. The successful detections of these molecules using aptamer-incorporating RLuc-DNA chimeraa will lead to immediate applications.

CHAPTER 5

Nonlinear Dynamics of Molecules

In Chapter 3 and 4 we demonstrated the manipulation of enzymatic activity using a DNA molecular spring on two entirely different types of enzymes, Guanylate Kinase (GK) and Renilla Luciferase (RLuc). These studies showed that the DNA molecular spring is indeed a general method to control enzymatic activity. The measurements of the GK and RLuc chimera are similar in that the enzymatic activity decreases drastically when the nick in the DNA spring is repaired. As we now understand that repairing the nick merely rigidifies the DNA spring slightly, then from where does this large change in enzymatic activity arises?

In a chimera, the protein and the DNA are mechanically coupled, where the DNA is bent and the protein is mechanically deformed. In this chapter, we explore the enzyme's mechanics by studying the coupling of the enzyme and the DNA of the RLuc chimera. The enzymatic response for different states of stress suggests that the enzyme undergoes a softening transition beyond a few Å deformation, similar to the softening behavior of the DNA spring beyond the elastic regime. Additionally, we find that the sensitivity of the chimera to small changes in the stiffness of the DNA spring arises from the combination of the mechanical nonlinearities of the DNA spring and the protein.

5.1 Introduction

5.1.1 Exploring the Nonlinear Dynamic Regime by Using DNA Molecular Springs

The catalytic reactions are often accompanied with conformational motions in enzymes. One nanometer scale conformational motion is not uncommon for an overall $\sim$ 5 nm enzyme size [4, 75, 76, 77, 78, 79], while motor proteins such as kinesin and myosin exhibit far larger conformational changes still. Such large motions must take place in beyond linear elasticity regime. It is therefore of considerable interest to understand the mechanics of these molecules beyond linear elasticity.

We explore this regime of mechanical perturbations using the RLuc-DNA chimera (see Chapter 4). The different states of stress are obtained by varying the length of the DNA spring and its state of hybridization (Fig. 5.1(c)). In this chapter we use two kinds of chimeras: RLuc with a 40mer spring and RLuc with a 60mer spring. Here, we use the 60mer chimera as an example. In ss chimera, i.e. RLuc with one ss DNA strand attached by two ends on the enzyme surface, there is no stress; in ds chimera with nick, i.e. the ss chimera hybridized with two sperate 30mer DNA, there is little stress due to the nick; in ds chimera no nick, i.e. the ss chimera hybridized with a 60mer complementary DNA, the stress is large. The enzymes' responses to different stresses are measured via the luminescence intensity.

The elastic energy of the system can be obtained using the elastic energy driven polymerization method (see Sec. 3.3.1), however, the elastic energy partitioning is still unclear. To make progress and disentangle the energy in the protein and DNA molecule, we first need a more accurate description of the DNA spring.

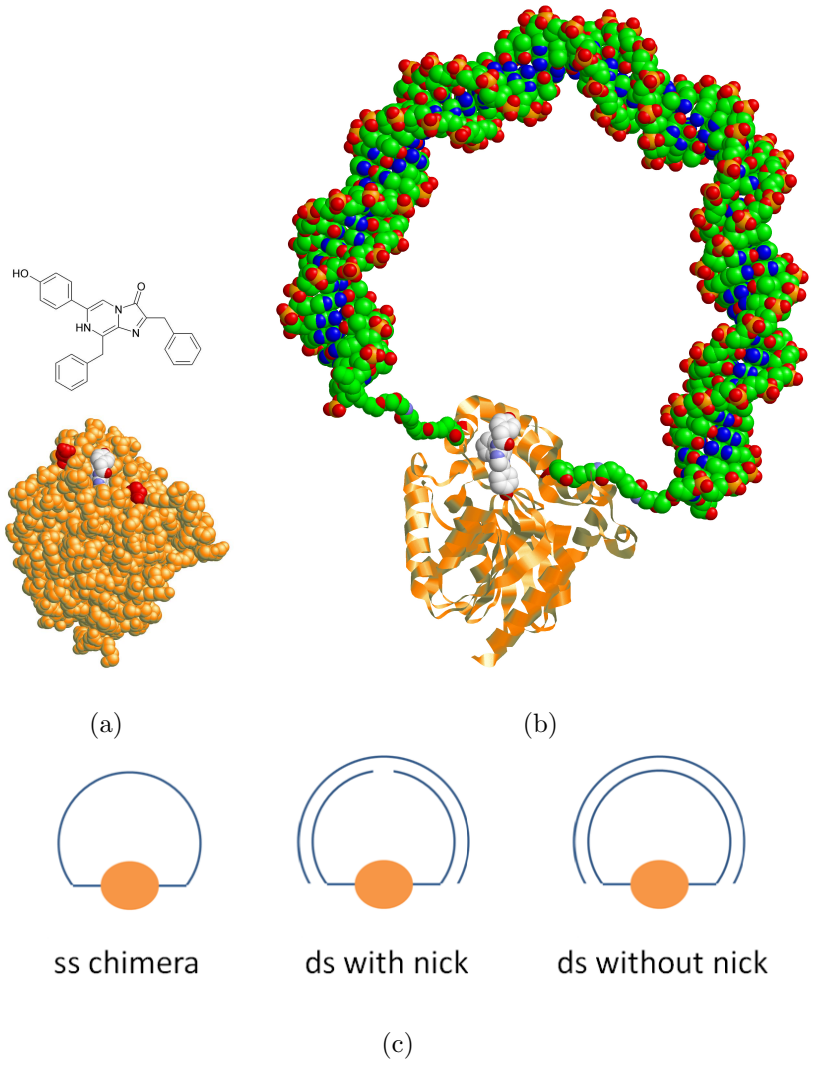

Figure 5.1: (a) Crystal structure of Renilla luciferase with bound substrate (coelenterazine) from the PDB structure 2PSJ. Residues 161 and 188, mutated to cysteins in the experiment, are colored red. The distance between these two residues is $\sim 2\,nm$. (b) Cartoon of the RLuc-DNA chimera with the DNA spring attached to sites 161/188. The RLuc structure is from PDB 2PSJ and DNA is from the nucleosome structure 1KX5. The protein, DNA, and cross-linkers are drawn approximately to scale. (c) Sketch of the different forms of the RLuc chimera used in this study. The ss chimera is under no stress, ds with nick under a small stress, ds without nick under a larger stress.

5.2 Elastic Energy of a Bent DNA

5.2.1 The Worm-like-chain Model

In large scale, the behavior of ds DNA can be well described by the worm-like-chain (WLC) model, which accounts for both the elastic energy and entropy of polymer chains. The bending elastic energy in the WLC language is the same as that of a thin rod in the linear elasticity regime:

$$E_{WLC} = \int_0^{2L} \frac{1}{2} \frac{B}{R^2(s)} \, ds \tag{5.1}$$

where B is the bending modulus, $2L$ the contour length of the ds DNA, R the radius of curvature and s the arc length along the rod. B is associated with the persistence length l_p, which is the length over which a polymer is basically straight, through a simple relation:

$$B = k_B T \times l_p \tag{5.2}$$

Under normal conditions, the persistence length of a ds DNA is $\sim$ 50 nm or 150 bp [13] while that of a ss DNA is $\sim$ 0.8 nm or 3 bp [11, 12].

Single molecule experiments, such as atomic force microscopy (AFM), optical tweezers and magnetic tweezers, are widely used to investigate the force-extension relation of a ds DNA (or a ss DNA). An interpolation formula, which is called the Marko-Siggia expression [11, 80],

$$\frac{F l_p}{k_B T} = \frac{1}{4(1 - \frac{x}{L})^2} - \frac{1}{4} + \frac{x}{L} \tag{5.3}$$

permits an evaluation of the extension x at a worm-like chain at an applied force. Though the results of single molecule force-extension experiments on $\sim$10 kbp DNA follow the WLC model to a great extent, this description must break down at small DNA scale.

5.2.2 Bending Behavior of a Short Piece of DNA

Many experiments demonstrate that a short piece of DNA is more flexible than predicted by the WLC model, where high-curvature configurations of DNA are involved when the DNA is bent. The cyclization efficiency measured in cyclization experiments of short DNA fragments, where different sizes of DNA fragments are ligated into circles, presenting indirect measurements of the bending energy of DNA, was much larger than theoretically expected [81], suggesting the development of sharp kinks in ds DNA [82, 83]. The AFM study by Wiggins et al. [84] also reported a softening transition of the DNA at small scale, where the energy depends on the bending angle linearly, rather than quadratically as deduced from the WLC model.

Contrary to the cyclization and AFM experiments, where the high energy states are generated by thermal fluctuations and thus statistically rare, we used a different approach to investigate the bending of short DNA [28, 29]. This method is similar to the elastic energy driven polymerization (see Sec. 3.3.1) but now the stretched part is a ss DNA strand instead of a protein. (Fig. 5.2) The structures can be fulfilled by hybridizing two ss DNA strands which are partially complementary to each other. With hybridization, a nick is generated in the middle of the ds part, allowing formation of dimers to release internal stress. The elastic energy in the molecule can be determined using Eq. 3.3:

$$2F_{el} = k_B T \ln\left(\frac{X_D}{{X_M}^2}\right)$$

and analyzing the monomer-dimer population obtained from gel electrophoresis. For constant ds DNA N_d and increasing length of ss DNA N_s, the ss spring becomes softer when the end-to-end distance (EED) z increases, and one obtains the total energy curve shown in Fig. 5.3. The transition in the energy curve corresponds to the formation of a kink in the ds DNA, where to the right of the transition, the ds DNA is smoothly bent while to the left it is kinked. The re-

sultant analytic expression of the elastic energy of a short ds DNA, given in [29], is:

$$E_{DNA}(z) = \begin{cases} \tau_c \; arccos(\dfrac{z}{2R}) & for \; 0 < z \leq z_c \\ \dfrac{5B}{L}\dfrac{z_0 - z}{2L} - T \; ln(\dfrac{2L - z}{2L - z_0}) & for \; z_c < z < z_0 \end{cases} \tag{5.4}$$

Here, B is the bending modulus for DNA linear elasticity (B = 200 $pN \times nm^2$), τ_c is the critical bending torque for kink formation, z is the EED of the DNA, $2L = 0.33 \times N_d$ is the contour length of the DNA, and $R = L(1 - 2\gamma^2/45)$, $z_0 = 2L(1 - LT/5B)$, $\gamma = L\tau_c/2B$. The upper form corresponds to the DNA being kinked, the lower to smoothly bent DNA. The critical EED z_c at which the DNA kinks is found by equating the upper and lower expressions.

This elastic energy function exhibits a softening transition governed by two parameters: the bending modulus for DNA linear elasticity B, and the critical bending torque for kink formation in DNA τ_c. The critical torque τ_c= 27 $pN \times nm$ with a nick [28, 29] and $\approx$ 31 $pN \times nm$ when the nick is repaired [30].

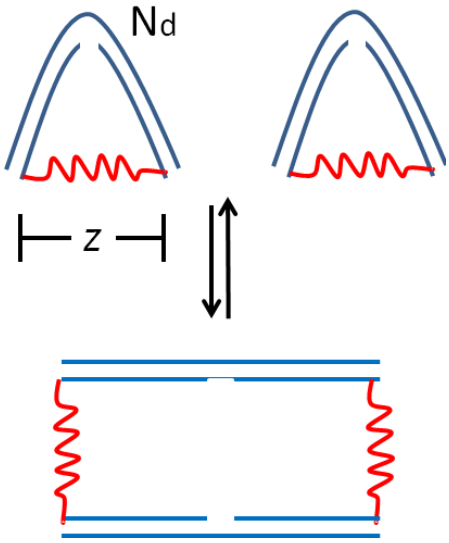

Figure 5.2: Sketch of the monomer-dimer equilibrium. The configuration on the top (i.e. a monomer) consists of two ss DNA which are partially complementary to each other. N_d is the number of bases in the ds part. In the monomer, the ds part is bent while the ss part is stretched. On the other hand, the formation of dimers will reduce the elastic energy and the entropy as well. The equilibrium is reached by a balance between the elastic energy and the entropic cost. Therefore, the elastic energy can be calculated by determining the population of monomers and dimers in equilibrium.

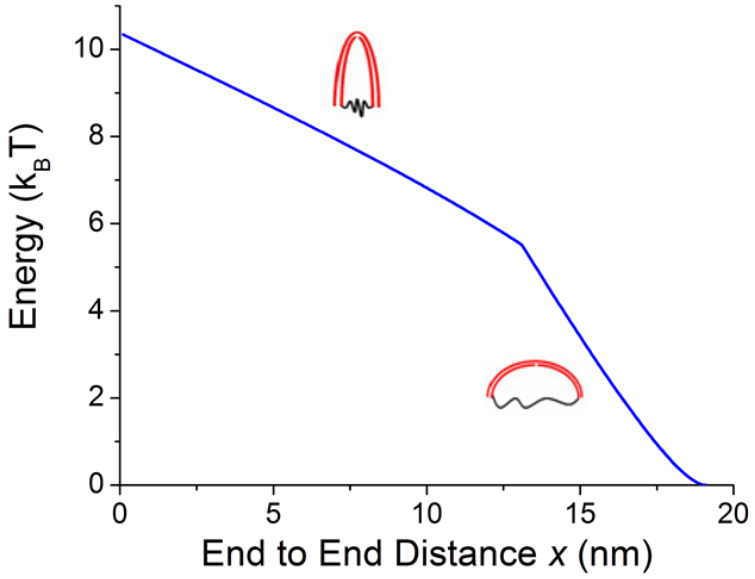

Figure 5.3: The elastic energy of a bent 60 bp ds DNA vs the end-to-end distance (EED) z of the DNA. This plot is generated by using Eq. 5.4, where the elastic energy function exhibits a softening transition governed by two parameters: the bending modulus for DNA linear elasticity B, and the critical bending torque for kink formation in DNA τ_c. Before the critical bending (i.e. $\tau < \tau_c$), the DNA is smoothly bent; after the critical bending, the DNA is kinked. The parameter values for this graph are: B = 200 $pN \times nm^2$ and τ_c= 27 $pN \times nm$.

5.3 Measurements of GK and RLuc Chimeras

5.3.1 Common Feature of the Activity Measurements

In both GK and RLuc chimeras, we observed that there is little effect on the enzymatic activity with a nick in the middle of DNA spring while repairing the nick increases the inhibition drastically (see Sec. 3.2 and 4.3.1). However, according to the discussion in Sec. 5.2.2, now we know that repairing the nick of the DNA spring merely increases the stiffness of the DNA slightly. Then, what is the mechanism accounting for this feature that the small change in DNA spring leads to the big change in enzymatic inhibition?

5.3.2 Two RLuc Chimeras with Different DNA Spring Lengths

In order to answer this question, we measure the response of the RLuc chimera to different states of stress. More specifically, we compare measurements with two different chimeras, made with DNA springs of length 40 and 60 bases, respectively, and we compare different states of hybridization of the DNA spring (Fig. 5.1(c)).

Fig. 5.4 shows the time courses of luminescence intensity for the RLuc60 and RLuc40 chimeras in three different hybridization forms: ligated ss (no stress: circles), ds nicked (small stress: diamonds), ds non-nicked (larger stress: squares). The nicked spring has a small effect on the activity of the enzyme, while the non-nicked spring slows down the enzyme drastically. Control experiments where the two-armed chimera is hybridized with two separate complementary strands (i.e. the DNA spring is disjointed so there is no stress) show that the mere presence of DNA in close proximity to the enzyme does not affect the activity [85].

The time course of the reaction (Fig. 5.4) is unusual because this enzyme becomes inactive after an average number of catalytic cycles of about 100. In addition, the product of the reaction is an inhibitor (it binds the active site rela-

tively strongly). We have already discussed these dynamics in detail in Sec. 4.3.1. In the following we use an integrated measure of activity, namely the area under the curves of Fig. 5.4 (from t = 0 to t = 120 s) as a single number reporting on the enzymatic activity (Fig. 5.5). Normalizing the activity A of the chimera in the absence of stress (ligated ss chimera) to 1 ($A(\text{ss}) = 1$) we find, for RLuc40:

$A(\text{nicked}) = 0.72 \pm 0.08$; $A(\text{ds}) = 0.15 \pm 0.01$

where ds stands for the double stranded non-nicked chimera (Fig. 5.5(b)). For RLuc60 the corresponding measurements, previously reported in Sec. 4.3.1, are:

$A(\text{nicked}) = 0.83 \pm 0.03$; $A(\text{ds}) = 0.36 \pm 0.01$

(Fig. 5.5(a)). Thus in both cases "repairing the nick" has a large effect on the enzyme's activity even though we believe that it increases the stiffness of the DNA spring only slightly [86, 87].

Intuitively, our first thought was to represent the protein as a linear spring. However, this assumption led to results that were incompatible with the experimental data, which we will discuss in Sec. 5.5.3. In the following, we try to interpret these measurements quantitatively using a model of two coupled nonlinear springs.

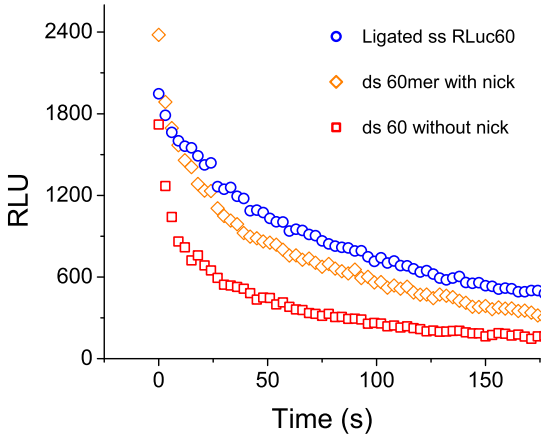

(a)

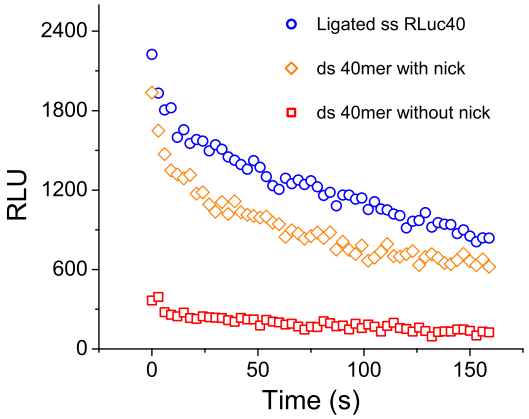

(b)

Figure 5.4: Time courses of luminescence intensity (arbitary units) of (a) the RLuc60 chimera and (b) the RLuc40 chimera for different states of mechanical stress. Blue circles: ligated ss chimera (zero stress); orange diamonds: ds chimera with nick (small stress); red squares: ds chimera with no nick (larger stress). Luminescence intensity is proportional to the reaction speed. The latter decreases over time due to combinational effects (Sec. 4.3.1): substrate consumption, product inhibition, and inactivation of the enzyme after a number of $\sim$100 turnovers. The conditions are: chimera concentration 2 nM, initial substrate concentration 1 μM. On the scale of this graph, the background of the measurement is essentially zero.

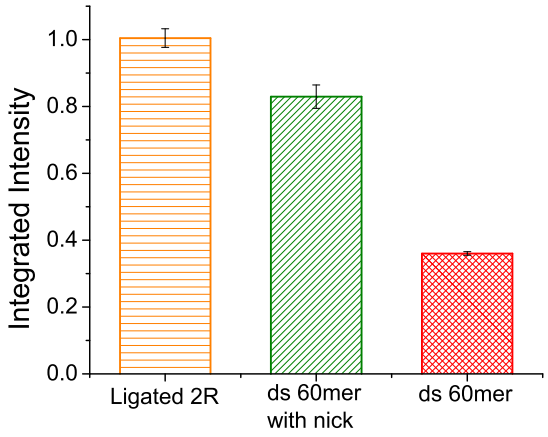

(a)

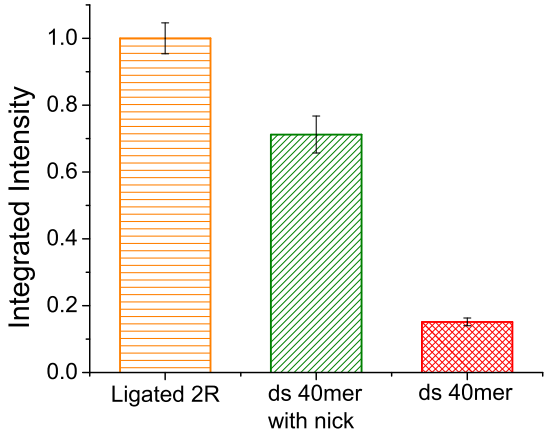

(b)

Figure 5.5: Integrated luminescence intensity (area under the time course curves of Fig. 5.4 from t =0 to t = 120 seconds) for different chimeras. (a) Ligated RLuc60 chimera, ss (no stress), ds with nick (small stress), ds without nick (larger stress). The intensity for the ss chimera is normalized to 1. (b) Ligated RLuc40 chimera with the same DNA spring configurations as in (a). The 40mer spring leads to more drastic inhibition to the enzyme compared to the 60mer spring. In both cases, "repairing the nick" in the DNA spring has a large effect on the activity of the enzyme. The error bars are standard deviations from three measurements for each construction.

5.4 A Model of Two Coupled Nonlinear Springs

The bending behavior of the DNA spring can be described well using Eq. 5.4. However, how should we interpret the protein spring? Can we use this knowledge of DNA to figure out some feature of the mechanics of the protein? The simplest thought is to represent the protein as a linear spring, nevertheless, it is insufficient to account for the measured response of the enzyme (see Sec. 5.5.3). Then what kind of nonlinearity will account for the experimental results?

In this section we will demonstrate that if we interpret both the DNA and the protein as a nonlinear spring, which displays a softening transition beyond the elastic regime, the large change in activity when the nick in the DNA is repaired can be derived accordingly.

5.4.1 DNA Spring and Protein Spring

We start from the assumption that continuum mechanics models may be appropriate for describing the response of biomolecules to external forces, in contrast to two-states (or few-states) models [88] which are frequently used to discuss protein dynamics. The measurements of Fig. 5.4 can not be reconciled with a two-states model (the individual enzyme is either folded, with activity 1, or unfolded, with activity 0) because the shape of the time course curves is very different for different stresses; we have already analyzed these shapes in [85]. The same conclusion can be drawn from our previous work with the Guanylate Kinase - DNA chimeras [21, 16]. At the level of models, the continuum mechanics point of view is supported by a number of successful implementations in the past, for instance the WLC model of DNA mechanics [11], the critical bending torque (CBT) model of DNA kinking [28, 29, 30], not to mention effective Hamiltonian models, such as the Peyrard-Bishop- Dauxois (PBD) model of DNA melting [89].

We use Eq. 5.4

$$E_{DNA}(z) = \begin{cases} \tau_c \; arccos(\dfrac{z}{2R}) & for\ 0 < z \leq z_c \\ \dfrac{5B}{L}\dfrac{z_0 - z}{2L} - T\ ln(\dfrac{2L - z}{2L - z_0}) & for\ z_c < z < z_0 \end{cases}$$

to describe the molecular DNA spring and plot this elastic energy function in Fig. 5.6 (pink curves).

For the enzyme, we assume an elastic energy function exhibiting a similar softening transition: a parabola up to a critical value of the deformaion x_e which then softens into a straight line:

$$E_{prot}(x) = \begin{cases} \dfrac{1}{2}Kx^2 & for\ 0 < x \leq x_e \\ \dfrac{1}{2}K{x_e}^2 + f_e(x - x_e) & for\ x > x_e \end{cases} \tag{5.5}$$

Here x is the deformation of the enzyme, and the parameter f_e which multiplies $(x - x_e)$ is the restoring force in the soft regime of this spring. This energy function is also shown in Fig. 5.6 (blue curve).

Now, how should we couple the DNA and the protein springs?

5.4.2 Energy Function of the Coupled Springs

Here we couple the DNA spring and the protein spring by enforcing the constraint that if the "enzyme spring" has EED $\Delta + x$, where $\Delta = 1.9$ nm is the distance between the Cys residues where the DNA spring is attached, measured on the protein's structure, then the "DNA spring" has EED $z = \Delta + 2H + x$, where H = 2.1 nm is the effective length of one cross-linker (linking the DNA to the Cys residue) and z is the argument of Eq. 5.4. We write the energy of the system as

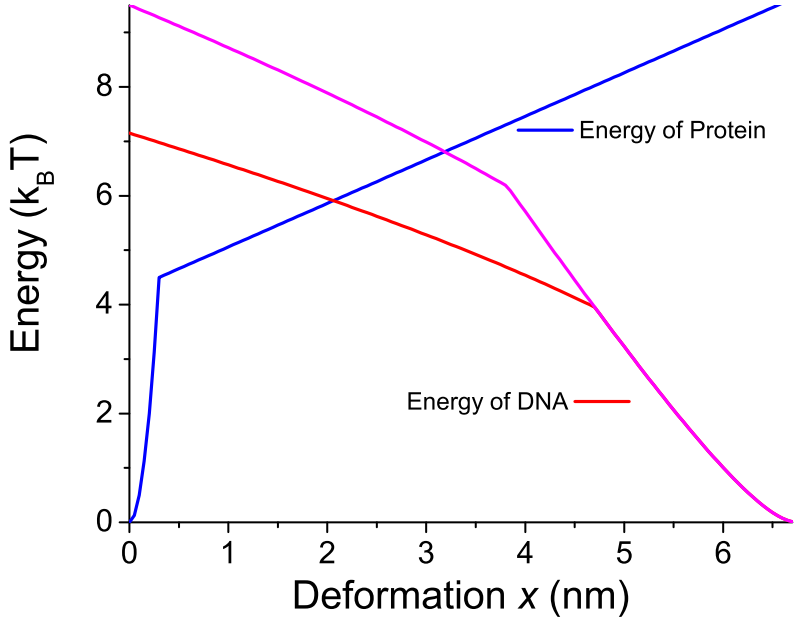

Figure 5.6: Elastic energy vs. deformation of the enzyme x, for the protein (blue) and the 40mer DNA spring (red and pink). The curves are plots of eqs. (1) and (2), respectively, and represent the model. The parameter values for this graph are: spring constant of the protein $K = 100\ k_BT/nm^2$, $x_e = 0.3$ nm, restoring force of the protein in the soft regime $f_e = 0.8\, k_BT/nm$, critical bending torque of the DNA $\tau_c = 27$ (red) and 36 (pink) pN $\times$ nm. The energy function of the DNA spring has been directly measured in experiments [27, 28, 29]. For the enzyme, we assume a similar softening transition beyond the parabolic regime.

a function of the deformation of the enzyme, x :

$$E(x) = E_{DNA}(\Delta + 2H + x) + E_{prot}(x) \tag{5.6}$$

and compute the partition sum:

$$Z = \int_0^{2L-(\Delta+2H)} e^{-E(x)/T}\, dx \tag{5.7}$$

From Z we obtain the thermodynamic quantities in the usual way, in particular we compute the elastic energy in the enzyme $E_p =< E_{prot} >$ and the enzyme deformation $< x >$. Now from the energy function in Fig. 5.6 it is clear that the ratio of the slopes in the soft regime for the enzyme spring and the DNA spring decides whether the system spends most of the time with a small $< x >$ (the enzyme is not much deformed) or a large $< x >$ (the enzyme is considerably deformed). Call f_{DNA} the slope of the DNA energy function in the soft regime (this is the restoring force of the DNA spring in the soft regime, which is approximately constant, see Fig. 5.6); f_e is the corresponding slope for the enzyme energy function (Eq. 5.5). Then we expect a transition in the behavior of the system roughly as the parameter f_e/f_{DNA} goes through 1.

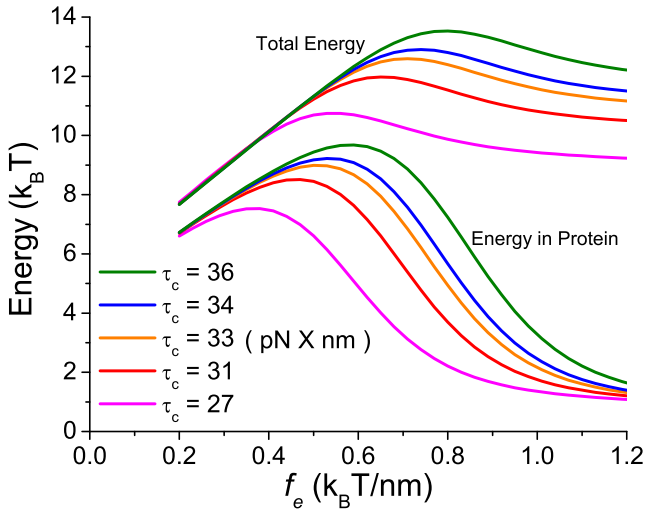

(a)

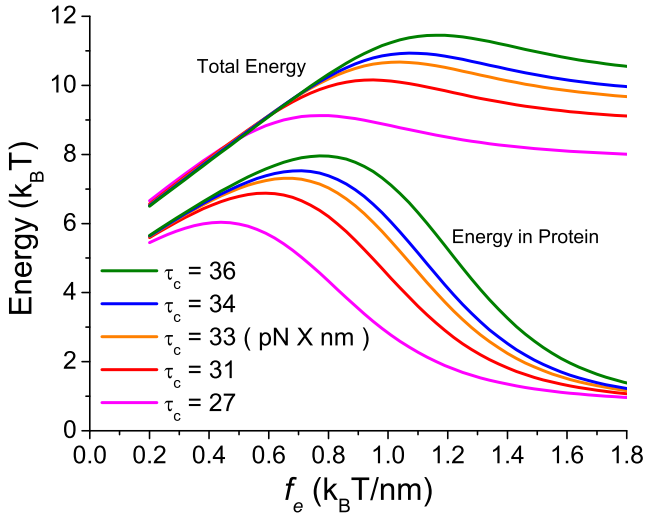

(b)

Figure 5.7: The total elastic energy of the chimera and the elastic energy injected in the protein, plotted vs. the protein restoring force f_e. The different curves correspond to different critical bending torques (τ_c) of the DNA spring, varying from 27 to 36 pN $\times$ nm. The measured value for nicked DNA is $\tau_c = 27\,pN\times$ nm. (a) RLuc60 chimera. (b) RLuc40 chimera.

In Fig. 5.7 we show the calculated elastic energies (the total elastic energy $E_{tot} =< E_{DNA} + E_{prot} >$ and the elastic energy in the enzyme $E_p =< E_{prot} >$) as a function of f_e (the restoring force of the enzyme in the softer regime), for different values of τ_c. Note that f_{DNA} is essentially proportional to τ_c (Eq. 5.4), in fact $f_{DNA} \approx \tau_c/2L$. From Fig. 5.7(a) we see that a relatively small increase in τ_c (the stiffness of the DNA spring) from the value 27 $pN \times nm$ measured for nicked DNA can cause a large change in the elastic energy injected into the enzyme, if the stiffness parameter f_e of the enzyme is within a relatively narrow range, approximately $0.6 < f_e < 1$ in units of k_BT/nm for the 60mer spring. Fig. 5.7(b) shows similar energy curves for the case of the 40mer DNA spring, where the corresponding interesting range for f_e is approximately $0.8 < f_e < 1.2$ in the same units. The overlap of these two ranges tells us that $f_e \approx 0.9\, k_BT/nm$.

5.4.3 Relation of Enzymatic Activity and Mechanical Stress

The next step is to obtain the connection between the mechanical model and the activity of the enzyme. The connection is of course not clear. Enzyme activity has to do with non-equilibrium dynamics [30], as well as statics. This is indeed a criticism one may level at the arguments above. Nevertheless, we find it instructive to ask what simple, plausible connection between equilibrium mechanics and activity would qualitatively reproduce the measurements.

The two simple possibilities are to use the energy E_p injected in the enzyme and write essentially $A \propto exp(-E_p/T)$ for the activity A, or use the deformation x of the enzyme and write $A = A(x)$. Choosing the second possibility, and once again the simplest approximation, namely an activity which decreases linearly to zero as the enzyme is deformed, we write:

$$A(x) = \begin{cases} 1 - \frac{x}{\lambda} & for\ 0 < x \leq \lambda \\ 0 & for\ x > \lambda \end{cases} \tag{5.8}$$

and calculate the observed activity accordingly:

$$< A >= \frac{1}{Z} \int_0^{2L-(\Delta+2H)} A(x)\ e^{-E(x)/T}\, dx \tag{5.9}$$

Now the question is whether the calculated activity $< A >$ compatible with our experimental results?

5.4.4 Results

Fig. 5.8 shows the enzymatic activity thus calculated vs f_e (the same representation as Fig. 5.7) for different values of τ_c (the DNA stiffness parameter). Because in the model the activity $< A >$ never reaches 1 (since $< x > \neq 0$ even with zero stiffness of the DNA spring), to compare to the normalized measurements we normalize the calculated activity curves to 1 for $f_e \to \infty$. Inspection of the graphs shows that the two measurements with the nicked DNA spring (60mer and 40mer), for which $\tau_c = 27\ pN \times nm$, are reproduced by the model with $f_e \approx 0.9$ k_BT/nm. Further, the measurements with the non-nicked spring are also reproduced with this same value of f_e if we assume that without nick $\tau_c \approx 36\ pN \times nm$. This value is about 15 % larger than the value $\tau_c = 31\ pN \times nm$ given in [30]. We have drawn in Fig. 5.8 (vertical bars) the range of values of f, basically $0.8 < f_e < 1$ in k_BT/nm, which lead to predictions, within the present model, qualitatively consistent with the measurements. On the other hand, without assuming a softening transition in the enzyme (i.e. if we treat the enzyme mechanically as a linear spring) we find that we cannot account for the measurements, as we discuss in the later section.

For reference, we also quote the values of the force exerted by the DNA spring on the enzyme, if the enzyme was not deformed. We use $\tau_c = 27\ pN \times nm$ for nicked DNA, $\tau_c = 36\ pN \times nm$ for non-nicked DNA, and $6.1\ nm$ for the DNA EED. From the derivative of (1) we then find: $F_{60}(nicked) = 1.5$ pN, $F_{60}(ds) = 2.0$ pN

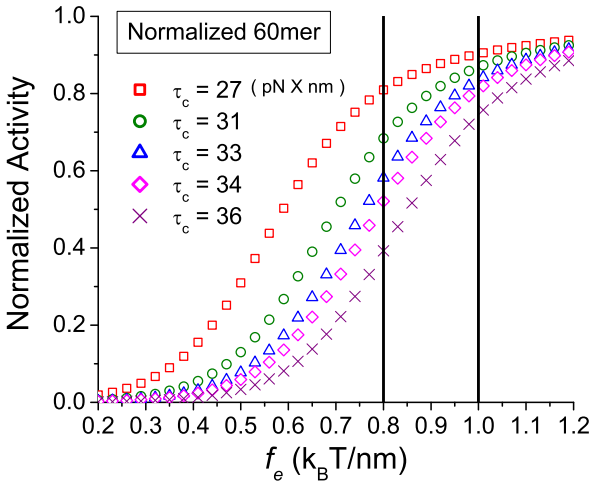

(a)

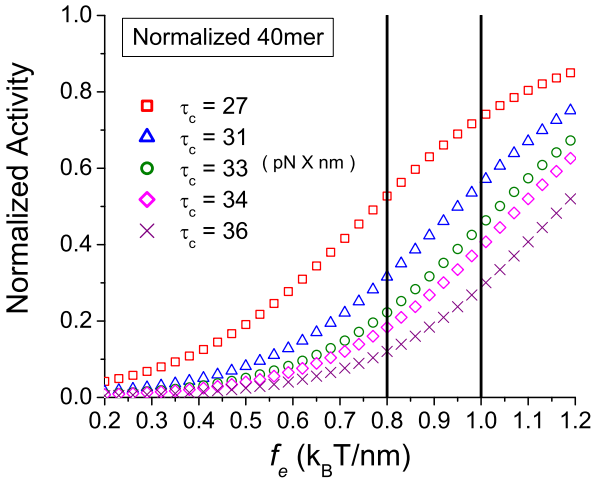

(b)

Figure 5.8: The calculated activity (A) vs. the restoring force f_e of the enzyme. A is calculated using Eq. 5.9 and normalized to 1 for $f_e \to \infty$. Here we assume that the activity decreases linearly to zero as the enzyme is deformed. (a): normalized activity vs. f_e for RLuc60; (b): same for RLuc40. The parameters used here are: x_e = 3 Å, K=100 k_BT/nm^2 and λ=1 nm. The vertical bars show the range of values of f_e which lead to agreement with the measurements of activity in Fig. 5.5, using $\tau_c = 27\ pN \times nm$ for the nicked DNA springs and $\tau_c = 36\ pN \times nm$ for the non-nicked springs.

for RLuc60, and $F_{40}(nicked) = 2.3$ pN, $F_{40}(ds) = 3.1$ pN for RLuc40.

5.4.5 Discussions

We assigned a value to the linear spring constant of the enzyme (K in Eq. 5.5) $K = 100\ k_BT/nm^2 = 400\ pN/nm$), which is compatible with neutron scattering and single-molecule pulling measurements (see Sec. 5.6), and a reasonable value $x_e = 3$ Å for the onset of the nonlinearity. Then we find that the constant force part of the energy function of the enzyme must have a slope $f \approx 0.9\ k_BT/nm \approx 4pN$. This force represents an average restoring force or free energy gradient arising when the structure is deformed. The microscopic picture is that the native (undeformed) structure is the global free energy minimum in the space of conformations of the polypeptide chain. This minimum results from many weak (non-covalent) bonds. However, alternative (deformed) structures are possible where some weak bonds are rearranged or lost: these are higher free energy states. In the real system, there is of course no reason that the free energy should increase linearly with the distance from the native state: this is a simplification of the model. Within this simplified picture, we do however find that, as an order of magnitude, our constant $f \approx 4$ pN is consistent with the restoring force envisioned in the viscoelastic relaxation model of enzyme action (5 pN) [30], with the similar restoring force which is the stall force of the motor kinesin (5 pN)[90], with the equilibrium unzipping force of DNA (12 pN)[91].

5.5 Other Evidences and Arguments

Using the two-coupled-nonlinear-springs model, we are able to derive the connection between equilibrium mechanics and activity, where the observation that small changes in the stiffness of the DNA lead to large changes in catalysis of the enzyme can be reproduced. In the following sections, we will discuss other

evidences and arguments which can support the validity of this model.

5.5.1 Elastic Energy of the Whole Chimera

There is one noteworthy feature. For the same value $f_e = 0.9\ k_BT/nm$, in the case of the nicked 60mer spring ($\tau_c = 27\ pN \times nm$), the total energy in the model is $E_{tot} \approx 9.5\ k_BT$ (Fig. 5.7(a)). This is in excellent agreement with direct measurements of the total elastic energy of several protein - DNA chimeras [18, 20] (although the protein for those chimeras was a different enzyme, see Sec. 3.3.3). Also in agreement with the conclusions in [20] is that the elastic energy in the protein ($E_p \approx 1.5\ k_BT$, Fig. 5.7(a)) is a small fraction of the total elastic energy E_{tot}.

5.5.2 Argument on the Energy Scale

With the model we compute the elastic energy injected into the enzyme, represented as a nonlinear spring. The connection to the measurements of activity comes from recognizing that, on fundamental grounds, for a multi-level system at temperature T it is impossible to change the occupation of a state or group of states by a factor χ unless one injects into the system an energy ΔE of at least $\Delta E \sim Tln\chi$. For RLuc40 we measure $A(nicked)/A(ds) \approx 5$, so by this argument the difference in elastic energy injected into the enzyme for the nicked and non-nicked case must be at least $\Delta E \geq 1.6\,kT$. Similarly, for RLuc60 we find $A(nicked)/A(ds) \approx 2.3$ and therefore the difference in injected energy for this case must be $\Delta E \geq 0.8\ k_BT$. Within the model (Eq. 5.5) for the equilibrium mechanics of the enzyme, these measurements then constrain the possible values of the restoring force f_e, namely $f_e \approx 1\,k_BT/nm \approx 4\,pN$.

5.5.3 Linear Spring Model being incompatible

The simplest mechanical representation of the enzyme, namely a linear spring characterized by one spring constant K, is not compatible with the present measurements. Namely, if we use in Eq. 5.5 the energy function of a simple spring: $E = \frac{1}{2}Kx^2$ and plot the elastic energy in the enzyme, E_p, vs the spring constant K for different values of τ_c (Fig. 5.9), we find the following. For the 60mer chimera, we look for the range of K values such that the elastic energy injected in the protein, E_p justifies the modulation of activity reported in Fig. 5.5. We are looking for $E_p \lesssim 1\ k_BT$ for the nicked ($\tau_c = 27\ pN \times nm$) state and $E_p \gtrsim 2\ k_BT$ for the non-nicked ($\tau_c = 36\ pN \times nm$) state. The corresponding range of K values from Fig. 5.9(a) is $0.15 < K < 0.25$ (in units of k_BT/nm^2). However, for the 40mer spring (Fig. 5.9b) this range is $0.25 < K < 0.5$. In fact, considering also that the nicked 40mer spring has a smaller effect on the enzyme activity than the non-nicked 60mer spring (Fig. 5.5), we see that we have to restrict the possible K values from Fig. 5.9b even further, perhaps $0.35 < K < 0.5$. In short, the two ranges of K values we get from Fig. 5.9(a)&(b) are essentially disjoint, or in other words, there is no one value of K which reasonably accounts for all the measurements. Worse, a mechanical model of the enzyme as a simple spring with a K value of this order, say K= 0.2 k_BT/nm^2 , is rather unphysical. For example, it predicts fluctuations in the size of the unperturbed protein of order $< x^2 >^{1/2} = \sqrt{\frac{k_BT}{K}} \approx 2nm$ (we use equipartition) which is unreasonably large. Indeed, many different scattering experiments [9, 92] and also MD simulations [56] find values of order $\sim$1Å for these fluctuations. By the equipartition argument above, values of the spring constant in the linear elasticity regime must therefore be at least 2 orders of magnitude larger, of order 100 pN/nm and above.

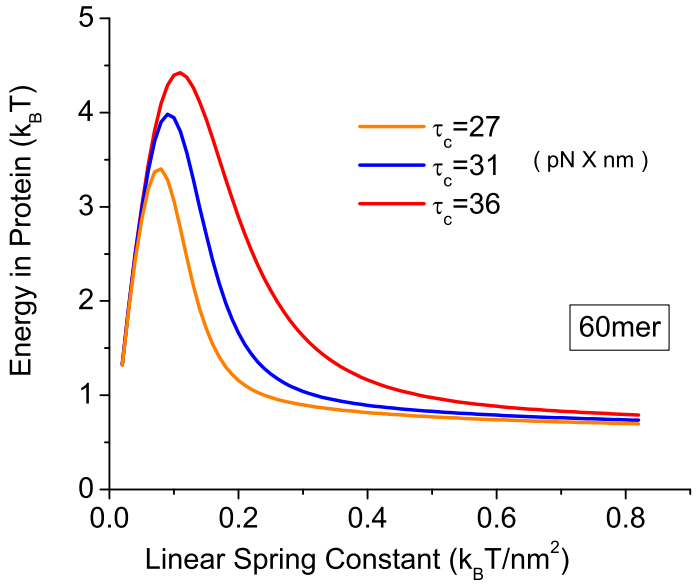

(a)

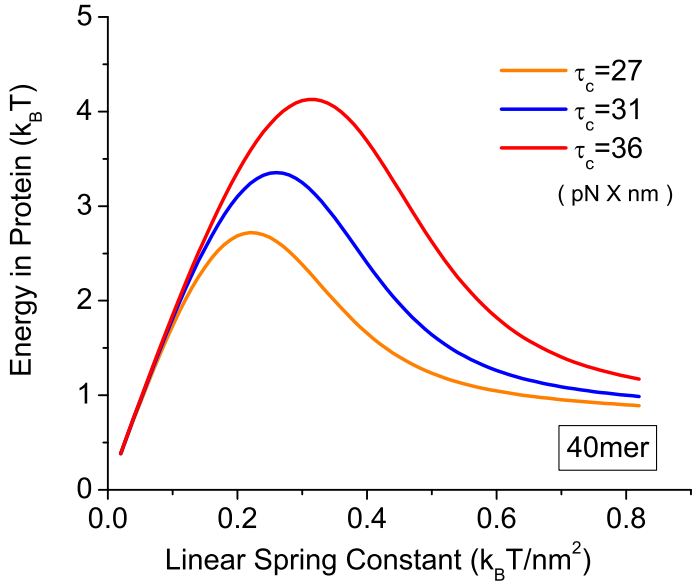

(b)

Figure 5.9: Elastic energy in the protein plotted vs. protein spring constant for the model where the protein behaves as a linear spring. (a) Results for RLuc60, for different values of τ_c; (b) results for RLuc40

5.5.4 Thermal Fluctuation of the Molecules

For the linear spring representation, with the K (barely) accounting for all the measurements ,the thermal fluctuation of the protein is in the order of few nm, which is rather unphysical (see Sec. 5.5.3).

On the other hand, for the nonlinear spring representation, with these values for f_e and K in the energy profile Eq. 5.5, the rms fluctuations of the x in the model without DNA (Eq. 5.5) are $< x^2 >^{1/2} \approx 0.5\, nm$, still too large but more reasonable than in the linear spring model. Further, this can be improved by choosing K even larger (but still within the range of spring constants found in the literature), for instance $K = 500\ k_BT/nm^2$ (2000 pN/nm) results in $< x^2 >^{1/2} \approx\ 0.2nm$ and otherwise the same qualitative picture for the graphs Figs. 5.7 and 5.8, merely leading to a smaller $f_e \sim 0.45\, k_BT/nm^2$.

5.5.5 Sensitivity to the Small Change in the Spring

From Fig. 5.10, where we plot the total energy of the model $E_{tot} = E_p + E_{DNA}$ vs the deformation x, for different values of f_e, the mechanism by which the nonlinearity of the two springs of the model (the enzyme and the DNA) produces the observed sensitivity of the system to small changes in the stiffness of one spring is apparent. One can see that for values of the ratio τ_c/f_e such that the linear part of the total energy graph (Fig. 5.10) is nearly horizontal, the system will exhibit anomalously large fluctuations: these are represented in Fig. 5.11 where we plot $< x^2 >^{1/2}$ vs f_e for different values of τ_c. For the non-nicked 60mer spring $\tau_c = 36\ pN \times nm$) and $0.8 < f_e < 1$ (in units of k_BT/nm) the model predicts fluctuations of order $< x^2 >^{1/2} \approx 4nm$, whereas for the nicked spring ($\tau_c = 27\ pN \times nm$) we find $< x^2 >^{1/2} \approx 2nm$. Such large fluctuations should be observable in single molecule FRET experiments, which are feasible with our chimeras, providing a possibility to further test the proposed softening transition

of the enzyme.

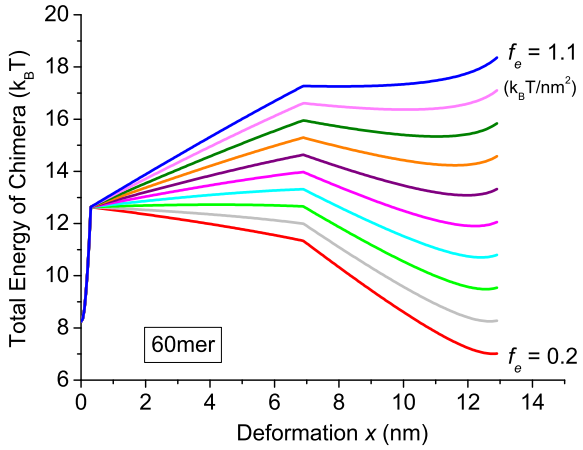

(a)

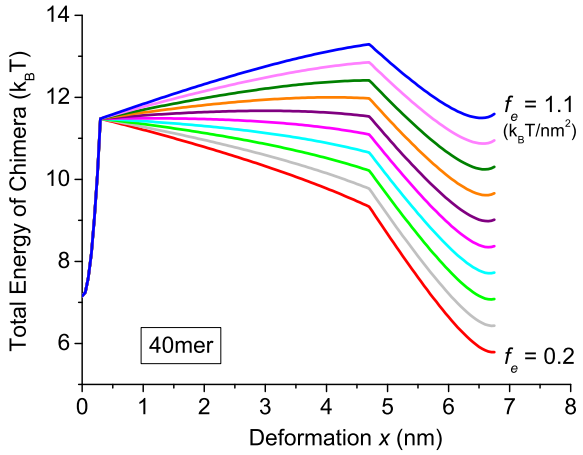

(b)

Figure 5.10: The elastic energy of the chimera plotted vs. the enzyme's deformation (x), for different values of the restoring force f_e (in steps of 0.1 k_BT/nm^2. Qualitatively, we expect a transition in the behavior of the system as the slope of the approximately linear part of this energy function goes through zero. (a) is RLuc60 and (b) is RLuc40. Note the different scales in the axis.

The parameters for this graph are: $x_e = 3$ Å, $K = 100\ k_BT/nm^2$ and τ_c=27 pN $\times$ nm.

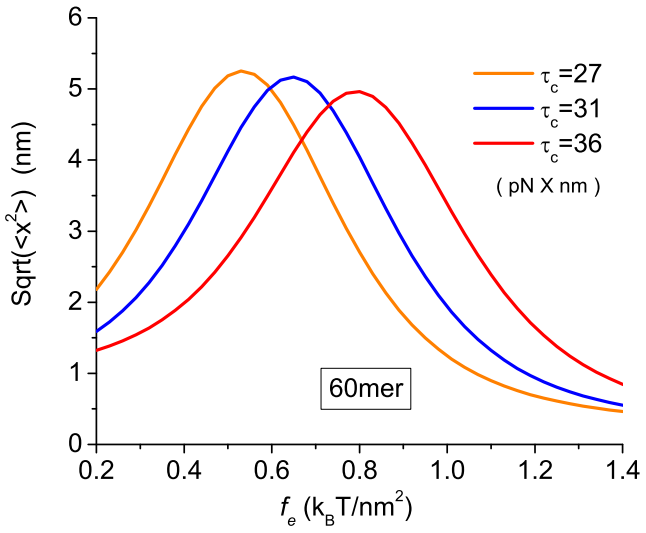

(a)

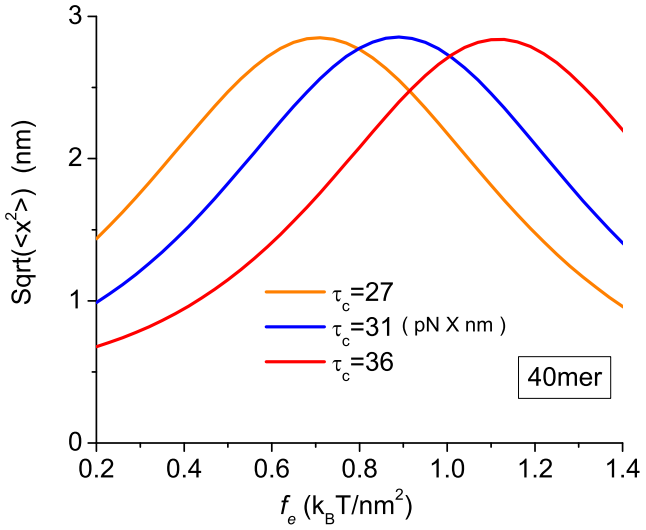

(b)

Figure 5.11: The thermal fluctuations (root mean square deformation) for the chimera vs. the restoring force of the protein f_e, for the values τ_c= 27, 31, 36 pN × nm. (a) RLuc60 (b)RLuc40

The parameter values for this graph are: x_e=3 Å and K=100 k_BT/nm^2.

5.6 Other Relevant Technical Strategies

In this section, we address several methods which have been used to investigate the flexibility and mechanical properties of proteins.

Neutron scattering experiments capture the thermal fluctuations of atoms in the structure. Usually this is combined with equipartition to calculate the "environmental force constant", or resilience, of the structure, using $< k >= k_B/(d < x^2 > /dT)$ [9, 92]. For example, the force constant of myoglobin at room temperature is 300 pN/nm, with root mean square fluctuations of 0.9 Å with respect to the equilibrium position [9]. Neutron scattering experiments are time-averaged, ensemble measurements, and the force constant obtained does not refer to a specific direction.

In contrast, in single-molecule force spectroscopy experiments the protein is stretched and unfolded by applying a mechanical force in a specific direction. The force-extension curves obtained from these pulling experiments are usually interpreted in terms of the worm-like-chain (WLC) model [11] for the unfolded part of the polypeptide, plus a two-states model for the unfolding transition. The measurements are fitted using the WLC parameters and rates for the unfolding transition, from which barrier heights and positions in the two-states model are estimated, yielding finally an estimate for a "spring constant" in the quadratic approximation for this two-states unfolding potential [93]. Orienting the protein construct in the apparatus via specific amino acid pairs on the protein surface, spring constants for different pulling directions have been measured [94]. For green fluorescent protein (GFP), these directional spring constants range from 1000 to 17000 pN/nm [94].

Our own approach of using a DNA molecular spring to mechanically perturb a protein evidently partakes of both methods, in that it is an equilibrium measurement but uses an externally applied, directional force.

5.7 Concluding Remarks

To summarize, we obtain precise measurements of the modulation of enzymatic activity of a luciferase coupled to DNA springs of different stiffness. Within a continuum mechanics framework where the enzyme is continuously and reversibly deformable, we infer from the measurements that the equilibrium mechanics of the enzyme must exhibit a softening transition beyond a few Å deformation, which mirrors a corresponding non-equilibrium transition discovered in earlier nano-rheology experiments [95, 25]. We propose that this may be a universal feature of the mechanics of compact biomolecules.

In addition, the coupling of two nonlinear molecules (the protein and the DNA) can account for our observation that the enzymatic activity decreases drastically when the nick of the DNA is repaired. More generally speaking, when two non-linear molecules are mechanically coupled, small changes in the stiffness of one of the molecules can lead to large changes in the elastic energy injected into the other molecule. This mechanism may be involved in many biological processes, where the behavior of one of the molecules can be greatly affected by finely tuning the property of the other one.

References

[1] DE Koshland Jr. Application of a theory of enzyme specificity to protein synthesis. *Proceedings of the National Academy of Sciences of the United States of America*, 44(2):98, 1958.

[2] Daniel E. Koshland. The keylock theory and the induced fit theory. *Angewandte Chemie International Edition in English*, 33(23-24):2375–2378, 1995.

[3] Alex Gutteridge and Janet Thornton. Conformational changes observed in enzyme crystal structures upon substrate binding. *Journal of Molecular Biology*, 346(1):21–28, 2005.

[4] Jaroslaw Blaszczyk, Yue Li, Honggao Yan, and Xinhua Ji. Crystal structure of unligated guanylate kinase from yeast reveals gmp-induced conformational changes. *Journal of Molecular Biology*, 307(1):247–257, 2001.

[5] Chung?Jung Tsai, Sandeep Kumar, Buyong Ma, and Ruth Nussinov. Folding funnels, binding funnels, and protein function. *Protein Science*, 8(6):1181–1190, 1999.

[6] David D Boehr, Ruth Nussinov, and Peter E Wright. The role of dynamic conformational ensembles in biomolecular recognition. *Nature chemical biology*, 5(11):789–796, 2009.

[7] K. Ravi Acharya and Matthew D. Lloyd. The advantages and limitations of protein crystal structures. *Trends in Pharmacological Sciences*, 26(1):10–14, 2005.

[8] J. C. Smith. Protein dynamics: comparison of simulations with inelastic neutron scattering experiments. *Quarterly Reviews of Biophysics*, 24(03):227–291, 1991.

[9] Giuseppe Zaccai. How soft is a protein? a protein dynamics force constant measured by neutron scattering. *Science*, 288(5471):1604–1607, 2000.

[10] Keir C Neuman and Attila Nagy. Single-molecule force spectroscopy: optical tweezers, magnetic tweezers and atomic force microscopy. *Nature methods*, 5(6):491–505, 2008.

[11] C Bustamante, JF Marko, ED Siggia, and S Smith. Entropic elasticity of lambda-phage dna. *Science*, 265(5178):1599–1600, 1994.

[12] D Bensimon, AJ Simon, V Croquette, and A Bensimon. Stretching dna with a receding meniscus: experiments and models. *Physical Review Letters*, 74(23):4754, 1995.

[13] Victor A. Bloomfield, Donald M. Crothers, and Ignacio Tinoco. *Nucleic acids: structure, properties, and functions*. University Science Books, 1999.

[14] Peter L Privalov. Protein folding. *Microcalorimetry of Macromolecules: The Physical Basis of Biological Structures*, pages 225–247, 1992.

[15] Brian Choi, Giovanni Zocchi, Stephen Canale, Yim Wu, Sum Chan, and L. Jeanne Perry. Artificial allosteric control of maltose binding protein. *Physical Review Letters*, 94(3):038103, 2005. PRL.

[16] Brian Choi, Giovanni Zocchi, Yim Wu, Sum Chan, and L. Jeanne Perry. Allosteric control through mechanical tension. *Physical Review Letters*, 95(7):078102, 2005.

[17] Brian Choi and Giovanni Zocchi. Guanylate kinase, induced fit, and the allosteric spring probe. *Biophysical Journal*, 92(5):1651–1658, 2007.

[18] Andrew Wang and Giovanni Zocchi. Elastic energy driven polymerization. *Biophysical Journal*, 96(6):2344–2352, 2009.

[19] Yong Wang, Andrew Wang, Hao Qu, and Giovanni Zocchi. Protein-dna chimeras: synthesis of two-arm chimeras and non-mechanical effects of the dna spring. *Journal of Physics: Condensed Matter*, 21(33):335103, 2009.

[20] Chiao-Yu Tseng, Andrew Wang, Giovanni Zocchi, Biljana Rolih, and Alex J. Levine. Elastic energy of protein-dna chimeras. *Physical Review E*, 80(6):061912, 2009.

[21] C.-Y. Tseng, A. Wang, and G. Zocchi. Mechano-chemistry of the enzyme guanylate kinase. *Europhysics Letters*, 91(1):18005, 2010.

[22] M Kurplus and J A McCammon. Dynamics of proteins: Elements and function. *Annual Review of Biochemistry*, 52(1):263–300, 1983.

[23] Alan Saghatelian, Kevin M. Guckian, Desiree A. Thayer, and M. Reza Ghadiri. Dna detection and signal amplification via an engineered allosteric enzyme. *Journal of the American Chemical Society*, 125(2):344–345, 2002.

[24] Mark J Zoller and Michael Smith. Oligonucleotide-directed mutagenesis using m13-derived vectors: an efficient and general procedure for the production of point mutations in any fragment of dna. *Nucleic Acids Research*, 10(20):6487–6500, 1982.

[25] Yong Wang and Giovanni Zocchi. Elasticity of globular proteins measured from the ac susceptibility. *Physical Review Letters*, 105(23):238104, 2010. PRL.

[26] KC Agarwal, RP Miech, and RE Parks Jr. Guanylate kinases from human erythrocytes, hog brain, and rat liver. *Methods in enzymology*, 51:483–490, 1978.

[27] Chandrasekhar V Miduturu and Scott K Silverman. Dna constraints allow rational control of macromolecular conformation. *Journal of the American Chemical Society*, 127(29):10144–10145, 2005.

[28] Hao Qu, Chiao-Yu Tseng, Yong Wang, Alex J. Levine, and Giovanni Zocchi. The elastic energy of sharply bent nicked dna. *Europhysics Letters*, 90(1):18003, 2010.

[29] Hao Qu and Giovanni Zocchi. The complete bending energy function for nicked dna. *Europhysics Letters*, 94(1):18003, 2011.

[30] Hao Qu, Yong Wang, Chiao-Yu Tseng, and Giovanni Zocchi. Critical torque for kink formation in double-stranded dna. *Physical Review X*, 1(2):021008, 2011. PRX.

[31] Guillaume Hible, Petya Christova, Louis Renault, Edward Seclaman, Andrew Thompson, Eric Girard, Hlne Munier?Lehmann, and Jacqueline Cherfils. Unique gmp?binding site in mycobacterium tuberculosis guanosine monophosphate kinase. *Proteins: Structure, Function, and Bioinformatics*, 62(2):489–500, 2006.

[32] Chenxiang Lin, Yan Liu, Sherri Rinker, and Hao Yan. Dna tile based self-assembly: Building complex nanoarchitectures. *ChemPhysChem*, 7(8):1641–1647, 2006.

[33] Tsu Ju Fu and Nadrian C. Seeman. Dna double-crossover molecules. *Biochemistry*, 32(13):3211–3220, 1993.

[34] Xiaojun Li, Xiaoping Yang, Jing Qi, and Nadrian C. Seeman. Antiparallel dna double crossover molecules as components for nanoconstruction. *Journal of the American Chemical Society*, 118(26):6131–6140, 1996.

[35] Rebecca Schulman and Erik Winfree. Synthesis of crystals with a programmable kinetic barrier to nucleation. *Proceedings of the National Academy of Sciences*, 104(39):15236–15241, 2007.

[36] Robert D. Barish, Rebecca Schulman, Paul W. K. Rothemund, and Erik Winfree. An information-bearing seed for nucleating algorithmic self-assembly. *Proceedings of the National Academy of Sciences*, 106(15):6054–6059, 2009.

[37] John C. Matthews, Kazuo Hori, and Milton J. Cormier. Purification and properties of renilla reniformis luciferase. *Biochemistry*, 16(1):85–91, 1977.

[38] Andreas Markus Loening, Timothy David Fenn, Anna M. Wu, and Sanjiv Sam Gambhir. Consensus guided mutagenesis of renilla luciferase yields enhanced stability and light output. *Protein Engineering Design and Selection*, 19(9):391–400, 2006.

[39] W W Ward and M J Cormier. An energy transfer protein in coelenterate bioluminescence. characterization of the renilla green-fluorescent protein. *Journal of Biological Chemistry*, 254(3):781–788, 1979.

[40] Y. Wang, G. Wang, D.J. O'Kane, and A.A. Szalay. *Bioluminescence and Chemiluminescence: Molecular Reporting with Photons*, pages pp. 419–422, 1997.

[41] Yao Xu, David W. Piston, and Carl Hirschie Johnson. A bioluminescence resonance energy transfer (bret) system: Application to interacting circadian clock proteins. *Proceedings of the National Academy of Sciences*, 96(1):151–156, 1999.

[42] Andreas Markus Loening, Timothy David Fenn, and Sanjiv Sam Gambhir. Crystal structures of the luciferase and green fluorescent protein from renilla reniformis. *Journal of Molecular Biology*, 374(4):1017–1028, 2007.

[43] John C. Matthews, Kazuo Hori, and Milton J. Cormier. Substrate and substrate analog binding properties of renilla luciferase. *Biochemistry*, 16(24):5217–5220, 1977.

[44] Jongchan Woo and Albrecht von Arnim. Mutational optimization of the coelenterazine-dependent luciferase from renilla. *Plant Methods*, 4(1):23, 2008.

[45] Sanjay Tyagi and Fred Russell Kramer. Molecular beacons: Probes that fluoresce upon hybridization. *Nat Biotech*, 14(3):303–308, 1996. 10.1038/nbt0396-303.

[46] Razvan Nutiu and Yingfu Li. Tripartite molecular beacons. *Nucleic Acids Research*, 30(18):e94, 2002.

[47] TomN Grossmann, Lars Rglin, and Oliver Seitz. Triplex molecular beacons as modular probes for dna detection. *Angewandte Chemie International Edition*, 46(27):5223–5225, 2007.

[48] Chunhai Fan, Kevin W. Plaxco, and Alan J. Heeger. Electrochemical interrogation of conformational changes as a reagentless method for the sequence-specific detection of dna. *Proceedings of the National Academy of Sciences*, 100(16):9134–9137, 2003.

[49] T. Andrew Taton, Chad A. Mirkin, and Robert L. Letsinger. Scanometric dna array detection with nanoparticle probes. *Science*, 289(5485):1757–1760, 2000.

[50] Shana O. Kelley, Elizabeth M. Boon, Jacqueline K. Barton, Nicole M. Jackson, and Michael G. Hill. Single-base mismatch detection based on charge transduction through dna. *Nucleic Acids Research*, 27(24):4830–4837, 1999.

[51] Yi Xiao, Xinhui Lou, Takanori Uzawa, Kory J. I. Plakos, Kevin W. Plaxco, and H. Tom Soh. An electrochemical sensor for single nucleotide polymorphism detection in serum based on a triple-stem dna probe. *Journal of the American Chemical Society*, 131(42):15311–15316, 2009.

[52] T. Gregory Drummond, Michael G. Hill, and Jacqueline K. Barton. Electrochemical dna sensors. *Nat Biotech*, 21(10):1192–1199, 2003. 10.1038/nbt873.

[53] Steve W. Lockless and Rama Ranganathan. Evolutionarily conserved pathways of energetic connectivity in protein families. *Science*, 286(5438):295–299, 1999.

[54] Jeeyeon Lee, Madhusudan Natarajan, Vishal C. Nashine, Michael Socolich, Tina Vo, William P. Russ, Stephen J. Benkovic, and Rama Ranganathan. Surface sites for engineering allosteric control in proteins. *Science*, 322(5900):438–442, 2008.

[55] Najeeb Halabi, Olivier Rivoire, Stanislas Leibler, and Rama Ranganathan. Protein sectors: Evolutionary units of three-dimensional structure. *Cell*, 138(4):774–786, 2009.

[56] Sophie Sacquin-Mora, Olivier Delalande, and Marc Baaden. Functional modes and residue flexibility control the anisotropic response of guanylate kinase to mechanical stress. *Biophysical Journal*, 99(10):3412–3419, 2010.

[57] Olivier Delalande, Sophie Sacquin-Mora, and Marc Baaden. Enzyme closure and nucleotide binding structurally lock guanylate kinase. *Biophysical Journal*, 101(6):1440–1449, 2011.

[58] Toru Nakatsu, Susumu Ichiyama, Jun Hiratake, Adrian Saldanha, Nobuyuki Kobashi, Kanzo Sakata, and Hiroaki Kato. Structural basis for the spectral difference in luciferase bioluminescence. *Nature*, 440(7082):372–376, 2006. 10.1038/nature04542.

[59] Alfred Pingoud and Albert Jeltsch. Structure and function of type ii restriction endonucleases. *Nucleic Acids Research*, 29(18):3705–3727, 2001.

[60] Hector Viadiu and Aneel K. Aggarwal. The role of metals in catalysis by the restriction endonuclease bam hi. *Nat Struct Mol Biol*, 5(10):910–916, 1998. 10.1038/2352.

[61] Yaakov Benenson. Biomolecular computing systems: principles, progress and potential. *Nat Rev Genet*, 13(7):455–468, 2012. 10.1038/nrg3197.

[62] Yaakov Benenson. Recombinatorial logic. *Science*, 340(6132):554–555, 2013.

[63] Omid C. Farokhzad, Jianjun Cheng, Benjamin A. Teply, Ines Sherifi, Sangyong Jon, Philip W. Kantoff, Jerome P. Richie, and Robert Langer. Targeted nanoparticle-aptamer bioconjugates for cancer chemotherapy in vivo. *Proceedings of the National Academy of Sciences*, 103(16):6315–6320, 2006.

[64] James S. Swensen, Yi Xiao, Brian S. Ferguson, Arica A. Lubin, Rebecca Y. Lai, Alan J. Heeger, Kevin W. Plaxco, and H. Tom Soh. Continuous, real-time monitoring of cocaine in undiluted blood serum via a microfluidic, electrochemical aptamer-based sensor. *Journal of the American Chemical Society*, 131(12):4262–4266, 2009.

[65] Maureen McKeague and Maria C. DeRosa. Challenges and opportunities for small molecule aptamer development. *Journal of Nucleic Acids*, 2012:20, 2012.

[66] Sumedha D. Jayasena. Aptamers: An emerging class of molecules that rival antibodies in diagnostics. *Clinical Chemistry*, 45(9):1628–1650, 1999.

[67] Sulay Jhaveri and Andrew Ellington. *In Vitro Selection of RNA Aptamers to a Small Molecule Target*. John Wiley and Sons, Inc., 2001.

[68] V. Bardoczy and T. Meszaros. Aptamer selection for macromolecular (protein) and for small molecule targets. *Proceedings of the Periodica Polytechnica Abstracts of PhD Conference*, 2006.

[69] Zsfia Balogh, Gergely Lautner, Viola Bardczy, Beata Komorowska, Rbert. E. Gyurcsnyi, and Tams Mszros. Selection and versatile application of virus-specific aptamers. *The FASEB Journal*, 24(11):4187–4195, 2010.

[70] K. Sefah, D. Shangguan, X. Xiong, M. B. O'Donoghue, and W. Tan. Development of dna aptamers using cell-selex. *Nature protocols*, 5(6):116–1185, 2010.

[71] Milan N. Stojanovic, Paloma de Prada, and Donald W. Landry. Aptamer-based folding fluorescent sensor for cocaine. *Journal of the American Chemical Society*, 123(21):4928–4931, 2001.

[72] Ryan Walsh and Maria C. DeRosa. Retention of function in the dna homolog of the rna dopamine aptamer. *Biochemical and Biophysical Research Communications*, 388(4):732–735, 2009.

[73] Louis C. Bock, Linda C. Griffin, John A. Latham, Eric H. Vermaas, and John J. Toole. Selection of single-stranded dna molecules that bind and inhibit human thrombin. *Nature*, 355(6360):564–566, 1992. 10.1038/355564a0.

[74] Shuichiro Uehara, Naohiko Shimada, Yoichi Takeda, Yoshikazu Koyama, Yoshifumi Takei, Hironori Ando, Susumu Satoh, Atsushi Uno, and Kazuo Sakurai. 3' poly(da)-tailed thrombin dna aptamer to increase dnase-resistance and clotting inhibitory activity. *Bulletin of the Chemical Society of Japan*, 81(11):1485–1491, 2008.

[75] W S Bennett and T A Steitz. Glucose-induced conformational change in yeast hexokinase. *Proceedings of the National Academy of Sciences*, 75(10):4848–4852, 1978.

[76] Nikolina Sekulic, Ludmila Shuvalova, Oliver Spangenberg, Manfred Konrad, and Arnon Lavie. Structural characterization of the closed conformation of mouse guanylate kinase. *Journal of Biological Chemistry*, 277(33):30236–30243, 2002.

[77] Georg E. Schulz, Christoph W. Mller, and Kay Diederichs. Induced-fit movements in adenylate kinases. *Journal of Molecular Biology*, 213(4):627–630, 1990.

[78] Paul Maragakis and Martin Karplus. Large amplitude conformational change in proteins explored with a plastic network model: Adenylate kinase. *Journal of Molecular Biology*, 352(4):807–822, 2005.

[79] Karunesh Arora and Charles L. Brooks. Large-scale allosteric conformational transitions of adenylate kinase appear to involve a population-shift mechanism. *Proceedings of the National Academy of Sciences*, 104(47):18496–18501, 2007.

[80] John F Marko and Eric D Siggia. Stretching dna. *Macromolecules*, 28(26):8759–8770, 1995.

[81] Timothy E Cloutier and Jonathan Widom. Spontaneous sharp bending of double-stranded dna. *Molecular cell*, 14(3):355–362, 2004.

[82] Quan Du, Chaim Smith, Nahum Shiffeldrim, Maria Vologodskaia, and Alexander Vologodskii. Cyclization of short dna fragments and bending fluctuations of the double helix. *Proceedings of the National Academy of Sciences of the United States of America*, 102(15):5397–5402, 2005.

[83] Quan Du, Alexander Kotlyar, and Alexander Vologodskii. Kinking the double helix by bending deformation. *Nucleic Acids Research*, 36(4):1120–1128, 2008.

[84] Paul A Wiggins, Thijn Van Der Heijden, Fernando Moreno-Herrero, Andrew Spakowitz, Rob Phillips, Jonathan Widom, Cees Dekker, and Philip C Nelson. High flexibility of dna on short length scales probed by atomic force microscopy. *Nature Nanotechnology*, 1(2):137–141, 2006.

[85] Chiao-Yu Tseng and Giovanni Zocchi. Mechanical control of renilla luciferase. *Journal of the American Chemical Society*, 135(32):11879–11886, 2013.

[86] Hao Qu and Giovanni Zocchi. How enzymes work: A look through the perspective of molecular viscoelastic properties. *Physical Review X*, 3(1):011009, 2013. PRX.

[87] Yongli Zhang and Donald M. Crothers. High-throughput approach for detection of dna bending and flexibility based on cyclization. *Proceedings of the National Academy of Sciences*, 100(6):3161–3166, 2003.

[88] Carlos Bustamante, Yann R. Chemla, Nancy R. Forde, and David Izhaky. Mechanical processes in biochemistry. *Annual Review of Biochemistry*, 73(1):705–748, 2004.

[89] Thierry Dauxois, Michel Peyrard, and A. R. Bishop. Entropy-driven dna denaturation. *Physical Review E*, 47(1):R44–R47, 1993. PRE.

[90] Mark J. Schnitzer, Koen Visscher, and Steven M. Block. Force production by single kinesin motors. *Nat Cell Biol*, 2(10):718–723, 2000. 10.1038/35036345.

[91] Simona Cocco, Rmi Monasson, and John F. Marko. Force and kinetic barriers to unzipping of the dna double helix. *Proceedings of the National Academy of Sciences*, 98(15):8608–8613, 2001.

[92] Frank Gabel, Dominique Bicout, Ursula Lehnert, Moeava Tehei, Martin Weik, and Giuseppe Zaccai. Protein dynamics studied by neutron scattering. *Quarterly Reviews of Biophysics*, 35(04):327–367, 2002.

[93] Matthias Rief, Julio M. Fernandez, and Hermann E. Gaub. Elastically coupled two-level systems as a model for biopolymer extensibility. *Physical Review Letters*, 81(21):4764–4767, 1998. PRL.

[94] Hendrik Dietz, Felix Berkemeier, Morten Bertz, and Matthias Rief. Anisotropic deformation response of single protein molecules. *Proceedings of the National Academy of Sciences*, 103(34):12724–12728, 2006.

[95] Yong Wang and Giovanni Zocchi. Viscoelastic transition and yield strain of the folded protein. *PLoS ONE*, 6(12):e28097, 2011.